MICROCOPY RESOLUTION TEST CHART
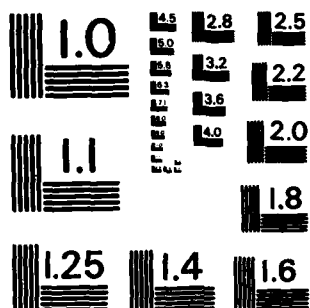
NATIONAL BUREAU OF STANDARDS-1963-A

AD A130627

AFWAL-TR-83-3013

AIRBORNE LIGHTNING CHARACTERIZATION

P.L. RUSTAN
Air Force Institute of Technology
Wright-Patterson AFB, Ohio 45433

B.P. Kuhlman
Flight Dynamics Laboratory
Wright-Patterson AFB, Ohio 45433

A. Serrano, J. Reazer, and M. Risley
Technology Scientific Services, Inc.
Post Office Box 3065, Overlook Branch
Dayton, Ohio 45431

January 1983

Final Report for Period June 1979 – August 1982

DTIC
SELECTED
JUL 2 5 1983

E

DTIC FILE COPY

FLIGHT DYNAMICS LABORATORY
AIR FORCE WRIGHT AERONAUTICAL LABORATORIES
AIR FORCE SYSTEMS COMMAND
WRIGHT-PATTERSON AIR FORCE BASE, OHIO 45433

83 07 22 048

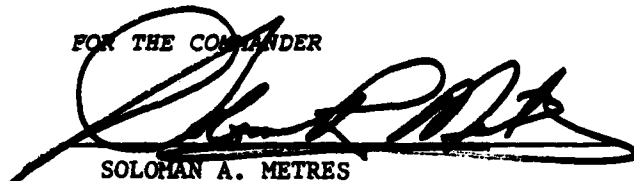This technical report has been reviewed and is approved for publication.

PEDRO L. RUSTAN, Jr.
Project Engineer

GARY A. DUBRO, Chief
Atmospheric Electricity Hazards Group
Vehicle Equipment Division
AF Flight Dynamics Laboratory

FOR THE COMMANDER

SOLOMAN A. METRES
Director, Vehicle Equipment Division
AF Flight Dynamics Laboratory

SECURITY CLASSIFICATION OF THIS PAGE *(When Data Entered)*

REPORT DOCUMENTATION PAGE		READ INSTRUCTIONS BEFORE COMPLETING FORM
1. REPORT NUMBER AFWAL-TR-83-3013	2. GOVT ACCESSION NO. AD-A130627	3. RECIPIENT'S CATALOG NUMBER
4. TITLE *(and Subtitle)* AIRBORNE LIGHTNING CHARACTERIZATION		5. TYPE OF REPORT & PERIOD COVERED Final June 1979 to August 1982
		6. PERFORMING ORG. REPORT NUMBER
7. AUTHOR(s) P.L. Rustan*, B.P. Kuhlman**, A. Serrano, J. Reazer, M. Risley***		8. CONTRACT OR GRANT NUMBER(s)
9. PERFORMING ORGANIZATION NAME AND ADDRESS Flight Dynamics laboratory (AFWAL/FIESL) Wright-Patterson AFB, OH 45433		10. PROGRAM ELEMENT, PROJECT, TASK AREA & WORK UNIT NUMBERS 62201F 24020223
11. CONTROLLING OFFICE NAME AND ADDRESS Flight Dynamics Laboratory (AFWAL/FIESL) Wright-Patterson AFB, OH 45433		12. REPORT DATE January 1983
		13. NUMBER OF PAGES 171
14. MONITORING AGENCY NAME & ADDRESS*(if different from Controlling Office)*		15. SECURITY CLASS. *(of this report)* Unclassified
		15a. DECLASSIFICATION/DOWNGRADING SCHEDULE

16. DISTRIBUTION STATEMENT *(of this Report)*

Approved for public release; distribution unlimited.

17. DISTRIBUTION STATEMENT *(of the abstract entered in Block 20, if different from Report)*

18. SUPPLEMENTARY NOTES

*Air Force Institute of Technology, WPAFB, OH 45433
**Flight Dynamics Laboratory, WPAFB, OH 45433
***Technology Scientific Services Inc., P.O. Box 3065, Overlook Br, Dayton, OH 45431

19. KEY WORDS *(Continue on reverse side if necessary and identify by block number)*

Airborne Lightning Test	Direct Strike
Aircraft Lightning	Lightning Waveforms
Lightning Tests	Lightning Far Field

20. ABSTRACT *(Continue on reverse side if necessary and identify by block number)*

This is an initial report of a three-year lightning characterization program performed by the Air Force Flight Dynamics Laboratory, Wright-Patterson Air Force Base, Ohio. The data were acquired in approximately 100 flight hours spaced over the summers of 1979 to 1981 in Central and South Florida.

A WC-130 aircraft was instrumented with eleven electric and magnetic field sensors at different locations. The aircraft was flown in the vicinity of active thunderstorms at altitudes between 1500 and 16000 feet mean sea level

DD FORM 1473 1 JAN 73   EDITION OF 1 NOV 65 IS OBSOLETE

SECURITY CLASSIFICATION OF THIS PAGE *(When Data Entered)*

Block 20 Continued

(MSL). To correlate the electric fields produced by the lightning flashes and the respective location of the flashes, a ground station network was employed. The ground network consisted of a central station where the electric field and very high frequency (VHF) radiation were measured and four remote stations arranged in a wye configuration with a 20 kilometer (km) radius for measuring VHF.

Fourteen channels of continuous analog data with 2 Mega hertz (MHz) bandwidth and ten channels of digital data of 164 microsecond (μsec) windows with 20 MHz bandwidth at a maximum rate of two data windows per second were recorded in the aircraft. Analog data for the electric field and VHF radiation with 2 MHz bandwidth were recorded at the central ground site. In addition, VHF radiation with 4 MHz bandwidth was recorded in modified video cassette recorders at all four ground sites. IRIG-B time code received at the ground site was retransmitted to the aircraft and remote stations and used for time synchronization. The aircraft and ground sensors were calibrated to detect lightning flashes between zero and 35 km away.

Accession For		
NTIS GRA&I	☒	
DTIC TAB	☐	
Unannounced	☐	
Justification		
By		
Distribution/		
Availability Codes		
Dist	Avail and/or Special	
A		

FOREWORD

This is the first report on an airborne lightning character-
ization program using a WC-130 aircraft to obtain electromagnetic
field data near thunderstorms in South Florida in the 1979-1981
time period. This analysis effort was performed in-house by the
Flight Dynamics Laboratory (AFWAL/FIESL) with cooperation with
the Air Force Institute of Technology and Technology Scientific
Services, Inc.

This work could not have been accomplished without the
assistance of certain individuals and groups during the entire
program. We express our deepest appreciation to Mr. Robert K.
Baum who was the principal investigator in this program during
the first two years. We are also grateful to Dr. Martin A. Uman
from the University of Florida for his constructive criticism of
different phases of the program. Special thanks are due to the
NOAA/RFC group at the Miami International Airport. This group
provided the aircraft and a very dedicated and knowledgeable crew
willing to fly it.

This work could not have started without the effort of Mr.
Gary DuBro, our group leader. Mr. DuBro obtained the funds for
the program and provided input throughout its completion. A word
of appreciation is also due to Major Charles Shubert who
coordinated the efforts of all the participants in the program in
the last three years.

During the nine months prior to the completion of this report
D. Jean-Patrick Moreau from the Office National d'Etudes et de
Recherches Aerospatiales, France, joined us as part of a data
exchange agreement with France. Dr. Moreau has been of great
assistance analyzing the 1981 data. Without his support, this
report could not have been completed at this time.

TABLE OF CONTENTS

LIST OF ILLUSTRATIONS

LIST OF TABLES

SUMMARY

This is an initial report of a three-year lightning characterization program performed by the Air Force Flight Dynamics Laboratory, Wright-Patterson Air Force Base, Ohio. The data were acquired in approximately 100 flight hours spaced over the summers of 1979 to 1981 in Central and South Florida.

A WC-130 aircraft was instrumented with eleven electric and magnetic field sensors at different aircraft locations. The aircraft was flown in the vicinity of active thunderstorms at altitudes between 1500 and 16000 feet mean sea level (MSL). To correlate the electric fields produced by the lightning flashes and the respective location of the flashes, a ground station network was employed. The ground network consisted of a central station where the electric field and very high frequency (VHF) radiation were measured and four remote stations arranged in a wye configuration with a 20 kilometer (km) radius for measuring VHF.

Fourteen channels of continuous analog data with 2 Mega hertz(MHz) bandwidth and ten channels of digital data of 164 microsecond (μsec) windows with 20 MHz bandwidth at a maximum rate of two data windows per second were recorded in the aircraft. Analog data for the electric field and VHF radiation with 2 MHz bandwidth were recorded at the central ground site. In addition, VHF radiation with 4 MHz bandwidth was recorded in

modified video cassette recorders at all four ground sites. IRIG-B time code received at the ground site was retransmitted to the aircraft and remote stations and used for time synchronization. The aircraft and ground sensors were calibrated to detect lightning flashes between zero and 35 km away.

This report presents a description of the aircraft and ground instrumentation used to accomplish the data acquisition for all three years. An analysis of the data collected during the first two years and a summary of about 40% of the events during the last year are also presented. Some of the most important results from the data analyzed to date are:

1) About half of the electric and magnetic field measurements of return strokes measured in the aircraft had a risetime, t_r, (fast transition to peak) between 100 and 200 nanoseconds (nsec). These results are comparable with those obtained by Weidman and Krider in 1978 and 1980 when it was found that some return strokes measured on the ground had average risetimes of 90 nsec during the fast transition.

2) The frequency transform of the airborne-measured return strokes decayed approximately as $1/f$ from 24 kilohertz (kHz) to 2 MHz and as $1/f^2$ from 2 MHz to 20 MHz. These results are comparable with those reported by Weidman et al., 1981, from derivative data recorded on the ground.

3) Correlated electric fields for return strokes at heights of 1500 to 16000 feet MSL have similar characteristics to those measured on the ground for lightning flashes between 10 and 20 km away. These results indicate that the aircraft resonances have no appreciable effect on the airborne measured field at these

distances. However, the electromagnetic field data collected in the near field as the aircraft flies around the thundercloud show the effect of the aircraft resonances.

4) There are electric and magnetic field pulses with rise-times on the order of 100 nsec which occur at times other than during the return stroke. These sharp pulses can be coupled through apertures and cause interference to aircraft electronics.

5) The electric field on the surface of aircraft flying in close proximity to a thunderstorm cell or inside the cell varies continuously. The charge on the surface of the aircraft producing this field could trigger a lightning flash with a nearby region which is oppositely charged. This discharge between the aircraft and its surroundings can start with leaders attaching to different areas of the aircraft. Electric field changes larger than 100,000 volts/meter (V/m) were measured on the surface of the aircraft during one of the direct strikes. The monitored induced voltage in the C-130 aircraft internal wiring was greater than 100 millivolts.

6) There were two direct lightning strikes to the aircraft during the 1981 flight test. Both of these strikes were triggered by the aircraft and can be interpreted as cloud-to-aircraft lightning discharges. These two flashes lasted about 400 msec and had a maximum pulse repetition rate of 10^4 pulses/sec. The maximum current for any of the pulses in these two strikes was 600 Amperes (A) and 3 kiloamperes (kA), respectively.

SECTION I

INTRODUCTION

In the ten years preceding the initiation of this program,
seven United States Air Force (USAF) aircraft were lost due to
confirmed lightning-related incidents. Lightning was cited as
the likely cause in two other major aircraft accidents, and 153
serious lightning-related mishaps were documented (Refs 1, 2, and
3). In the five-year period from 1972 to 1977, the USAF finan-
cial loss exceeded 21 million dollars. Similar reports for
commercial aircraft indicate one serious lightning strike about
every 3,000 flight hours (Ref 4).

Coupled with the ever present lightning hazards to the
aircraft are the changing effects on the aircraft introduced by
two emerging technologies: microelectronics and advanced struc-
tural materials. The application of these technological advances
to aircraft results in a potentially increased
susceptibility/vulnerability of electronic equipment to circuit
transients and an increase in the electromagnetic energy coupled
into the aircraft circuitry. Therefore, the advantages achieved
in aircraft performance and flexibility may be offset because of
the higher susceptibility to electromagnetic transients. This is
a major concern in new generation aircraft.

To determine the electromagnetic coupling to the aircraft
for direct and nearby lightning, the Air Force Wright Aeronauti-
cal Laboratories (AFWAL) started a three-year (1979-81) airborne
lightning characterization program. The WC-130 aircraft shown in

1

Figure 1 was instrumented with wideband electromagnetic field sensors and flown in close proximity to active thunderstorms to record the characteristics of the electric and magnetic fields in the aircraft environment.

The three-year program was evolutionary. In the first year, a fairly simple system was used and a small amount of useful data was obtained (Ref 5). The main emphasis during the first year was to capture data windows of 2048 points of the largest electric and magnetic field radiation incident on the aircraft from lightning flashes 5 to 20 km away. For this purpose four aircraft sensors were designed and the interface instrumentation was developed. The results of the first year were used to provide design criteria for improved instrumentation.

A new system was implemented during the second year and sufficient data were collected to analyze the system performance and determine adequate correlation methods for air and ground data. During the second year the number of aircraft sensors was increased from four to eleven and new instrumentation was developed to correlate ten data windows of 164 μsec. Even though some continuous electric field and VHF radiation were recorded in a ground network and in the aircraft, instrumentation problems did not allow proper correlation of the results.

During the third and final year additional changes were incorporated which resulted in consistent sets of airborne and ground data which are being used to characterize the lightning threat to aircraft in flight. The final experiment consisted of the WC-130 instrumented with eleven sensors to measure the electric and magnetic fields and the current density external to the

2

Figure 1.   The WC-130 Aircraft

aircraft. The fields detected by these sensors were recorded continuously with 2 MHz response. In addition, digital data with 20 MHz frequency response were recorded in sample data windows of 164 μsec at a rate of about two per second. The ground network consisted of a set of four VHF stations located about 20 km apart and an electric field station. The data obtained from the multiple VHF stations were used to determine the location of the lightning channel and the data from the ground electric field station were used for ground-aircraft correlation. IRIG-B time code with one millisecond (msec) resolution recorded on the ground was transmitted to the aircraft to obtain correlated airborne and ground recordings. Ground and airborne data were obtained from discharges 1 to 30 km apart at heights of 1500, 5000, 8000, and 15000 feet. Data were also obtained in two direct strikes to the aircraft.

Even though a large amount of fine structure data recorded on the ground during ground and cloud flashes[Refs 5, 13-17], very limited data [Refs 13 to 17] have been collected during actual aircraft flight. This report presents the first simultaneous measurement of electromagnetic fields produced by lightning on an aircraft and at the ground. Once the correlation between airborne and ground data is understood, it should be possible to directly relate ground data to the aircraft environment.

This report discusses all aspects of the data acquisition, data processing procedures, and data interpretation. The test environment and a detailed discussion of the airborne and air-

4

craft sensors and their interfaces are presented. Even though the aircraft sensors have been used in ground-based electromagnetic pulse (EMP) and lightning tests, the application of these sensors in an airborne lightning test environment has not been fully described. Block diagrams are shown for all the experiments. The full description of the the ground and airborne instrumentation given in Section II is needed to understand the limitations of the data being reported. Section III presents the technique used for processing and describes how the raw data recorded by the analog and digital recorders are processed to obtain the displays presented in this report. Sections IV and V contain the most important part of the report, data interpretation. The first part of the data display and interpretation consists of near and far field data which are shown in Section IV. In many cases correlated ground and airborne records are shown. A discussion of the risetime and frequency content is given for the near and far field data. Two direct lightning attachments are discussed in Section V. Section VI provides conclusions based on our experiments and recommendations for designing a more ideal experiment to collect this type of data.

SECTION II

DATA ACQUISITION

The intent of the instrumentation described herein was to employ digital and analog data acquisition equipment to obtain inflight lightning data. A ground station network was designed to relate the inflight electromagnetic energy coupled during the different phases of ground and cloud flashes with ground data. Most of the aircraft flights were in the vicinity of the ground station sites at a nominal altitude of 4 km mean sea level (MSL). The aircraft was restricted from penetrations into developed storm cells, so most of the inflight data reported here were obtained from 5 to 30 km from the lightning channel.

The electromagnetic radiation produced by the lightning current spans the frequency spectrum from near DC to the Gigahertz (GHz) range (Ref 18). The amplitude of this radiation is frequency dependent. As the frequency increases from 10 kHz to about 100 MHz, the amplitude of the electric field decreases and the number of radiation pulses increases (Refs 19 and 20). Radiation from return strokes, which is predominant at VLF, decreases inversely with frequency from 10 kHz to 2 MHz and inversely with the square of the frequency beyond 2 MHz (Ref 21).

To determine the frequency range over which the WC-130 aircraft will have the highest coupling, the lightning spectrum and the dimensions of the aircraft must be considered. Previous tests performed in the NASA Learjet aircraft (Ref 15) indicated

that maximum coupling to the aircraft occurs at a frequency which is determined by the nose-to-tail and wing-to-wing dimensions. Figure 2 shows the WC-130 aircraft dimensions. The 97.75 ft from nose-to-tail and 132.6 ft from wing-to-wing correspond to frequencies of 10.1 and 7.4 MHz, respectively. These frequencies are usually referred to as the fundamental aircraft resonant frequencies. It is expected that these frequencies and those corresponding both to twice and to one half of the fundamental wavelength will couple the most energy into the aircraft. To include the resonant frequencies, it was decided to measure the electromagnetic energy coupled to the aircraft with instrumentation having a frequency response of at least 20 MHz.

1. GROUND AND AIRBORNE DATA

Previously, it was determined that the electromagnetic energy must be recorded with an upper frequency response of at least 20 MHz. In addition, since ground data are usually recorded from DC to 2 MHz (Refs 6 to 12), and both sets of data must be correlated, an overall frequency range from near DC to 20 MHz was chosen for the airborne instrumentation. Since the effects on aircraft circuits should be related to the skin currents resulting from nearby and direct strikes, the parameters measured should include induced and conducted skin currents and radiated electric and magnetic fields. Consequently, the aircraft instrumentation included sensors for measuring all these parameters.

To determine the three dimensional structure of the lightning channels which are radiating the electromagnetic energy,

7

29 FT. 1 IN.

97 FT. 9 IN.

52 FT. 8 IN.

132 FT. 7 IN.
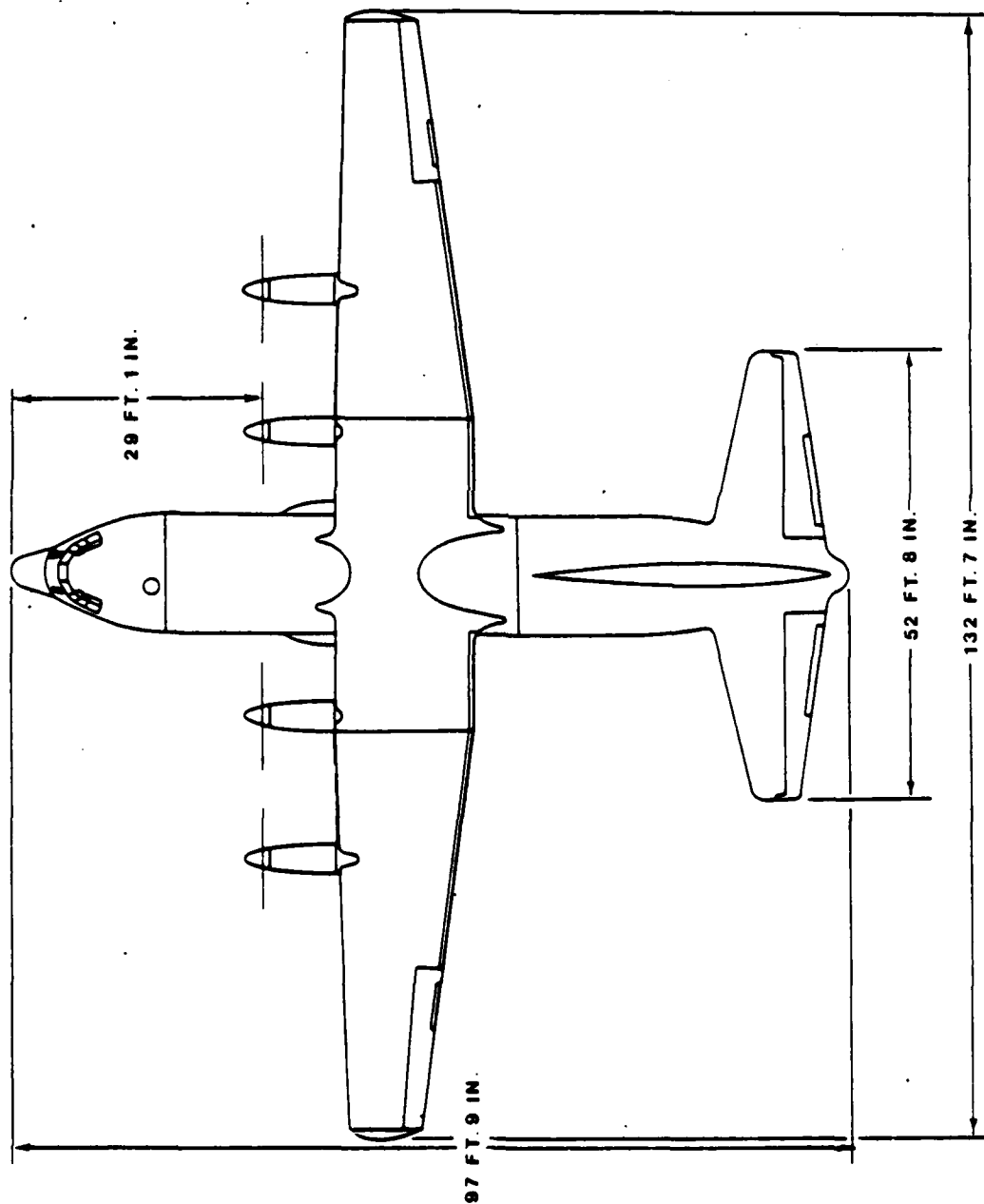
Figure 2. WC-130 Aircraft Dimensions

8

four VHF stations were installed about 30 km apart. These stations recorded the VHF radiation whenever the aircraft flew in the neighborhood of a thunderstorm within 25 km of the central site of the ground network. All these ground and airborne measurements are needed to provide proper identification of the events in a lightning discharge which produce the most severe threat to the aircraft.

2. TEST ENVIRONMENT

Figure 3 shows a conceptual view of the test environment. The ground and airborne data are correlatd by a timing code (IRIG B) transmitted from the central ground station for recording in the aircraft and at the remote ground stations. Electric field and VHF radiation were recorded at the Cowpens site. Only VHF radiation was recorded at the remote sites. The aircraft was equipped with various sensors.

3. AIRCRAFT SENSORS

Three basic types of sensors were used on the aircraft during the three-year program: electric field sensors, magnetic field sensors, and current density sensors (Refs 22-24). For each sensor, the proper circuit configuration was used to determine a calibration constant relating the electric field, magnetic field, and current density to the recorded voltage. Even though some variations of the basic sensor design have been used over the last three years, only the basic sensor type is discussed for the three electromagnetic readings. The principles of operation

WC-130
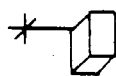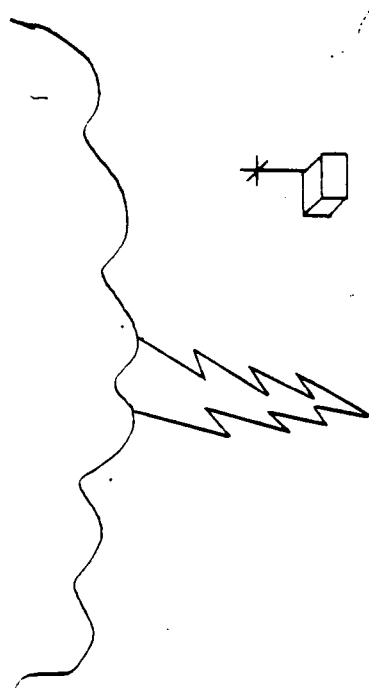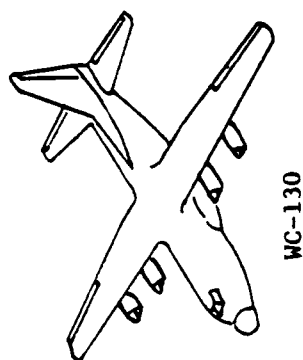
Airglades Site

Cal. Pulse

Time Code

Wilson Ward Site
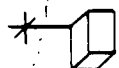
Cowpens Site

Devil's
Garden Site
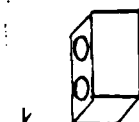
Instrumentation
Van & E-Field
System
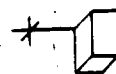
Keri Site

Vertical &
Horizontal Sync. Pulses

WINK TV
Fort Myers
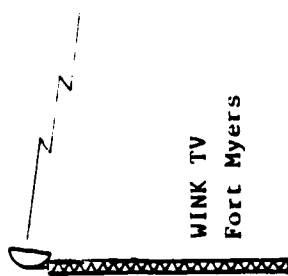
Figure 3. Conceptual View of Test Environment

of the sensors are based on Maxwell's equations.

a.   Electric Field Sensor

A dipole sensor was used to measure the vertical compo-
nent of the incident electric field. Figure 4a shows the basic
configuration. The electric field perpendicular to the plates
induces a voltage between the plates. Figure 4b shows all the
basic circuit elements in the sensor. C and G represent the
capacitance and conductance, respectively, between the parallel
plates. The stray capacitance, C_s at the sensor output and the
line resistance, R, are also considered in the electric field
sensor equivalent circuit in Figure 4b.   The sensor output is
matched to a 50 ohm line. In air, the conductivity between
plates will be about 10^{16} siemens/centimeter and a typical value
for C is about 1 picofarad (pFd). Therefore, G can be neglected
over the entire frequency range. In addition, the line
resistance R is negligible with respect to the load. Figure 4c
shows the remaining elements. The sensor current can be deter-
mined using the Norton equivalent circuit in Figure 4d and the
equation

$$I_{in}(\omega) = V_{in}(\omega) \; j\omega C = j\omega C \; d \; E(\omega) \qquad (1)$$

where $E(\omega)$ is the electric field sensed between the plates and d
is their separation.   But since the capacitance between the
plates is

$$C = \epsilon_o A/d \qquad (2)$$

11
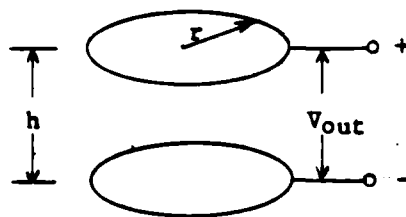
a. Parallel Plate Dipole
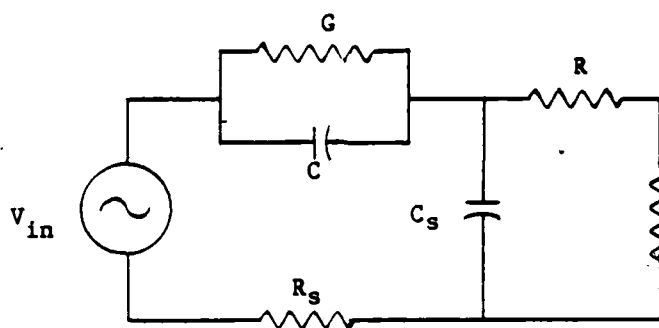
b. Electric Field Equivalent Circuit
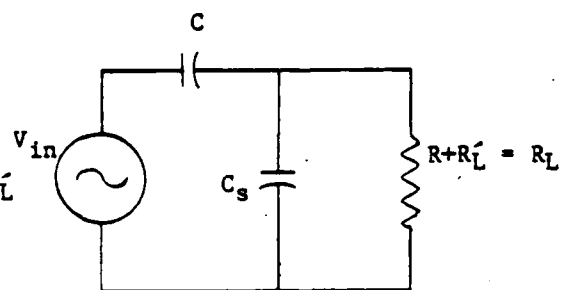
c. First Approximation
   Equivalent Circuit
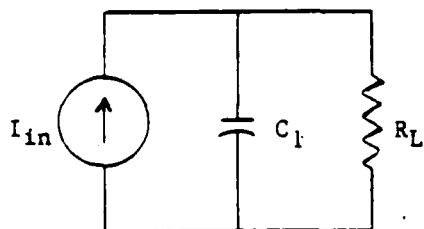
d. Simplified Current Equivalent
   Circuit
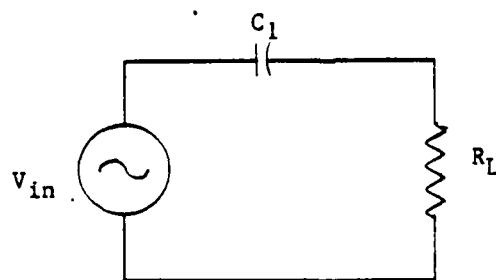
e. Simplified Voltage
   Equivalent Circuit

Figure 4. Electric Field Sensor and Equivalent Circuits

where A is the plate area, substituting (2) in (1) we get

$$I_{in}(\omega) = j \omega \epsilon_o A \, E(\omega). \tag{3}$$

Defining $C_1 = C + C_s$, the equivalent circuit in $\qquad$ (4) Figure 4e is obtained. Therefore,

$$V_{in}(\omega) = I_{in}(\omega)/j\omega C_1 = (\epsilon_o A/C_1) \, E(\omega) = d_1 E(\omega) \tag{5}$$

where, as expected, the input voltage between the plates is proportional to the electric field and d_1 is the equivalent plate separation (.101 m). The equivalent sensor capacitance C_1 was calculated to be 7.1 pFd (Ref 25).

From Figure 4e the output voltage V_{out} can be calculated as:

$$V_{out}(\omega) = [R_L/(R_L+1/j\omega C_1)]V_{in}(\omega) = [j\omega R_L C_1/(1+j\omega R_L C_1)]V_{in}(\omega)$$
$$= [j\omega R_L \epsilon_o A/(1+j\omega R_L C_1)] \, E(\omega) \tag{6}$$

Two extreme cases can be observed from equation (6). First, for $\omega \ll 1/R_L C_1$ then

$$V_{out}(\omega) = j\omega \quad R_L \epsilon_o A \, E(\omega) \tag{7}$$

which implies that the measured voltage is proportional to the derivative of the electric field. Second, for $\omega \gg 1/R_L C_1$ then

$$V_{out}(\omega) = (\epsilon_o A/C_1) \, E(\omega) = d_1 E(\omega) \tag{8}$$

where the measured voltage is proportional to the electric field.

Since R_L = 50 ohms (ω) and C_1 = 7.1 pFd, then $1/2\pi\ R_L C_1$ = 447 MHz, and over the frequencies of interest $\omega \ll 1/R_L C_1$ the output voltage is always proportional to the derivative of the electric field.

In the time domain,

$$V_{out}(t) = \epsilon_o A\ R_L\ \frac{dE(t)}{dt} = K_E\ \frac{dE(t)}{dt} \qquad (9)$$

where K_E is the electric field sensor calibration constant. For $A = 0.1\ m^2$, $K_E = 4.425 \times 10^{-11}$ m-sec.

The sensor was calibrated using a $50\,\Omega$ parallel plate transmission line. A continuous wave test was performed using a sinusoidal excitation input over the frequency range from 0.1 to 20 MHz. The theoretical value of K_E and the experimental value determined from the tests were within 10%.

The frequency response of the sensor is linear from near DC to almost 20 MHz. However, the sensor output is extremely low at low frequencies and the practical lower frequency limit is determined by the dynamic range of the data link. The dynamic range of the data link is limited at the low end by the noise level of the light emitting diode (LED) and its electronics and by the transmission medium. By laboratory testing, it was determined that the lowest sinusoidal amplitude that could be detected was about 50 microvolts (μV). A simplified analysis was performed to estimate the practical low frequency response of the electric field data channel. For analysis purposes, the radiated electric field was assumed to have a double exponential waveform, i.e.,

$$E(t) = E(e^{-\alpha t} - e^{-\beta t}) \qquad (10)$$

14

From equation (9) and the derivative of equation (10) we get:

$$V_{out}(t) = k_E E(\beta e^{-\beta t} - \alpha e^{-\alpha t}) \qquad (11)$$

The frequency domain response can be obtained by the Laplace Transform of equation (11) which gives:

$$V_{out}(s) = \frac{K_E E \ s \ (\beta - \alpha)}{(s+\alpha) \ (S+\beta)} \qquad (12)$$

Since $s = j\omega$:

$$V_{out}(j\omega) = \frac{j\omega K_E E(\beta - \alpha)}{(\alpha + J\omega)(\beta + J\omega)} \qquad (13)$$

The Magnitude of (13) is

$$V_{out}(\omega) = \frac{K_E E(\beta - \alpha) \ \omega^{\frac{1}{2}}}{(\alpha^2 + \omega^2)^{\frac{1}{2}}(\beta^2 + \omega^2)^{\frac{1}{2}}} \qquad (14)$$

Since the output of the sensor is the summation of the inputs at all frequencies within its bandwidth:

$$V_{out}(t) = \int_0^{20 \ MHz} V_{out}(j\omega)e^{j\omega t} \ df \qquad (15)$$

Equations (14) and (15) were used for radiated electric field peak amplitudes of 20 volts/meter (V/m) and 10 kilovolts/meter (kV/m), a sensor calibration constant of 4.425×10^{-11} and α and β constants of 1.4×10^4 and 7×10^7 radians/second, respectively, to produce a double exponential with an approximate risetime (10%-90% of peak) of 100 nsec. The results from equation (15) indicate that all the frequency components must be used to yield a voltage level above the noise threshold of the data channel for an electric field of 20 V/m. For an electric field

of 10 kV/m, the corresponding value is about 500 Hz. However, the practical low frequency response of the E-field sensor when the derivative value was recorded was about 1 kHz. The 20 V/m and 10 kV/m electric field values correspond to distances from the source of 30 km and 0.5 km (Ref 7), respectively.

b. Magnetic Field Sensor

The magnetic field sensor consisted of a one turn cylindrical Moebius loop (Ref 25) with a frequency response higher than 20 MHz. The sensor diameter was 0.124 m and the loop was constructed with semirigid coaxial cable to yield an equivalent area, A, of 0.02 m^2. The sensor was installed with the bottom of the loop about eight inches above the aircraft skin. Figure 5a shows the basic configuration. From Faraday's Law, it is known that a variation in the flux produces an induced voltage. Figures 5b and c show the sensor voltage and current equivalent circuits. R_s is the resistance in the turns of the wire, R_L is the load resistance, and L is the sensor inductance derived from Faraday's Law. The effect of R_s can be neglected by choosing it much smaller than R_L. Since the input voltage is proportional to the derivative of the magnetic field density times the sensor area, the output voltage across R_L will be

$$V_{out}(\omega) = j\omega B(\omega)A\frac{R_L}{R_L + j\omega L} \tag{16}$$

For

$$\omega << \frac{R_L}{L} \qquad V_{out}(\omega) = j\omega AB(\omega) \tag{16a}$$
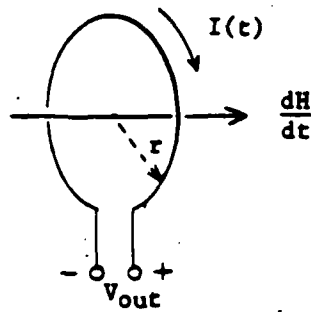
a. Inductive Loop
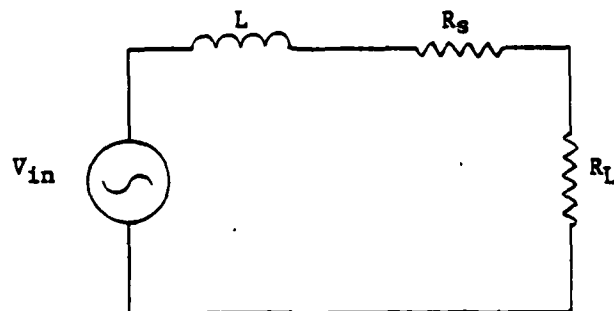
b. Simplified Voltage Equivalent
Circuit
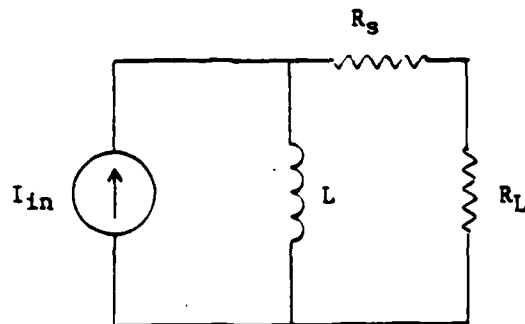
c. Simplified Current Equivalent
Circuits

Figure 5. Magnetic Field Sensor and Equivalent
Circuits

and the sensor voltage is proportional to the derivative of the magnetic field density. For $\omega >> \frac{R_L}{L}$

$$V_{out}(\omega) = \frac{AR_L}{L} B(\omega) \qquad (17)$$

and the sensor voltage is proportional to the magnetic field. For the magnetic field sensors used, the measured value of L was 0.9 micro Henries (μh) and R_L was 100Ω. Therefore, $\frac{R_L}{2\pi L} = 17.7$ MHz and the voltage reading was always proportional to the derivative of the magnetic field. In the time domain

$$V_{out}(t) = A_{eq} \frac{d}{dt} B(t) = K_B \frac{d}{dt} B(t) \qquad (18)$$

The value of $K_B = A_{eq} = .02$ m^2 was verified with the parallel plate transmission line using the continuous wave test. The theoretical and experimental values agreed within 5%.

The low end frequency response of the magnetic field channel was estimated in the same manner as was that of the electric field data channel. Using 0.6 and 0.01 A/m for the magnitudes of the magnetic field at 1 and 30 km, respectively, the low end frequency responses were estimated to be 20 kHz and 500 Hz, respectively.

c. Skin Current Sensor

The skin current sensors operate on the same principle as the magnetic field sensors. From Ampere's Law it is known that

$$\oint H \cdot dl = \int_s J_s \cdot ds + \frac{\partial}{\partial t} \int_s D \cdot ds. \tag{19}$$

But the magnetic flux incident on the sensor will be due to the conduction current J because the induction term is negligible for no apertures. Applying boundary conditions for a conductor, H must be equal to J_s, so that:

$$B/\mu_0 = J_s \tag{20}$$

Using (18) and (20) the output voltage of the sensor can be expressed as:

$$V_{out} = A\mu_0 \frac{dJ_s}{dt} \tag{21}$$

Equation (21) is valid for good conductors with negligible skin depth over the frequencies of interest (mainly between 0.1 and 20 MHz).

The skin current sensor consisted of the same type of loop as used for magnetic field measurements except that the bottom of the loop was at the skin surface. The sensors were calibrated in the parallel plate transmission line using the same technique as for the magnetic field sensors.

4. OVERALL AIRCRAFT INSTRUMENTATION

The number of sensors used in the aircraft was increased from four in 1979 to 11 in 1980 and 1981. To accommodate this increase, the aircraft instrumentation was appropriately updated. Additional changes in the data recording capabilities were introduced in 1981. To fully understand the recorded data, the time and frequency domain characteristics of the equipment used must be known. Therefore, the descriptions of the airborne instrumen-

19

tation are separated for the three years.

a. 1979 Airborne Instrumentation

One electric (Ḋ), one magnetic (Ḃ), and two skin current sensors, (J̇), were used in 1979. Figure 6 shows the relative locations of the sensors on the aircraft. Table 1 summarizes the sensor identification and specifications. All the sensors were prototypes built at the Air Force Wright Aeronautical Laboratory.

Figure 7 shows a block diagram of the aircraft instrumentation. The sensor outputs were connected to a transmitter unit via a 100 Ω twinax cable. The transmitter unit consisted of an amplifier and optical modulator module. The transmitter output was sent to a receiver unit via a fiber optic cable. The receiver unit consisted of an optical demodulator module and an amplifier whose output was buffered before being recorded on magnetic tape. The data to be digitized was taken through an anti-aliasing filter to limit its bandwidth and then digitized by a transient recorder which permitted temporary storage, display on a CRT and/or permanent storage on magnetic floppy disk via a digital processor.

Table 2 summarizes the mechanical and electrical characteristics of the fiber optic components. The data link consisted of a Meret Inc. Model 27802 Transmitter Receiver system with type DR fiber optic cable assembled by Meret Inc.

The analog recorder was an Ampex Model AR-700 14 channel recorder with a frequency response from 300 Hz to 300 kHz (Ref 5). In addition to the four data channels, two other channels were used to record a 1 kHz reference signal and an IRIG B time
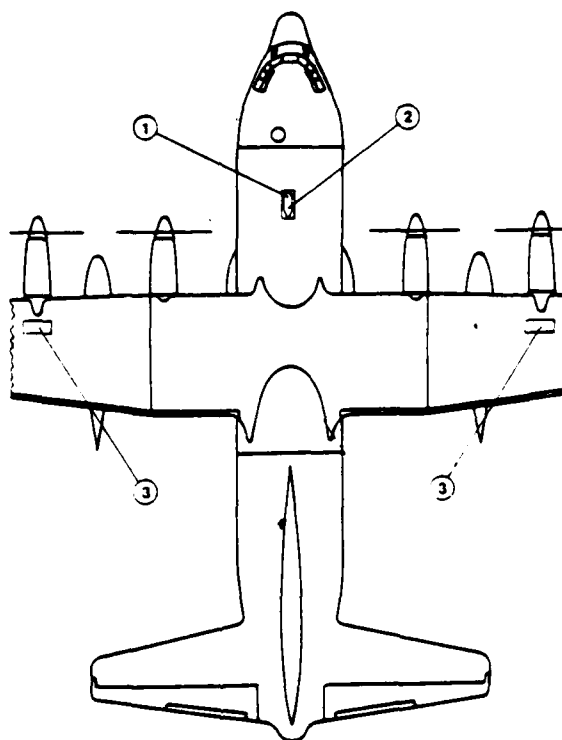
1. E-Dot   3. J-Dot
2. B-Dot

Figure 6. FY79 Sensor Locations

TABLE 1

FY 79 SENSOR IDENTIFICATION AND SPECIFICATIONS

Type Sensor	Description	A (m^2)	t_r(nsec) 10%-90%	3dB(MHz) Bandwidth	Dynamic Range of Data Channel*	Location
B	Prototype 4-turn cylindrical loop	0.051	18	19	3.5×10^{-5} to 3.5×10^{-2} A/m or 3.5×10^{-6} to 3.5×10^{-3} A/m	Upper fuselage centerline, forward of wing
D	Prototype Parallel plate with ground plane	0.032	10	35	20 V/m to 20 KV/m or 2 V/m to 2 KV/m	Upper fuselage centerline, forward of wing
J	Prototype 2-turn shielded	0.016	22	16	1.5×10^{-4} to 0.15 A/m or 1.5×10^{-4} to 1.5×10^{-2} A/m	Upper right outer wing on out board engine dry bay access panel
J	Prototype 2-turn shielded	0.016	22	16	1.5×10^{-4} to 0.15 A/m or 1.5×10^{-4} to 1.5×10^{-2} A/m	Upper left outer wing on out board engine dry bay access panel

*Dynamic range was switch selectable by changing amplifier gain from 10 to 100.
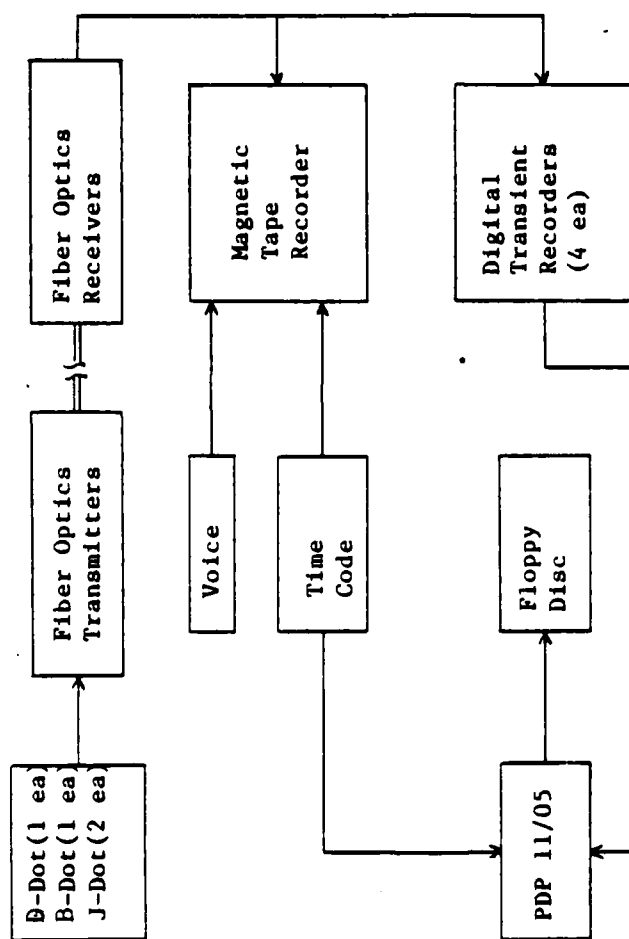
Figure 7. FY79 Airborne Instrumentation Block Diagram

TABLE 2

FIBER OPTICS SYSTEM CHARACTERISTICS

a. Mechanical

No. of fibers, approx.	19
Individual fiber diam.	85 microns
Core diameter	68 microns
Bundle diameter	0.43 mm
Numerical aperture	0.48
Est. insertion loss	13 dB
Optical attenuation at 800 to 900 nm	80 dB/Km
Jacket Material	Kevlar & Teflon
Usable temp. range	-55° to 150° C
Weight	14 gm/m
Minimum bend radius	19 mm
Outside diameter	3.81 mm
Max. recommended tensile loads	50 Kg
Ferrule part no.	97012

b. Electrical

Electrical bandwidth	DC to 25 MHz
Dynamic range	60 dB
Max. input, pk-pk	3 V
Min. input, pk-pk	3 mV
System linearity	1%
Second harmonic, max.	-40 dB
Output signal range for 3 V pk-pk	0.5 V
for 3 mV pk-pk	0.5 mV
System transfer ratio	-7.8 dB
Output noise pk-pk, DC-20 MHz	0.5 mV
RMS	0.1 mV
Input impedance, 10 MHz	1 Megohm
Input offset	0 V
Output impedance	<20 ohms
Output offset	1.6 V
Max. output DC current	5 mA
Power supply Transmitter	+6V @ 150 mA, +12 @ 2 mA
Receiver	-40v @ 0.1 mA

code.

The anti-aliasing filters were manufactured by Metropole Products Inc. Four manually selected (short coaxial cable jumpers) filters were provided for each of the four data channels. A particular filter (2,4,10 or 20 MHz) was chosen depending on the sweep rates selected on the transient recorders.

The digitizing recorders were four Biomation Model 8100's operated as single channel recorders. These units have 8 bit resolution and 2 K storage capacity. The analog outputs of the four recorders were displayed in pairs on two Tektronix Model 603 display monitors by using two Biomation Model 355 multiplexers. The recorder digital outputs were interfaced to a Digital Equipment Corporation PDP 11/05 processor by means of a DR-11 interface. Computer programs were written to store the data on a magnetic floppy disk.

b. 1980 Airborne Instrumentation

Table 3 summarizes the characteristics of the eleven sensors used in 1980. All sensors were manufactured by the EG&G Company in Albuquerque, New Mexico, and were designed to sense either electric or magnetic fields. Skin currents were also measured by properly scaling the output of the magnetic field sensor. There were two types of sensors used to measure the electric field, a Hollow Spherical Dipole (HSD), and a Flush Plate Dipole (FPD). The HSD was mounted on the curved conducting surface of the upper fuselage centerline (aft of wing). Using the EG&G designation, the HSD sensor will be referred to as the Q sensor. Three FPD sensors were mounted on the aircraft, one on the upper forward fuselage, one on the left wing tip, and one

TABLE 3

1980 SENSOR IDENTIFICATION AND SPECIFICATIONS

Sensor Type	Model No.	Equiv. Area A (m^2)	Rise time (nsec) t_r 10-90%	Bandwidth 3dB (MHz)	Dynamic Range	Location
Q	HSD-S1A(R)	0.1	7.4	45	0.2 V/m to 2 KV/m	Upper fuselage centerline (aft of wing)
B	CML-S7A(R)	0.02	9	38	4×10^{-4} to 4 A/m	Upper fuselage centerline (forward of wing)
B	CML-S7A(R)	0.02	9	38	4×10^{-4} to 4 A/m	Upper fuselage centerline (forward of wing)
J	CML-S7A(R)	0.02	9	38	0.4 to 400 A/m	Upper fuselage centerline (aft of wing)
J	CML-S7A(R)	0.02	9	38	0.4 to 400 A/m	Lower left outer wing at fuel pump access panel
J	CML-S7A(R)	0.02	9	38	0.4 to 400 A/m	Upper left outer wing on outboard engine dry bay access panel
J	CML-S7A(R)	0.02	9	38	0.4 to 400 A/m	Lower right outer wing at fuel pump access panel
J	CML-S7A(R)	0.02	9	38	0.4 to 400 A/m	Upper right outer wing on outboard engine dry bay access panel
D	FPD-2A(R)	0.02	5	70	113 V/m to 113KV/m	Upper forward fuselage centerline
D	FPD-2A(R)	0.02	5	70	113 V/m to 113KV/m	Lower aft empennage
D	FPD-2B(R)	0.02	5	70	113 V/m to 113KV/m	Upper left wing tip

26

wing tip, and one below the aircraft tail. The FPD sensor
mounted on the left wing tip was built to adapt to the curvature
of the wing tip. Because of their location on the aircraft struc-
ture, the sensors at the wing tip and below the tail were not
exactly parallel to the ground and the detected electric field
should be multiplied by approximately 1.02 to obtain the vertical
component of the electric field. These FPD sensors will be
referred to as $\dot{D}$ sensors to follow EG&G designation. The
remaining sensors consist of a Cylindrical Moebius Loop (CML).
The CML sensors used to measure the B-field are scaled according
to equation (18), whereas the CML sensors used to measure the
skin currents are scaled by using equation (21). The CML sensors
are referred to as B-Dot ($\dot{B}$) if scaled to measure the B-field and
J-Dot ($\dot{J}$) if scaled to measure the skin current. Figure 8 shows
the relative locations of these sensors on the aircraft. These
locations were chosen to minimize the effect of the aircraft on
the sensor inputs. Figure 9 is a photographic view of the three
types of sensors shown in Figure 8. Figure 9a shows the forward
upper fuselage (FUF) sensors. The D-Dot circular FPD sensor is
in the front and the B-Dot CML sensors are under the pod. Fig 9b
shows a view of the CML sensors under the pod. Fig 9c shows the
pod covering the rear upper fuselage while Fig 9d shows the J-Dot
and Q-Dot sensors under the pod. Finally, Fig 9e shows an iso-
lated J-Dot sensor in the left wing. The B-field sensors were
installed with their bottoms about 8 inches above the aircraft
skin while the J-Dot sensors were installed with their bottoms at
the aircraft skin surface.
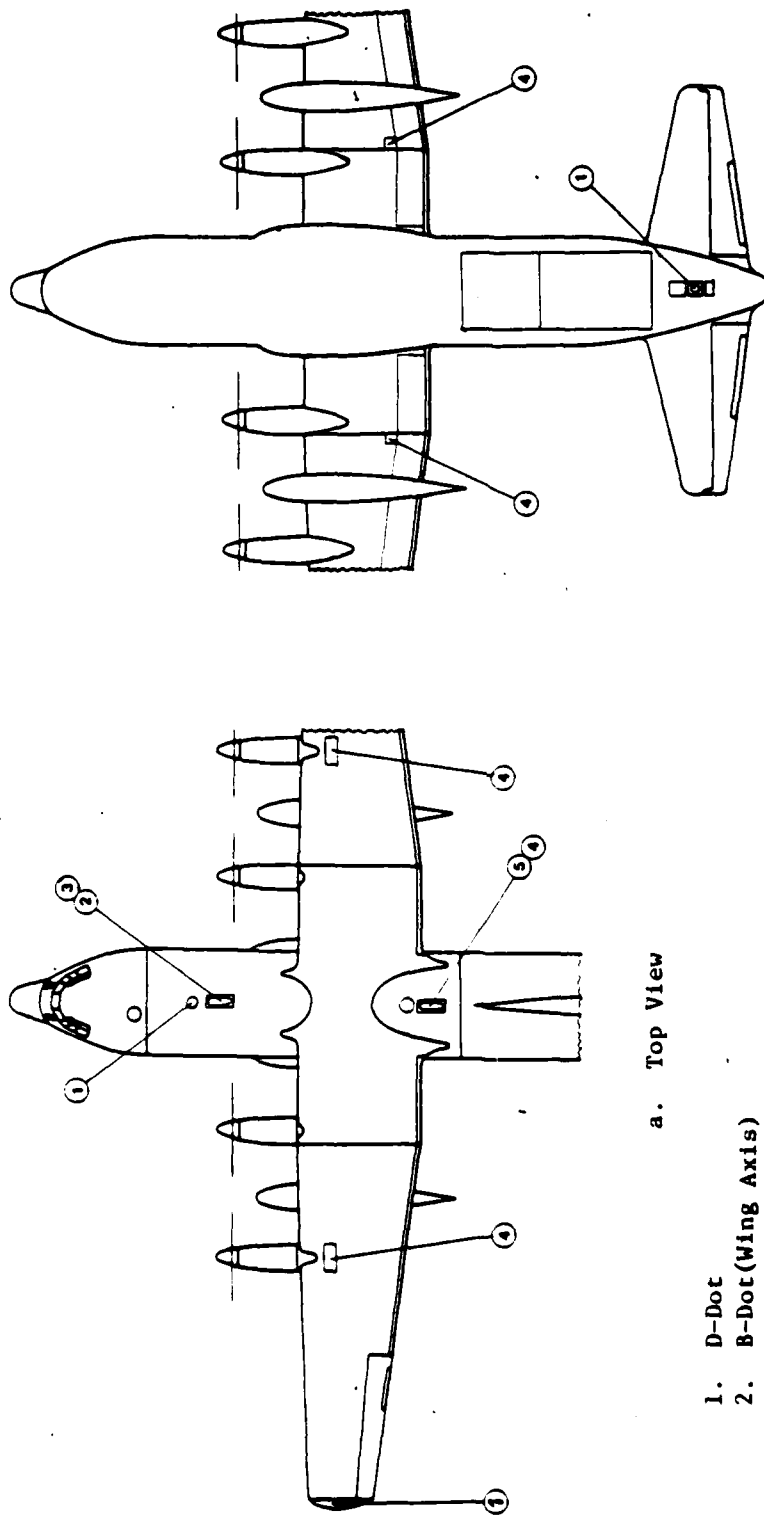
b. Bottom View

a. Top View

1. D-Dot
2. B-Dot(Wing Axis)
3. B-Dot(Fus. Axis)
4. J-Dot
5. Q-Dot

Figure 8.   FY80/81 Sensor Locations

23

a. Upper Fuselage D Sensor and Pod Covering B Sensors

b. B Sensors (Pod Removed)
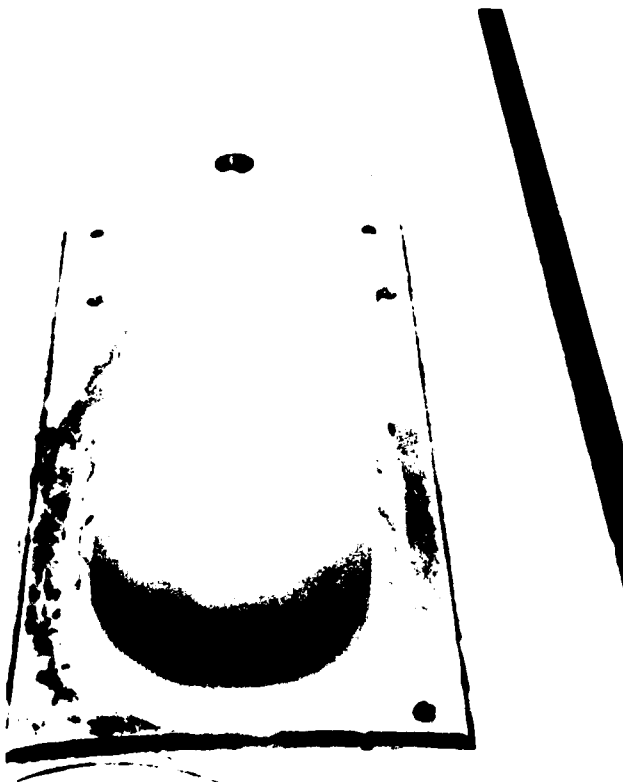
c. Pod Covering Rear Upper Fuselage Q and J Sensors

Figure 9. Aircraft Sensor Installations
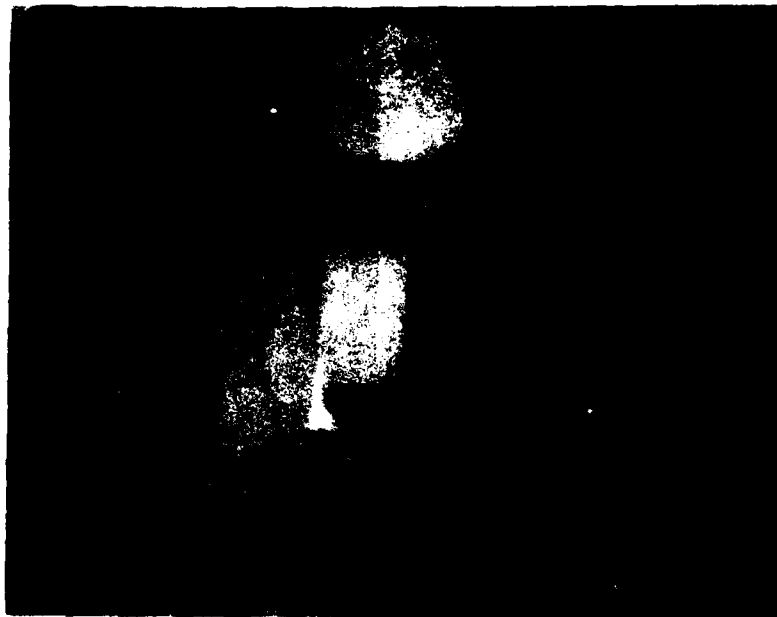
d. Q̇ and J̇ Sensors (Pod Removed)
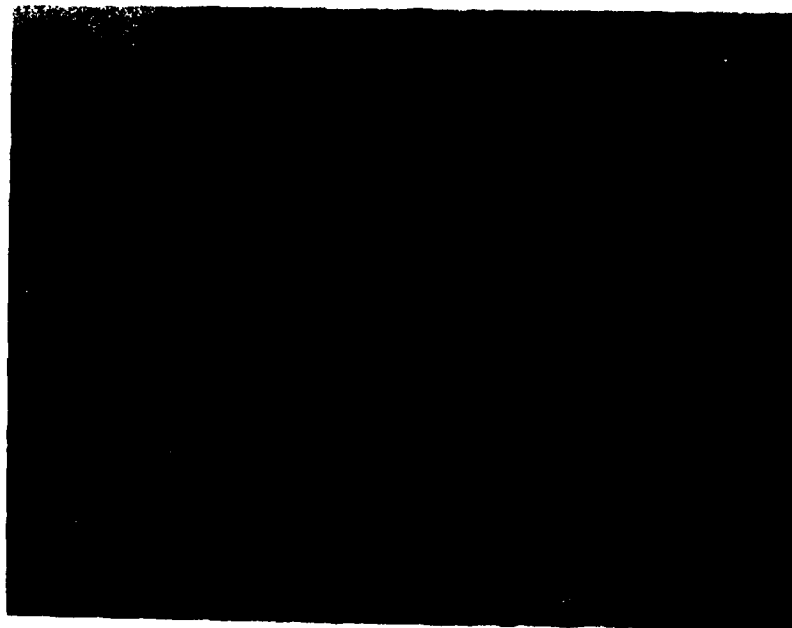
e. Upper Wing J̇ Sensor

Figure 9. Aircraft Sensor Installations (concluded)

Figure 10 shows a block diagram of the 1980 aircraft instrumentation. The following changes were made from the 1979 configuration:

a) The number of sensors was increased from four to eleven.

b) A single, ten channel digitizing transient recorder (DTR) with 8 bit resolution and 8 K storage capacity per channel replaced the four individual recorders.

c) A 28 channel analog recorder was used to increase bandwidth from 300 kHz to 2 MHz.

d) The digital record length was increased from the 40 sec obtained in the Biomation 8100 to 164 µsec at the same sample rate of 20 nsec.

e) Logarithmic amplifiers were used at the output of the sensors to increase the input dynamic range to 80 dB.

f) Digital data were encoded and recorded directly on magnetic tape instead of through the processor on floppy disks.

g) The rate of acquisition and storage of digital data was increased from four simultaneous displays of 40 µsec records approximately every 2 sec to ten simultaneous displays of 164 µsec records about every 400 msec.

h) The frequency response of the sensors and their interface was extended to at least 25 MHz.

i) The anti-aliasing filters were replaced with individual filters at frequencies of 5, 10, and 20 MHz which were mounted at the fiber optics receivers.

The ten channel digitizing transient recorder (DTR) model 7901 was developed by Micro Pro Inc. specifically for this appli-

31
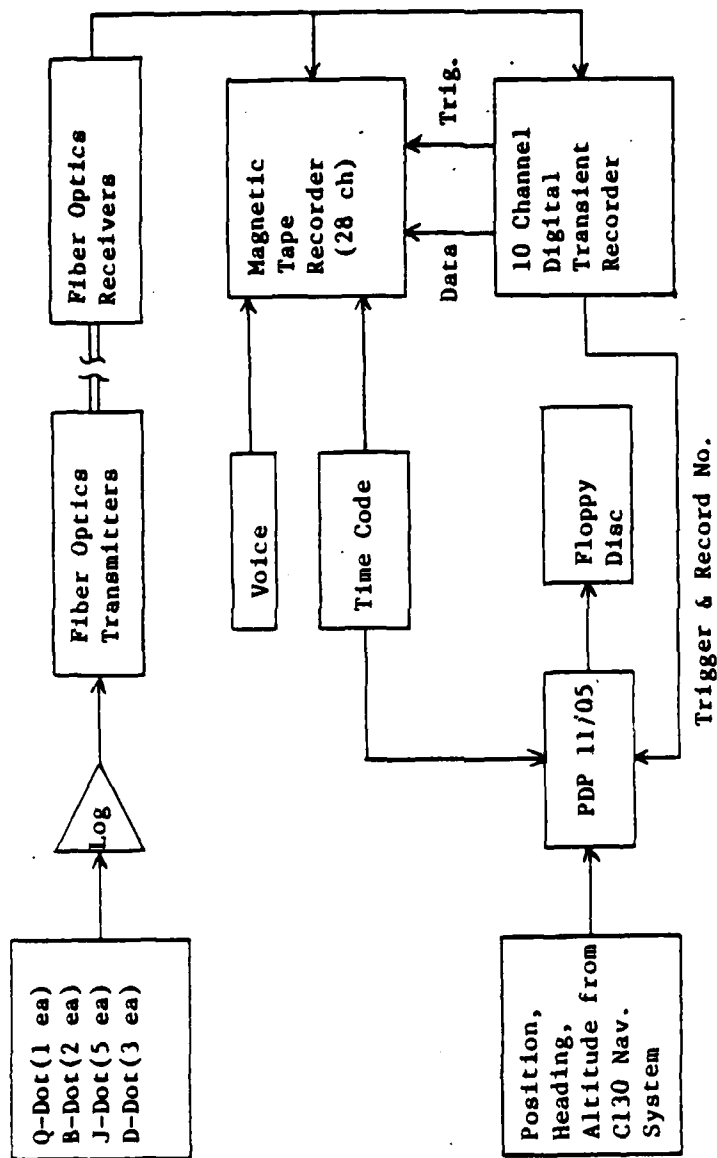
Figure 10. FY80 Airborne Instrumentation Block Diagram.

cation. This unit digitizes a data window of the incoming analog data and stores it. Upon external command (by the operator or the PDP 11/05 processor), the unit encodes the digital data using a Manchester phase modulated code and outputs the data for recording on magnetic tape. The digital data can also be stored on floppy disks. However, this method is not used during data acquisition because of the limited capacity of the disks and the longer time needed to store data as compared to dumping onto tape. For processing, a ten channel decoder is used to convert the data stored on magnetic tape back to digital format.

In addition to the sensor data, the aircraft position, heading, and altitude were stored on magnetic disk via the PDP 11/05 processor. A pulse unit and an antenna were installed for communication with the ground sites.

c. 1981 Airborne Instrumentation

Figure 11 shows the instrumentation used in 1981. The D-Dot FUF sensor output was integrated near the antenna and transmitter. This hardware integration was required to extend the low frequency response to near DC. The $\dot{D}$ output of the fiber optic receiver was stored in two FM channels with different gains. Since the frequency response of this channel was from DC to 500 kHz, these data were used to establish correlation between the ground and airborne electric field readings. Results of this correlation for a number of lightning flashes are given in this report. The Q-Dot, B-Dot and the remaining D-Dot sensor outputs were transmitted with fiber optic cables and recorded in two different forms. One output was left in derivative form, logged,

33
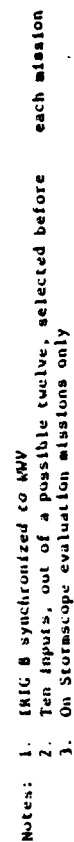
Figure 11. Airborne Instrumentation Block Diagram

Notes:
1. IRIG B synchronized to KMV
2. Ten inputs, out of a possible twelve, selected before each mission
3. On Stormscope evaluation missions only

34

stored in the DTR, and transferred to magnetic tape. The other output was integrated and could be recorded in analog form on direct record channels of the instrumentation recorder. Because of noise problems, the outputs from the fiber optic receiver for the latter signals could only be integrated down to 3 KHz.

Once the aircraft was instrumented as shown in Figure 11, the electric and magnetic field sensors were calibrated. Figure 12 shows the parallel plate calibration for the FPD sensors in the forward upper fuselage. In the illustrated technique, a rectangular pulse with known magnitude, risetime and falltime was incident at the parallel plate and the response at the recorder input was measured with an oscilloscope. Using this technique, the value of K_E in equation (9) and the frequency response of the sensors were determined.

The overall dynamic range of the integrated output from the electric and magnetic fields was designed for lightning flashes from 0.5 km to 30 km. In case of a direct strike, however, the output from the FPD sensor on the left wing tip was set for a maximum electric field of 320,000 V/m (change made July 21st) and the $\dot{J}$ sensors were always calibrated to measure skin currents on the order of kiloamperes.

A Ryan Stormscope was mounted in the aircraft as part of a second program to evaluate its performance and was used to assist in determining the relative locations of atmospheric electrical activity. Figure 13 shows the Stormscope antenna which was located on the rear lower fuselage forward of the FPD D sensor. With the exception of the Stormscope display unit, all the air-

Figure 12. Parallel Plate Calibration for the FPD
            Sensor at the Forward Upper Fuselage
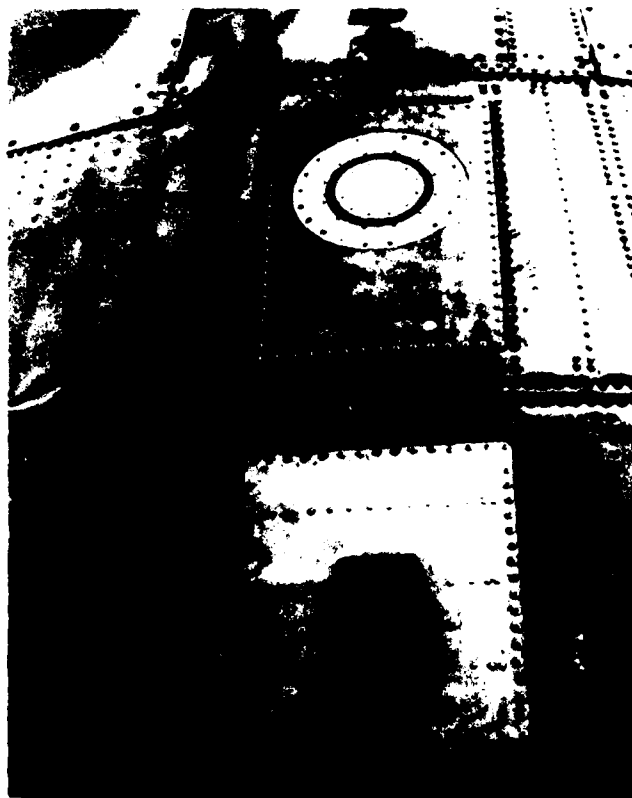
Figure 13. Rear Lower Fuselage View Showing the
Stormscope Antenna (Bottom Center)
and FPD Sensor (Upper Center).

craft instrumentation needed for operator interaction was located in one rack. Figure 14 shows a picture of that rack.

A periodic calibration pulse with controlled output amplitude, frequency, and repetition rate was built and mounted in the aircraft. This calibration was transmitted to the ground to correlate the airborne and ground events.

A new experiment was added in 1981. Internal wires were run along the trailing edge wing of the left wing box and within the fuselage nose-to-tail. Induced transients on these wires were measured and recorded on the magnetic tape recorder.

5. GROUND STATIONS

Correlated airborne and ground electric field readings were essential to compare the characteristics of the electric field readings recorded in the aircraft with those recorded on the ground. In addition, a ground VHF measuring network was designed to determine the location of the VHF sources produced by each flash (Refs 26-28).

Figure 15a shows the instrumentation van used to record the electric field and VHF radiation produced by lightning. This van was located at the Cowpens site shown in Figure 3. On top of the van were two electric field antennas, a VHF omnidirectional antenna, and a Stormscope antenna. A thunder microphone was located on the side of the van and a WWV antenna was placed in a small tower ne... the van. The electric field, VHF, thunder, and time code data were recorded continuously on strip charts and magnetic tape recorders. Figure 15b shows the main instrumenta-

Figure 14. Aircraft Instrumentation Rack

a. Instrumentation Van
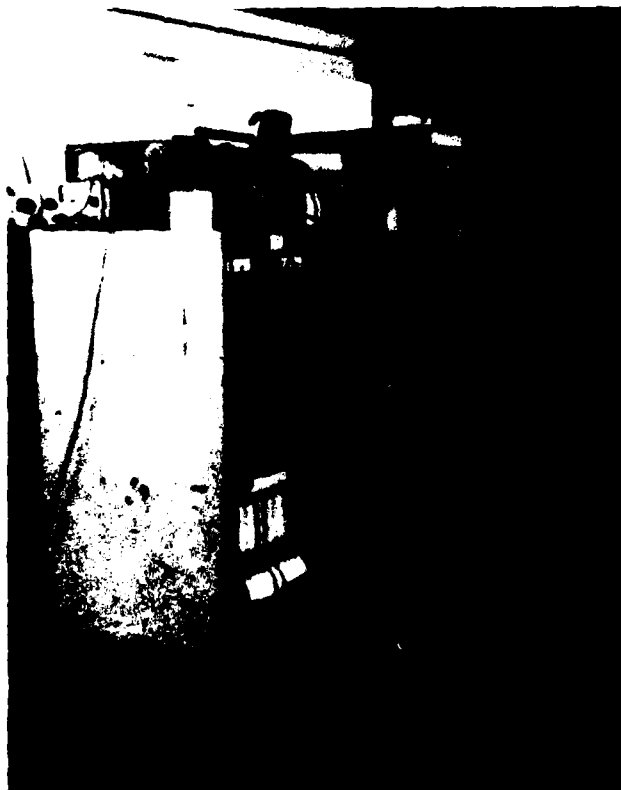
b. Instrumentation Rack
   inside Instrumentation Van

Figure 15.   Cowpens Site
             Ground Station

tion rack used in the van.

Figure 16 shows a block diagram of the electric field
system. The system was designed by Lightning, Location, and
Protection, Inc. (Ref 29) and consisted of two plates of 0.02 and
0.5 m^2 and two integrators and amplifier circuits. The voltages
at the four output terminals were recorded on direct and FM
channels of the instrumentation tape recorder with a frequency
response of 500 kHz for FM and 2 MHz for direct. The outputs
were also recorded on a strip chart. From the output voltage the
electric field is easily obtained from

$$E = \frac{C}{\epsilon_o S} V \qquad (20)$$

where E is the electric field, C the integrator capacitor, ϵ_o
is the permittivity of free space, S the area of the plate and V
the detected output voltage. Therefore, E = kV, where k is the
calibration constant for each one of the output terminals. The
IRIG B time code with 1 msec resolution was also recorded on the
instrumentation tape recorder and slow code was recorded on the
strip chart. The integrator outputs in Figure 16 were adjusted
manually to correct for drift.

To determine the position of the VHF sources a "difference
in the time arrival" hyperbolic system was instrumented. The
basic configuration and distance between the stations were simi-
lar to previous systems designed by Lennon (Ref 26) and Proctor
(Refs 28 and 30). The four VHF stations were located approxima-
tely 20 km apart as shown in Figure 17. The station at Devil's
Garden was used as a reference. A fifth station was located at
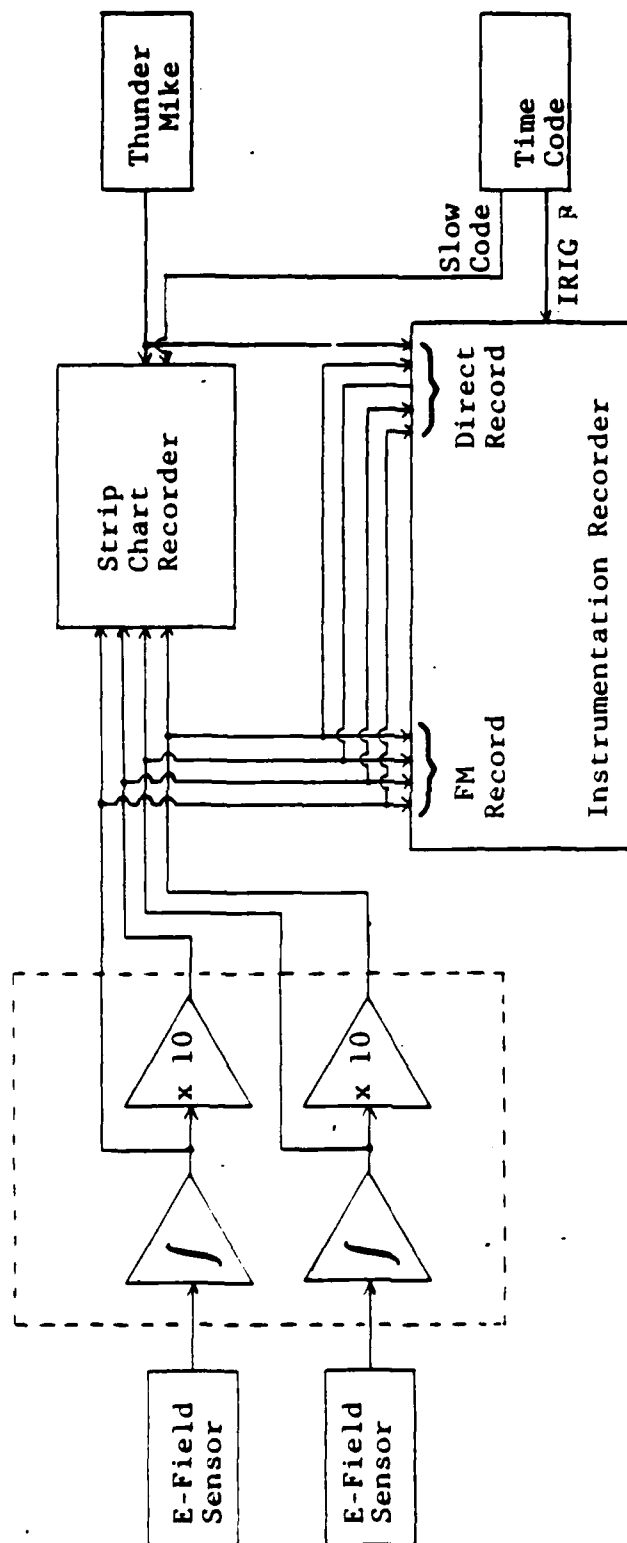
Figure 16. Block Diagram of Ground Station Electric
Field Recording System

North

West ——————————————————————————————— East

⊙ Airglades Airport
   (7.48,15.2)

Devil's Garden

(0.0,0.0)

⊙ Cowpens
   (0.54,-5.39)
   Site of E-Field Recorder and Van

⊙ KERI
   (-19.6,-0.5)

Range from Devil's Garden
Airglades   16.9
Cowpens   5.42
KERI   19.6
Wilson Ward   18.4

South

⊙ Wilson Ward (9.32,-15.9)
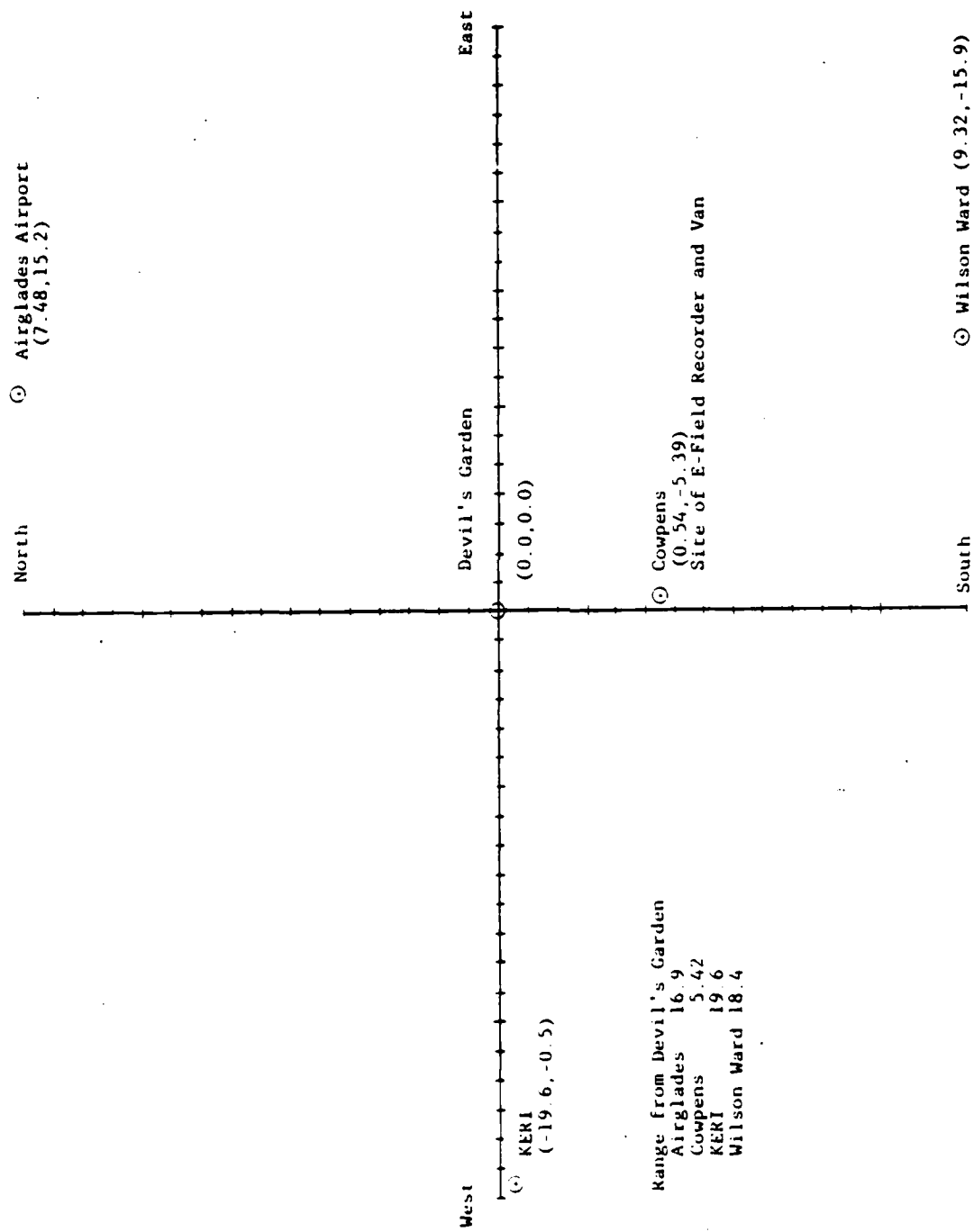
Figure 17.   VHF Ground Station Network
             (Coordinates & Distances in Kilometers)

Cowpens, site of the E-field recorder and mobile van. The VHF radiation at the Cowpens station was recorded in the analog magnetic recorder simultaneously with the electric field. The VHF radiation detected in omnidirectional antennas at all sites was processed through a 63 MHz bandpass filter with a bandwidth of 6 MHz, envelope detected, log amplified, and recorded in a modified RCA 201 Video Cassette Recorder.

Figure 18 shows a block diagram of the instrumentation used to detect the VHF radiation. To align the VHF radiation on the four sites, time correlation between the data traces must be established to about a tenth of a microsecond. Reference signals from a local TV station and time code were used to obtain the needed time correlation.

IRIG B time code with 1 msec resolution was received at the Cowpens station from WWV in Ft. Collins, Colorado. This signal was recorded in the analog tape recorder. In addition, the received time code signal was modulated at 138 MHz and transmitted to the other four stations and the aircraft. The detected signal at the four sites was recorded on the audio track of the video cassettes. The signal transmitted to the aircraft was used to synchronize an on-board clock to the same time code references as in the ground stations. The antenna needed to transmit the time code signal to the remote stations and the aircraft was also located on top of the tower. This last antenna was used for calibration purposes by transmitting a pulse at the Cowpens site and measuring the difference in the time of arrival at each of the remote sites. Figure 19a is a photographic view of the 100

44

Commercial
Broadcast
Vert. & Horiz.
Sync Pulses

Lightning VHF
& Cal. Pulses

On/Off
Signal

IRIG B
Time Code

TV RF Section Used to
Derive VSP's & HSP's

Modified
Video Video Tape
Recorder

Audio

Vert. & Horiz.
Sync Pulses

Data

63 MHz
Filter

Log

Playback

To Instrumentation
Recorder
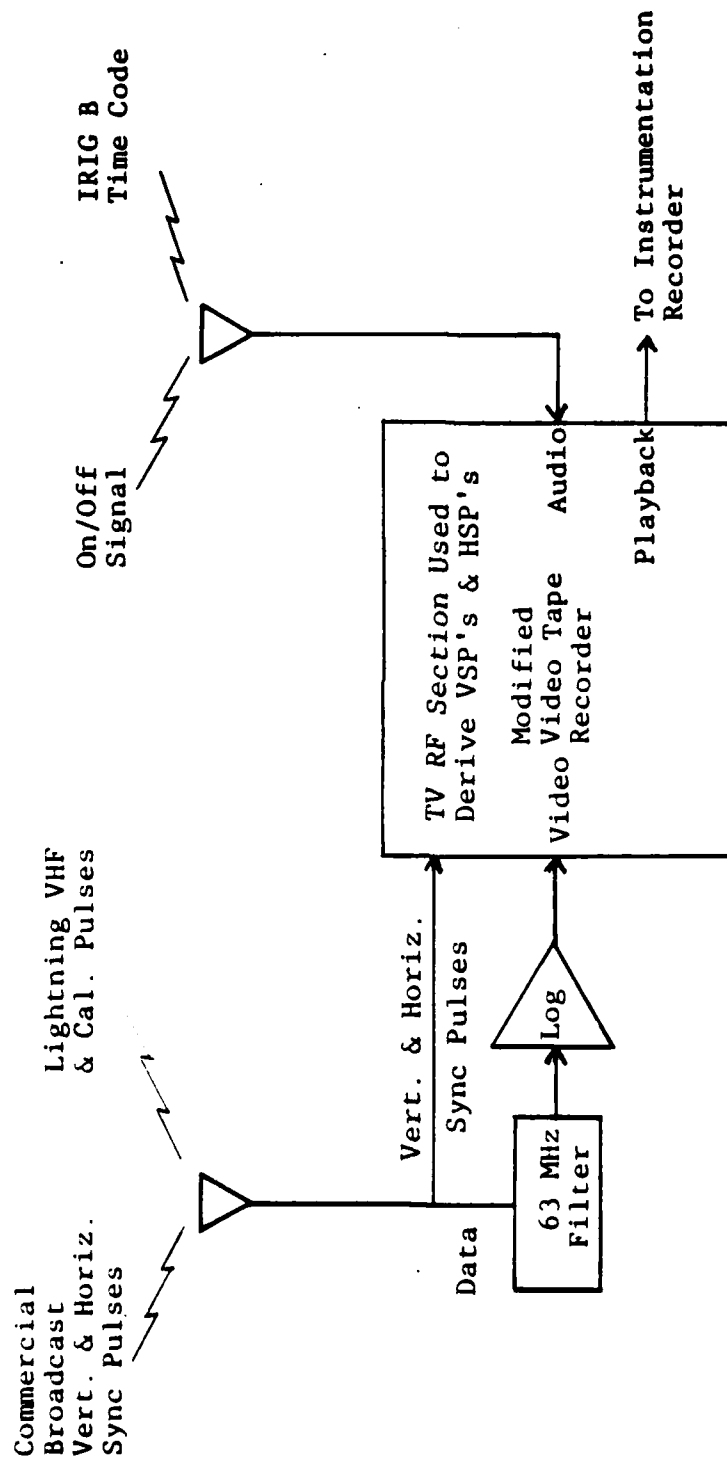
Figure 18. Block Diagram of VHF Recording System

45

a. 100 ft. Antenna Tower at
    Cowpens Site

b. *Typical Remote*
    VHF Station

Figure 19. Ground Station Installations

46

ft tower with the two antennas on the top. Figure 19b shows one of the remote VHF stations. The recorder was kept inside the barrel next to the antenna.

Horizontal and vertical sync pulses from WINK-TV at Ft. Myers, Florida were recorded in the video cassette recorders and also used for calibration. The vertical sync pulses (VSP) have a risetime of a few microseconds, a duration of about 200 μsec, and a repetition rate of 1.6 msec. The time at which the VSP occurs can be related to the IRIG B. The horizontal sync pulses (HSP) have a risetime of less than one microsecond, a duration of a few microseconds, and a repetition rate every 63 μsec. The rising edges of the HSP within two VSP between the Devil's Garden station and each one of the remote sites were aligned. Since the VHF data were recorded in the same track as the TV reference pulses, the time difference between corresponding VHF pulses was determined. In addition to alignment of the VHF pulses by using the TV reference signals, VHF calibration pulses were transmitted from the Cowpens station and recorded in all four stations. To ensure that the VHF sources were correct, calibration pulses were also transmitted from the aircraft in some of the flights and recorded at all the ground sites. The source location of these pulses can be determined and compared with the known aircraft location which was updated and recorded every five seconds.

Figure 20 shows the VHF radiation recorded in the video cassette at the four stations during the preliminary breakdown of a ground flash in the summer of 1979. The difference in the time of arrival is then obtained by using cross-correlation and pattern recognition techniques as described by Rustan (Ref 27).
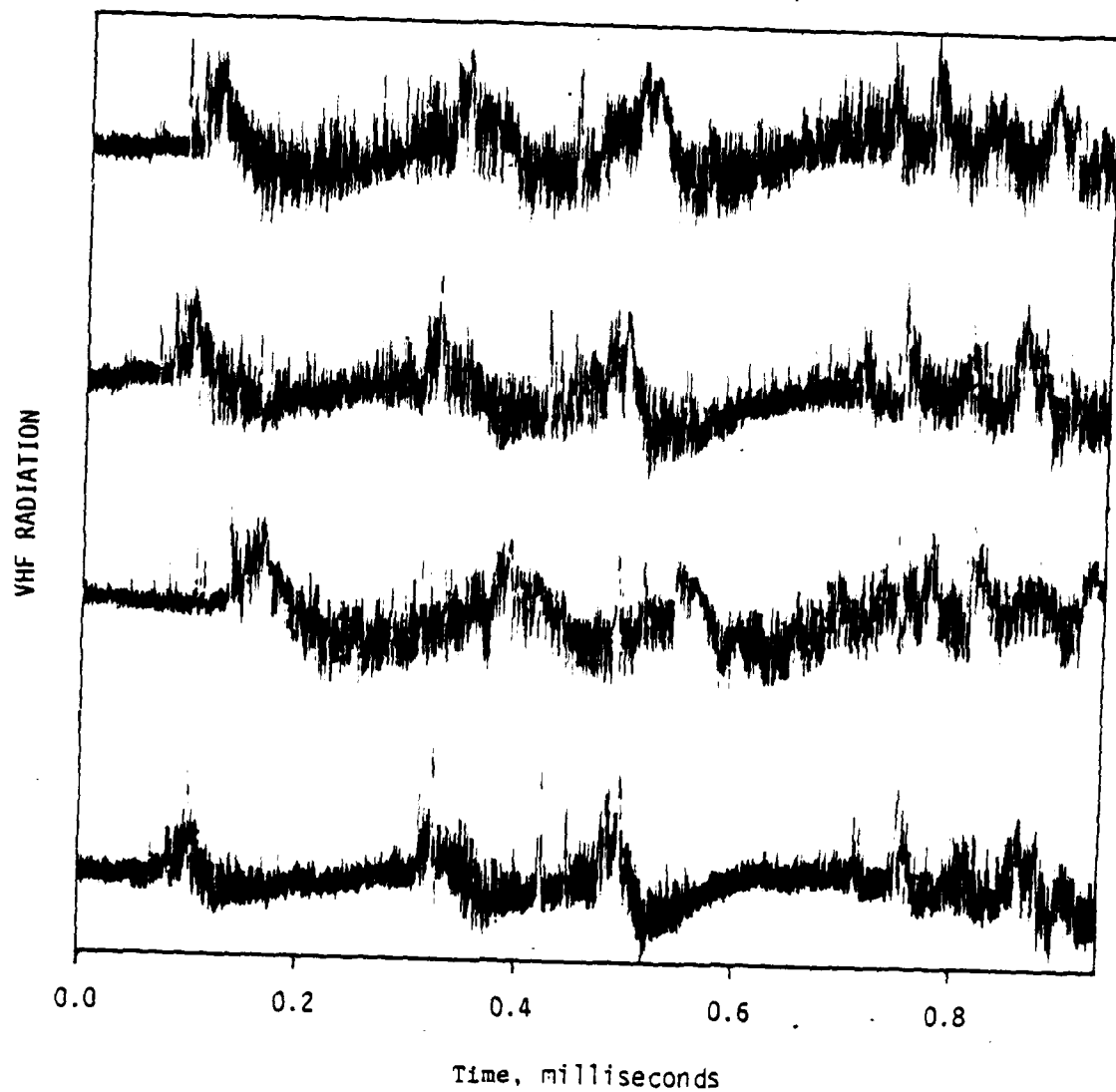
Figure 20.   FY79 Recording of One Event at
Four VHF Stations

48

SECTION III

DATA PROCESSING

1. AIRBORNE DATA

Data acquired during flight by the ten channel transient digitizer were encoded and stored in a magnetic tape recorder with a 2 MHz frequency response as shown in the instrumentation block diagram. During the 1980 and 1981 programs, the data windows consisted of ten simultaneous channels of 8192 samples with an eight bit resolution. In 1979, Biomation 8100's with 2048 samples and an eight bit resolution were used.

Figures 21a and b show the techniques used to transfer digital and analog data from magnetic tape to floppy disks. The data windows recorded in the Honeywell 101 were read into the Micro Pro decoder unit, then transferred and stored in digital form in the PDP 11/05 computer. For subsequent data identification, sweep rate, input range, trigger delay time, and the file and channel number of the data were also stored. Since the computer memory in the PDP 11/05 was limited to 10K, the data windows were read into the computer and stored on disks as two 4096 data arrays.

Figure 22 shows an expanded view of the instrumentation used at the output of the fiber optic receivers. Since there were eleven aircraft sensors, an integrated D output at the sensor, and two internal wires to be monitored for transients, but only ten DTR channels, a channel selection was performed prior to each

49
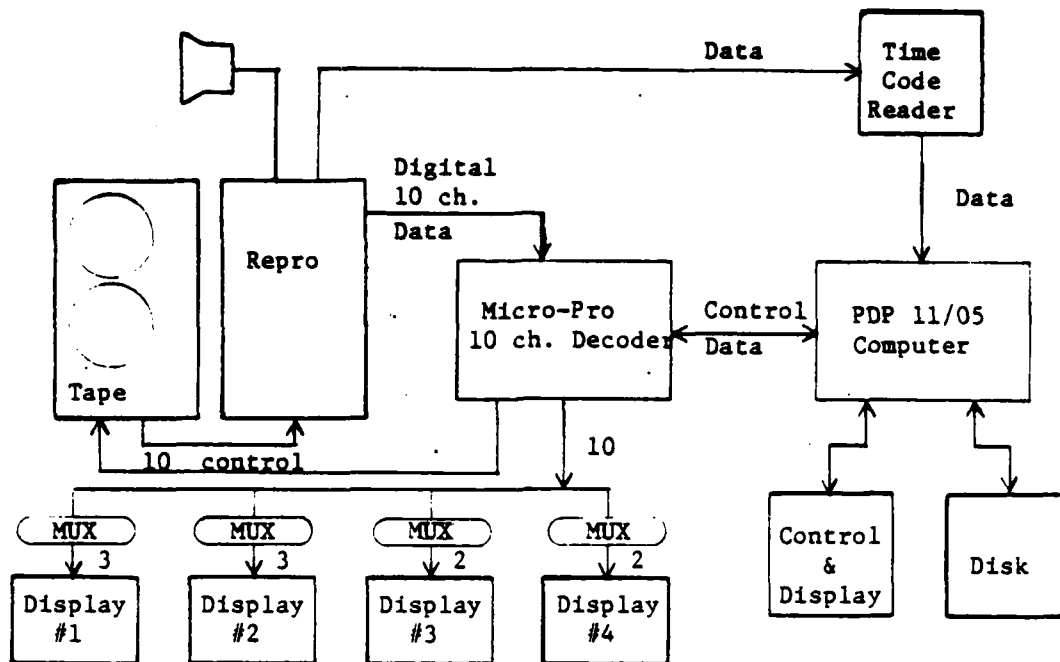
a.   Digital Data Transfer
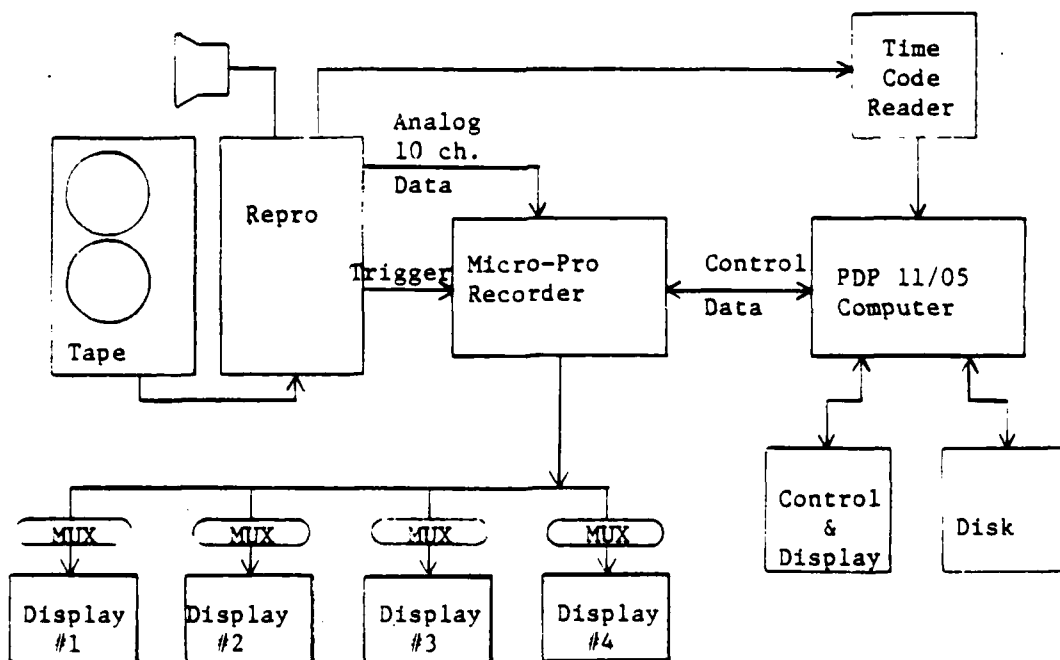
b.   Analog Data Transfer

Figure 21.   Techniques for Transferring Digital and
Analog Data to Floppy Disk

50
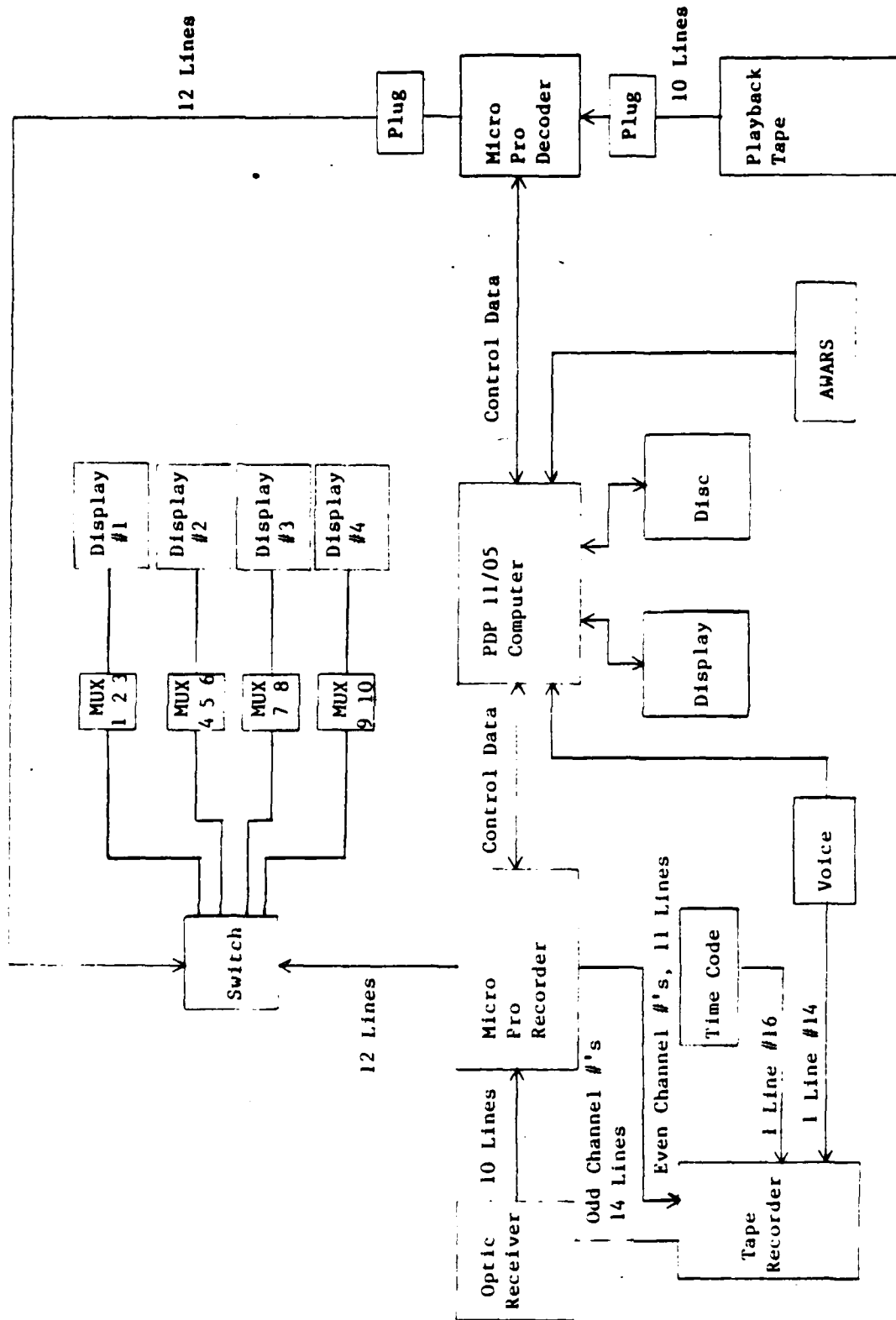
Figure 22. Expanded View of Instrumentation Used at the Output of the Fiber Optic Receivers

flight.

The logged output data stored on floppy disks in the PDP 11/05 were first antilogged. A logarithmic fit was made to the data using linear regression techniques and measurements of output vs input voltage through the logarithmic amplifier systems.

The resulting antilog equation for the $\dot{B}$ and $\dot{Q}$ sensors was

$$V_{in} = \log^{-1} \left(\frac{V_{out} - .6647}{.2163} \right) \tag{21}$$

and for the $\dot{J}$ and $\dot{D}$ sensors was

$$V_{in} = \log^{-1} \left(\frac{V_{out} - .0888}{.0383} \right) \tag{22}$$

Before the data were antilogged, the recorded output was scaled to the input range and the DC offset removed. Figures 23a and c show an example of typical scaled and antilogged waveforms recorded on the $\dot{Q}$ and $\dot{B}$ sensors during a flight on 8 September 1980.

The recorded voltage output of the sensor was integrated and properly scaled to determine corresponding readings of electric and magnetic fields. From Gauss's law, the current flowing in the cable connected to the electric field plate is given by

$$I(t) = \epsilon_o S \frac{dE(t)}{dt} \tag{23}$$

Since the voltage is measured across a 5C Ω load, equation (23) can be solved for the E-field as

52

a. Rate of Change of Electric Field

b. Electric Field

c. Rate of Change of Magnetic Field
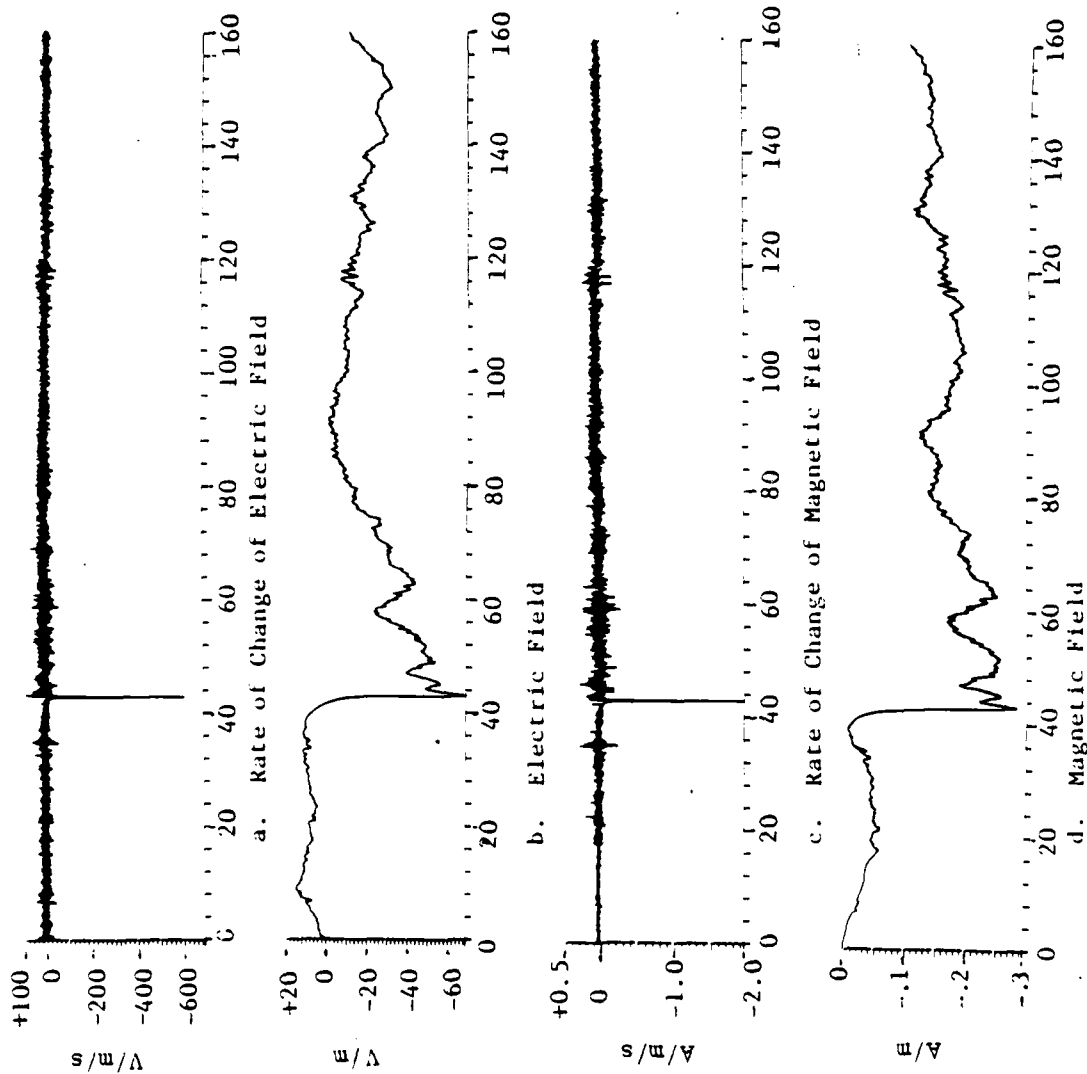
d. Magnetic Field

Figure 23. FY 80 Electric (Top Two) and Magnetic (Bottom Two) Field Waveforms Time in Microseconds

53

$$E(t) = \frac{1}{\epsilon_o S \ R} \int_0^t v(\lambda)\,d\lambda \tag{24}$$

The equivalent sensor area was 0.1 m^2 for $\dot{Q}$ and .02 m^2 for $\dot{D}$. Using time in microseconds, the integrated value of $v(t)$ has to be multiplied by 22598.9 and 112994 for $\dot{Q}$ and $\dot{D}$, respectively. From Faraday's law, the detected voltage between the wires connecting to the magnetic field sensor is

$$V(t) = \mu_o S \ \frac{dH(t)}{dt} \tag{25}$$

which can be solved for H as

$$H(t) = \frac{1}{\mu_o S} \int_0^t v(\lambda)\,d\lambda \tag{26}$$

With an equivalent area, A, of 0.02 m^2 for the $\dot{B}$ and $\dot{J}$ sensors, and time in microseconds, the integrated value of $v(t)$ will have to be multiplied by 39.7887 to obtain the corresponding values of $H(t)$.

The integration of the data windows was performed in the PDP 11/05 using the standard trapezoidal approximation. That is,

$$y(n) = y(n-1) + \frac{T}{2} [x(n) + x(n-1)] \tag{27}$$

where $y(n)$ is the output, $x(n)$ is the input, and T is the time between samples. Figures 23b and d show typical records of the electric and magnetic field recorded in a 164 usec window after integration.

54

2. GROUND DATA

Even though the VHF data in the different stations can be properly displayed as shown in Figure 20, instrumentation problems in 1979 and 1980 did not allow proper correlation of the electric field and VHF records at the central ground site and the corresponding VHF records at all the remote locations. These problems were corrected during 1981 and simultaneous records of the wideband electric field and VHF records were obtained at the Cowpens site and compared with the remote sites. Figure 24 shows a typical record of the VHF and the E-field during the beginning of a cloud-to-ground flash. Figure 24 was obtained by slowing down the analog tape and displaying the data in a 10 kHz ES 100 Gould Strip Chart recorder.

3. DATA ANALYSIS

The data analysis and interpretation presented in this report are based on the airborne data samples obtained in the Biomation (1979) and the the DTR (1980), and on partial results of the airborne and analog data analysis for correlated airborne and ground data in 1981. The 1981 data interpretation includes:

(1) A correlation between the ground and airborne electromagnetic field records for simultaneous lightning flashes 10 to 35 km away.

(2) Analysis of airborne analog and digital records of lightning strikes 2 to 10 km from the aircraft.

(3) Analysis of two lightning direct strikes to the air-
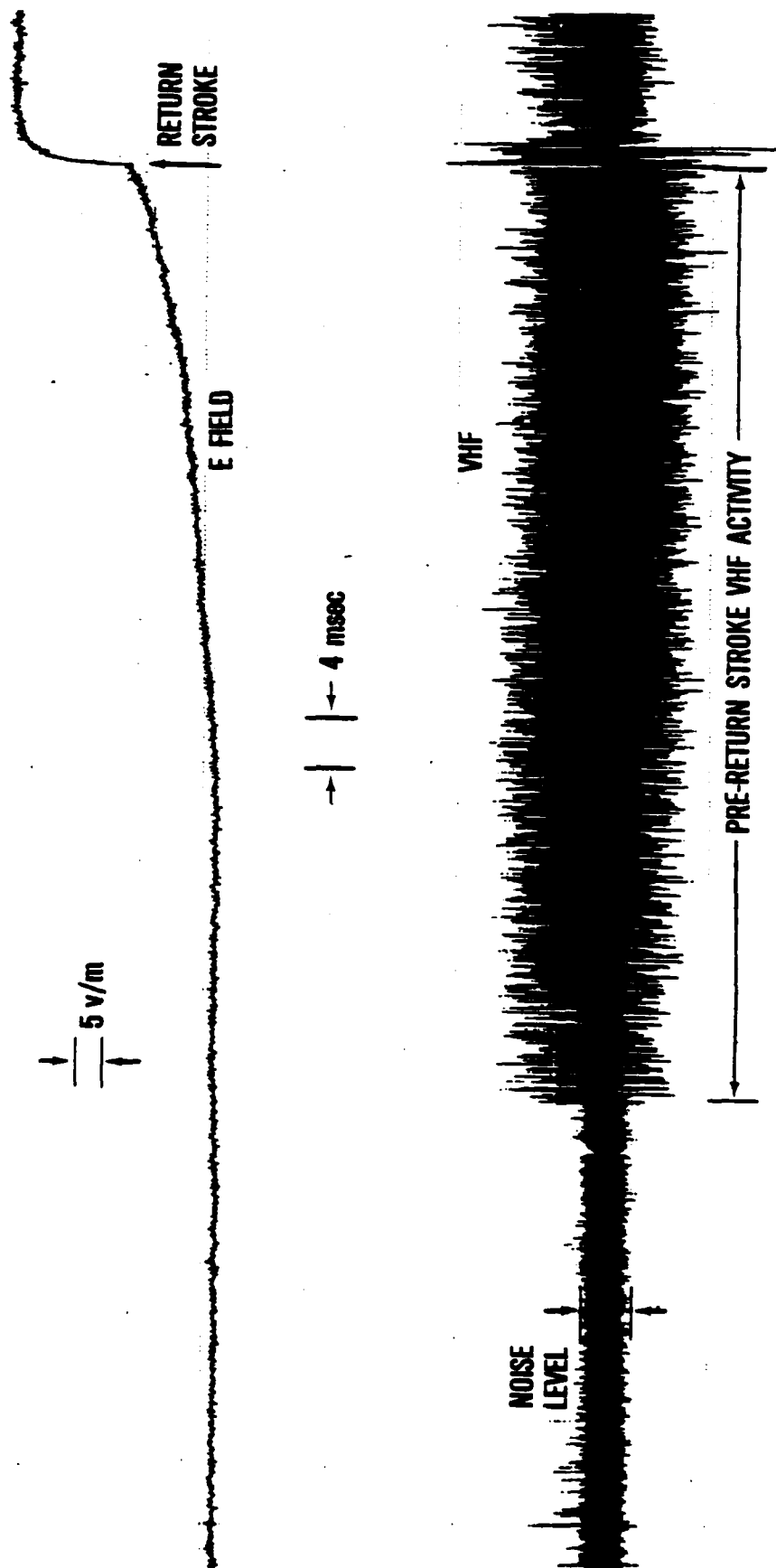
Figure 24 Correlated VHF and Electric Field During the Initiation of a Typical CG Flash at About 20 km Away.

56

craft.

Items (1) and (2) will be discussed in Section IV after the results of the 1979 and 1980 data are presented. Item (3) will be discussed in Section V.

SECTION IV

ANALYSIS OF FAR-FIELD LIGHTNING DATA

During 1979, airborne electric and magnetic fields for data windows of 2048 samples every 10 or 20 nsec were obtained for six flights. In 1980, the data window was increased to 8192 samples every 20 nsec and airborne data were obtained during three flights. Data for direct strikes were not obtained during these two years. Data were obtained from 25 triggered times in both 1979 and 1980 with peak airborne electric fields of 4 to 127 V/m. For each of these 50 waveforms, total windows of 40.96 μsec for the 1979 data and 163.84 μsec for the 1980 data were analyzed for the electric field and the two directional components of the magnetic field. The results of the 1979 and 1980 programs are summarized first, followed by partial results for some of the ten successful flights during 1981.

1. RESULTS OF THE 1979 AND 1980 TESTS

The only useful data recorded in these two years were obtained with the airborne digital system. Since these records were of relatively short duration compared to the entire lightning flash, it was not possible to determine with certainty whether the event captured was a stepped leader, return stroke, dart leader, K-change, etc. Since the physics of each process in a lightning flash is different, the amount of interpretation

58

possible for the 1979 and 1980 results was limited. This limita-
tion was eliminated in 1981 by ensuring that continuous electric
field records were recorded in the aircraft and on the ground.

The amount of pre-trigger recording was set at approximately
25% of the data window. The trigger level was set to record any
waveforms where dE/dt exceeded about 1×10^7 V/m/s. That is, a
minimum of 10 V/m difference in the field over one microsecond
was needed to produce a trigger. The use of the derivative
trigger allowed detection of very fast, low magnitude electric
field pulses which could cause electrical upsets to aircraft
circuitry if they coupled to the aircraft. On the other hand,
the differential trigger system might not detect a slowly
increasing electric field which could produce sufficient charge
in the aircraft to trigger a lightning discharge. The use of the
differential trigger resulted in the acquisition of many low
magnitude pulses with very fast risetimes in both 1979 and 1980.

a. Time Domain Analysis

Peak electric fields, risetimes and polarities for
selected 1979 and 1980 data are summarized in Tables 4 and 5.
The criterion used to select these waveforms was the peak field
value. Only events with peak field values greater than 4 V/m
were included. The waveforms marked with an R are similar to
those identified by Weidman and Krider (Ref 6) as return strokes
during ground measurements. Many of these events coincided with
visual lightning observed from the cockpit. The A designation is
given to any other recorded event that does not have characteris-
tics similar to those of return strokes. The ΔE shows the

TABLE 4

1979 ELECTRIC FIELD DATA

File Number/Date	Peak Field (V/m)	Risetime (ns)	ΔE (V/m)	ΔE/Risetime V/m/s	Polarity
1/(8-23) R	14.4	220	5.7	2.6×10^7	-
8/(8-23) A	16.2	612	12.4	2.0×10^7	+
9/(8-23) R	27.1	215	8.6	4.0×10^7	+
10/(8-23) R	37.0	705	20.6	2.9×10^7	+
11/(8-23) R	15.2	100	4.5	4.5×10^7	+
11/(8-23) R	15.2	118	3.4	2.9×10^7	+
13/(8-23) R	36.6	512	26.6	5.2×10^7	+
14/(8-23) R	45.9	131	8.1	6.2×10^7	+
6/(8-27) R	22.4	131	8.3	6.3×10^7	+
1/(8-31) A	50.3	240	27.3	1.1×10^8	-
7/(9-25) R	15.3	131	6.1	4.7×10^7	+
8/(9-25) R	62.0	129	21.3	1.7×10^8	+
9/(9-25) R	68.3	97	26.9	2.7×10^8	+
10/(9-25) A	62.7	119	36.3	3.1×10^8	-
11/(9-25) R	77.0	108	35	3.2×10^8	+
11/(9-25) A	59.1	468	44.4	9.5×10^7	+
13/(9-25) R	100.6	119	49.1	4.1×10^8	+
14/(9-25) R	126.6	132	42.2	3.2×10^8	+
15/(9-25) R	100.8	181	33.8	1.9×10^8	+
2/(9-26) A	63.1	277	33	1.2×10^8	+
2/(9-26) A	39.2	105	23.9	2.3×10^8	+
4/(9-28) A	18.5	146	9.2	6.3×10^7	-
5/(9-28) A	77.0	107	49.5	4.6×10^8	-
5/(9-28) A	99.8	133	48.3	3.6×10^8	-
5/(9-28) A	56.8	118	56.8	4.8×10^8	-

TABLE 5

1980 ELECTRIC FIELD DATA

File Number	Peak Field (V/m)	Risetime (ns)	ΔE (V/m)	ΔE/Risetime (V/m/s)	Polarity
87 R	28	99	10.9	1.1×10^8	-
89 R	10.3	83	3.5	4.3×10^7	-
91A-A	18.5	86	9.0	1.0×10^8	+
91B-A	22.8	132	13.3	1.0×10^8	+
91C-A	21.4	190	17.4	9.1×10^7	+
99A-A	12.6	105	5.3	5.0×10^7	+
99B-A	4.9	95	4.9	5.2×10^7	+
99C-A	13.6	224	8.3	3.7×10^7	-
101A-A	14.7	138	12.8	9.3×10^7	-
101B-A	15.0	191	10.4	5.4×10^7	+
106 R	20.8	615	13.9	2.2×10^7	+
114A-A	22.9	198	8.6	4.3×10^7	+
114B-A	25.0	235	13.2	5.6×10^7	+
120 A	12.2	111	9.0	8.1×10^7	+
133 R	18.7	179	11.4	6.4×10^7	-
135 R	42.9	212	16.5	7.7×10^7	-
136 R	53.3	135	45.6	3.4×10^8	-
138A-A	11.8	195	6.6	3.4×10^7	+
138B-A	13.1	197	6.1	3.1×10^7	+
146 A	17.4	118	6.6	5.6×10^7	-
149 R	16.8	142	4.9	3.5×10^7	-
150 R	53.7	227	27.2	1.2×10^8	-
151 R	20.8	299	10.3	3.4×10^7	-
152 R	16.1	195	6.8	3.5×10^7	-
154 R	15.9	135	9.5	7.0×10^7	-

increment of the electric field over which the risetime was measured. This value was sometimes substantially different from the peak field because of the slow front of the wave (Ref 6).

The data from 1980 had to be anti-logged before further processing. For both years, the data were numerically integrated using equation (27). Figure 23 illustrates the electric and magnetic field for a typical R waveform before and after integration. Figure 23b shows the characteristics of a return stroke waveform which includes a slow front of 1-3 μsec and a fast front on the order of a few hundred nanoseconds.

There are no standard techniques for measuring the risetime for this type of waveform. Baum (Ref 5) and Weidman and Krider (Ref 6) chose to use 10-90% of the fast front of the waveform, as illustrated in Figure 25. However, Fisher and Uman (Ref 8), Lin and Uman (Ref 31), and Tiller et al. (Ref 7) measured the rise-time (zero to peak) of the entire waveform. The earlier technique is probably more meaningful because it excludes the slower field changes of the slow front which are probably due to an upward going ground discharge. The earlier technique, however, does not produce consistent results because of the difficulty in determining the slow-fast front transition point. Different researchers using this technique might not agree on the choice of the transition point and could obtain results that vary by several tens of nanoseconds.

Because of the importance of risetime measurements in determining the lightning threat, an effort was made to develop a consistent method of calculating risetimes. This was accomplished by determining derivative values point by point for

62
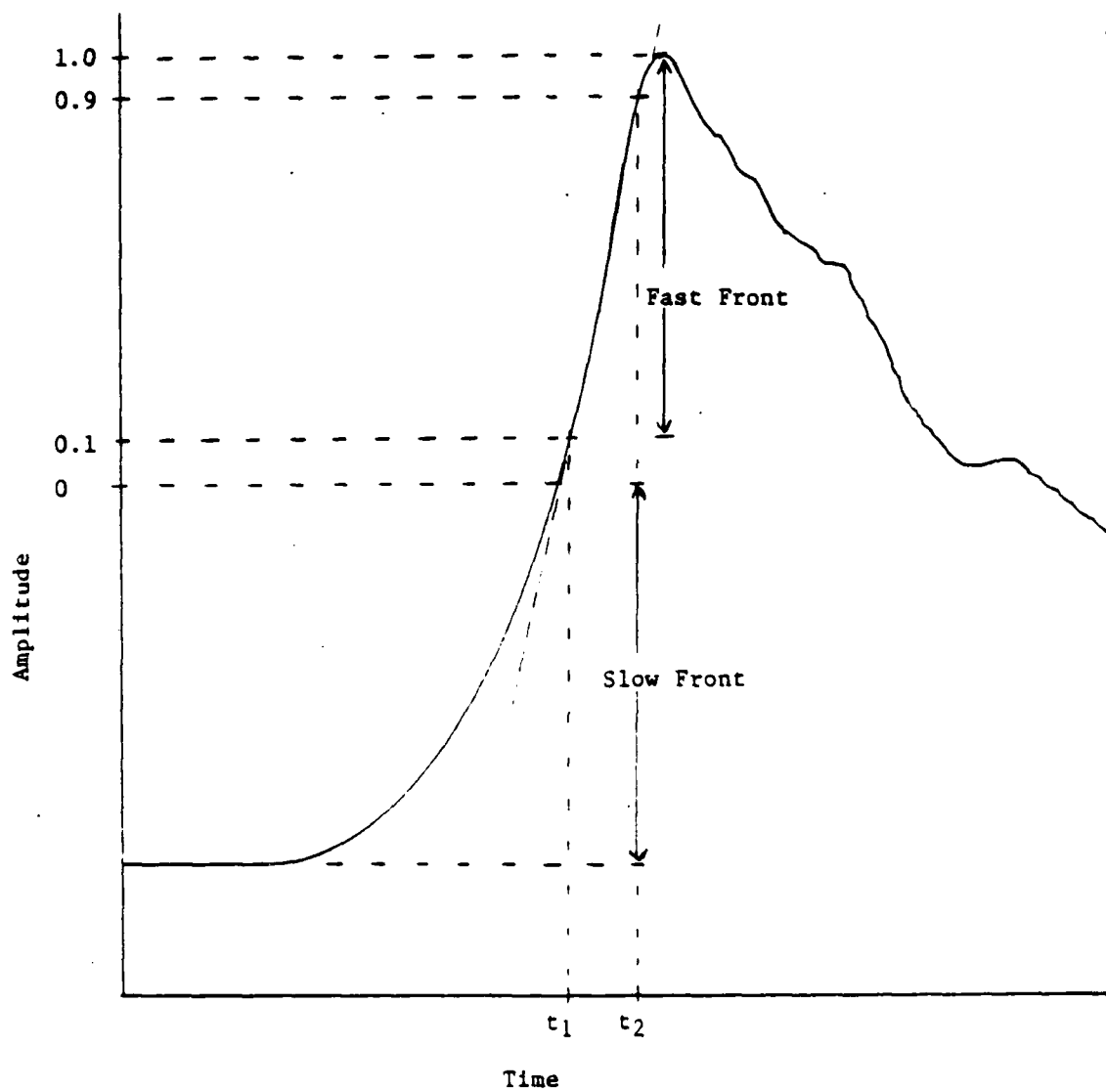
Rise Time $t_r = t_2 - t_1$

Figure 25. Illustration of How the 10% - 90% Rise Times of Lightning Waveforms were Determined by Baum (Ref. 5)

all the data in the fast front part of the curve. This deriva-
tive array will show a maximum at the time when the E-field is
changing most rapidly. By trial and error it was found that
taking 1.35 times the standard deviation of the maximum field
change and using this value as the point for beginning the rise-
time calculation produced consistent values irrespective of the
slow-fast transition point chosen by the operator. If only one
standard deviation was used, the maximum did not include enough
points to satisfy visual determinations of the faster risetime
range while using two standard deviations included so many points
that the consistency of the technique was impaired. Figure 26
shows four typical waveforms with risetimes calculated using this
technique. The second mark in the graphs shows the initial point
used to measure the risetime. Using this technique the average
risetime obtained in 1979 was 214 nsec with a standard deviation
of 167 nsec and in 1980 was 181 nsec with a standard deviation of
105 nsec. The fastest and slowest risetimes were 97 nsec and 705
nsec for 1979 and 83 nsec and 615 nsec for 1980. Figure 27 shows
a histogram of the risetimes for all 50 events. It is important
to note that since these data were recorded in the air, it should
have less attenuation of the high frequency components than
similar data recorded on the ground.

Figures 28 and 29 show correlated electric and magnetic
field events on different time scales. Even though it is theore-
tically possible to integrate the recorded derivative readings
and obtain a frequency response from near DC to about 23 MHz,
sensor output voltages below 50 μV fall within the noise level
and frequency response below about 600 Hz is not recovered. The
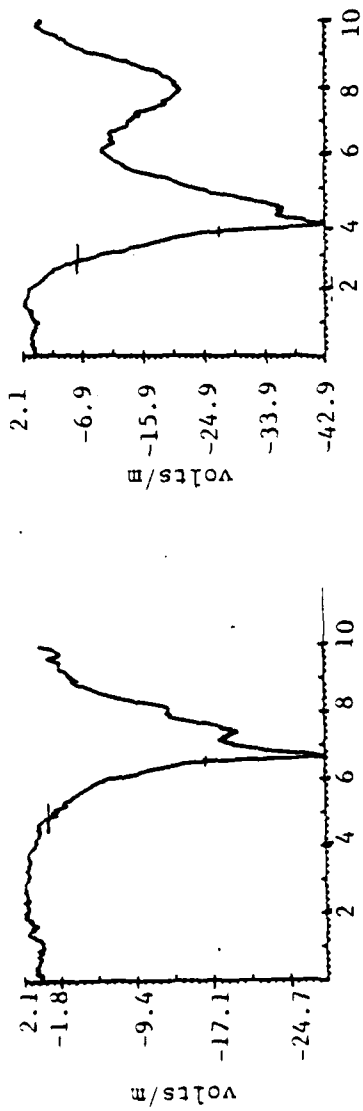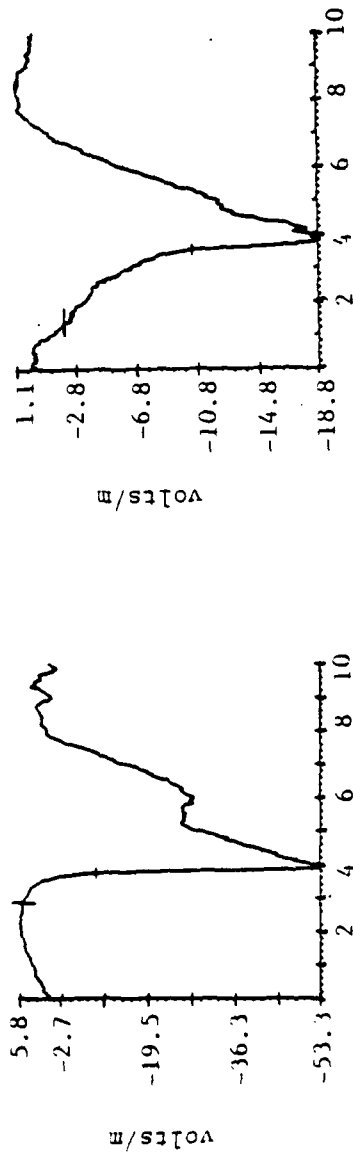
Figure 26. Typical Results of Rise Time Determination Technique (Wide mark is starting point operator input, short mark section of waveform that defines rise time). Time in Microseconds.
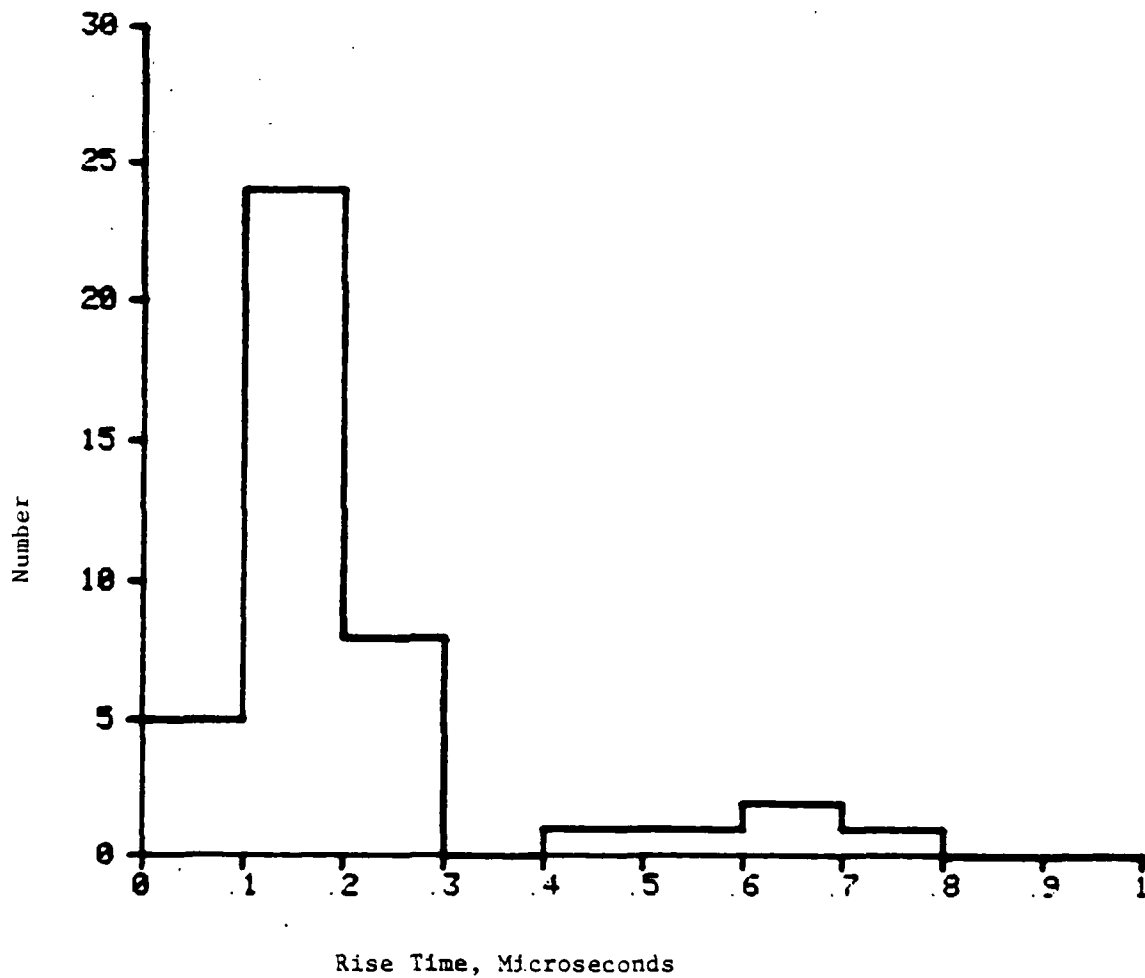
Figure 27.   Histogram of FY 79/80 Rise Time Data
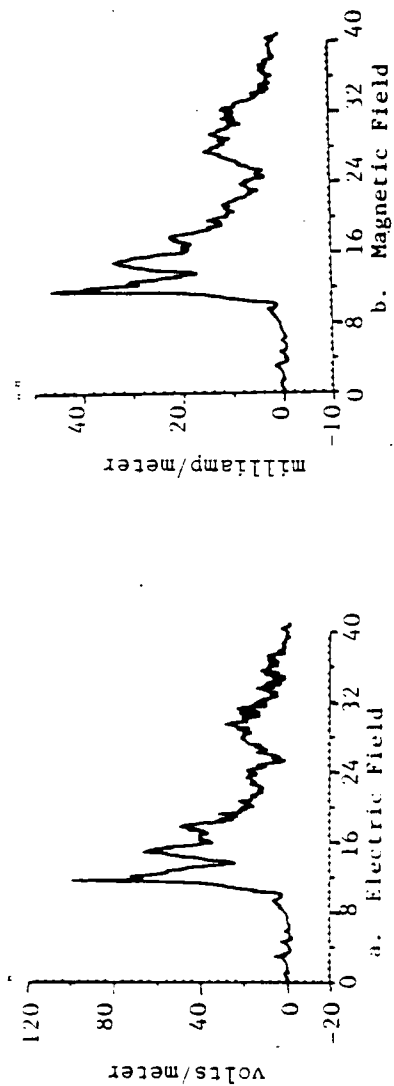
Figure 28. FY79 Correlated Electric and Magnetic Field Waveforms
(Time in Microseconds)

a. Electric Field

b. Magnetic Field Waveforms
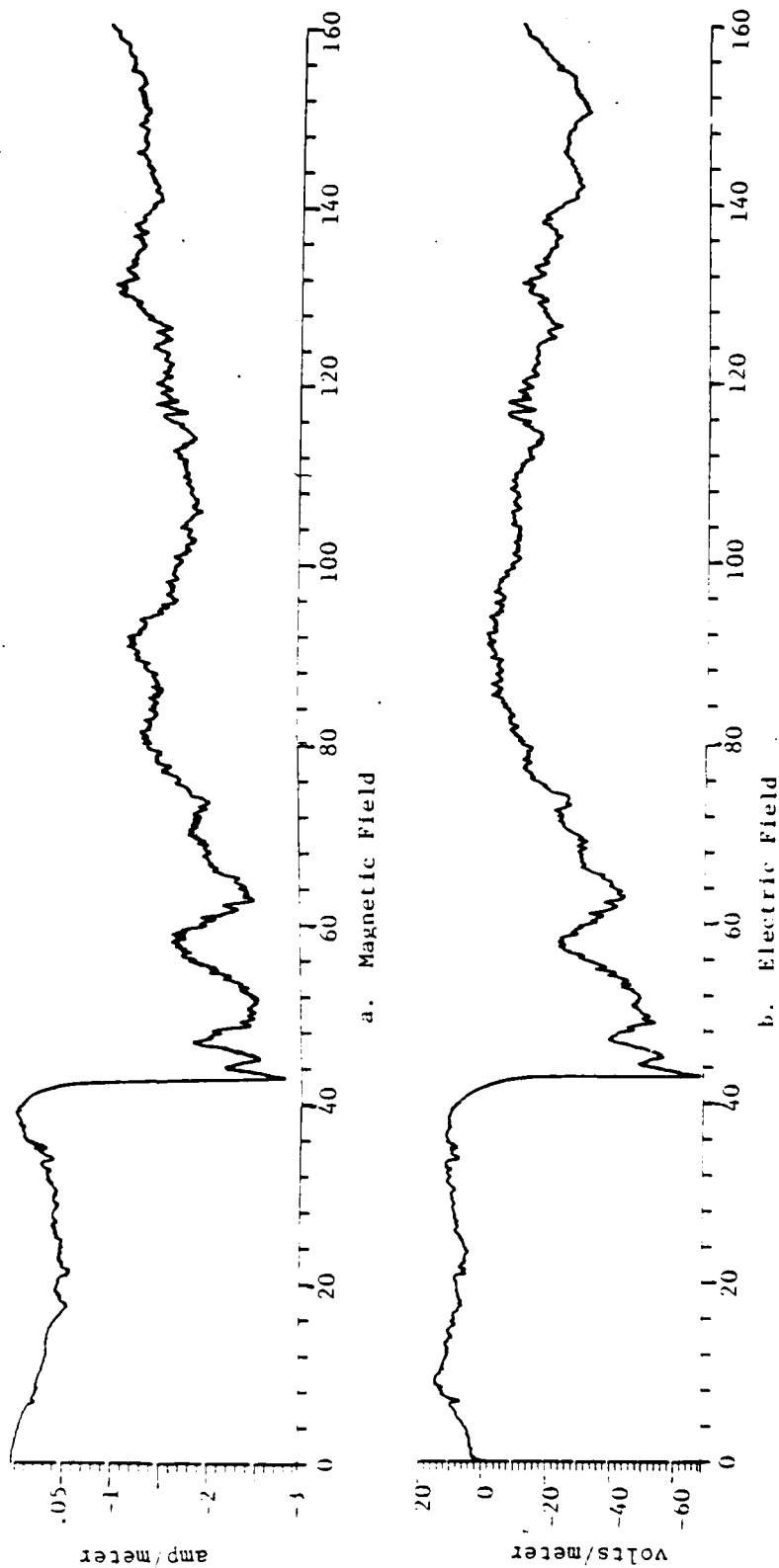
Figure 29. FY80 Correlated Electric and Magnetic Field Waveforms
(Time in Microseconds)

a. Magnetic Field

b. Electric Field

67

upper frequency response is limited by the characteristics of the software integration routine with a 20 nsec sample interval. Taking into account the lack of low frequency response and the fact that to observe the electrostatic component of the electric field this low frequency response is needed (Refs 7,8), it is expected that the peak airborne electric field measured between 4 and 127 V/m is mainly due to the radiation field and some induction field. The similarities between the electric and magnetic field waveforms in Figure 23 are then justified. Furthermore, the ratio between the radiation components of the electric and magnetic fields should be the impedance of free space (Ref 32), and values between 200 and 620 ohms were obtained for the data shown in Tables 4 and 5. Therefore, it was concluded that for some of the acquired data the airplane was closer than the 10 to 50 km range from the flash that would be expected for the magnitude levels that were obtained.

b. Frequency Domain Analysis

The Fast Fourier Transform (FFT) was calculated for some of the 50 sample data windows recorded in 1979 and 1980 using a PDP 11/05 computer. Even though a 163.84 usec data window was available in 1980, the FFT were only calculated for the 40.96 usec data window which shows the significant triggered event because of computer memory limitations. Since most of the magnetic field data windows were very similar to those of the electric field, the FFT's were only computed for the electric field waveforms.

68

Figure 30 shows FFT records for two 1979 and two 1980 triggered pulses. The labeled (a) and (b) events correspond to file numbers 13 and 15, 25 Sep 79 in Table 4. The events labeled (c) and (d) are file numbers 136 and 150 in Table 5. As can be seen in Tables 4 and 5, the risetimes and peak fields of these events were typical of the acquired data.

The FFT was calculated by using a rectangular window for the 40.96 μsec record length. For this data window the FFT samples are spaced 24.4 kHz apart and the repetition frequency is 50 MHz. Since the magnitude of the FFT has a half wave symmetry, only information between 24.4 kHz and 25 MHz is meaningful. The magnitude of the FFT was plotted in a logarithmic graph as shown in Figure 30. Therefore, as the frequency increases the samples become closer together.

Analysis of these data shows that the spectrum of the triggered waveform decreases at a rate faster than $1/f$ from 24.4 kHz to about 2 MHz. Between 2 and 5 MHz there is an increase in the spectrum which produces a difference in its rate of change and is probably due to aircraft resonances. No other effect in this data appears to be produced because of the presence of the aircraft. In the frequency range from 5 MHz to 20 MHz the frequency spectrum decreases at a rate faster than $1/f^2$. The rates of $1/f$ for the lower frequency range and $1/f^2$ for the higher frequency range have been suggested in the literature (Refs 18, 33) as a good approximation of the spectrum of return strokes. However, the previously reported spectrum data applies for data recorded on the ground. Figure 31 compares a typical spectrum
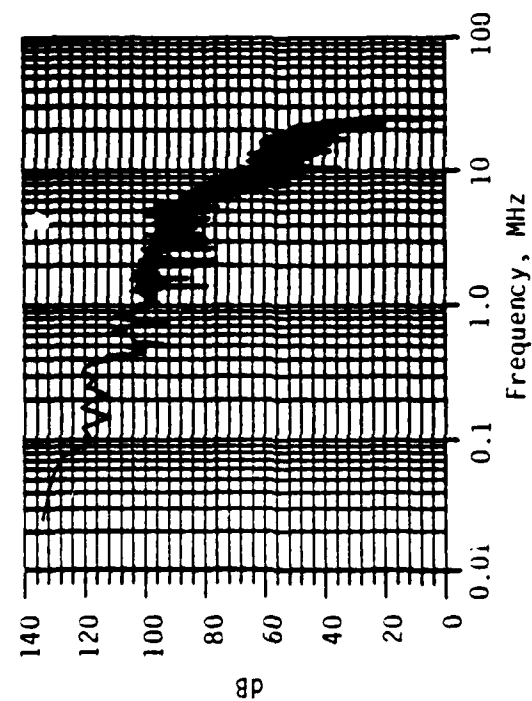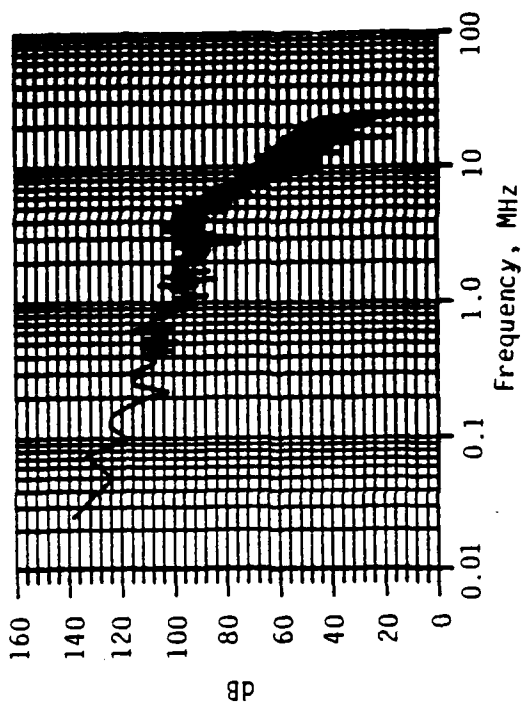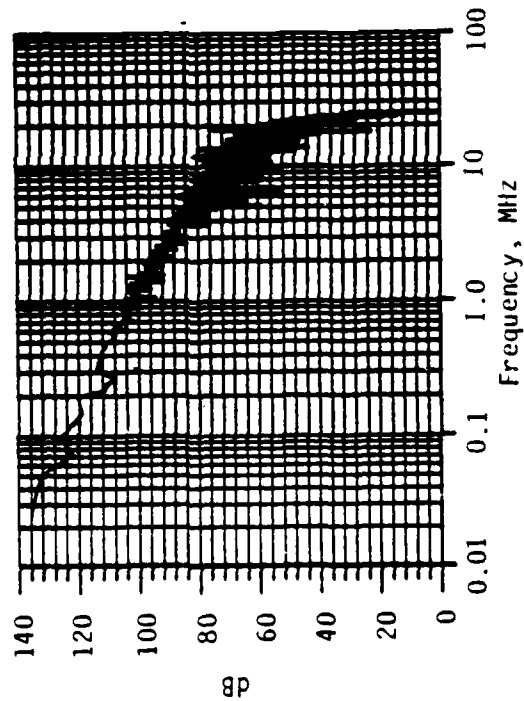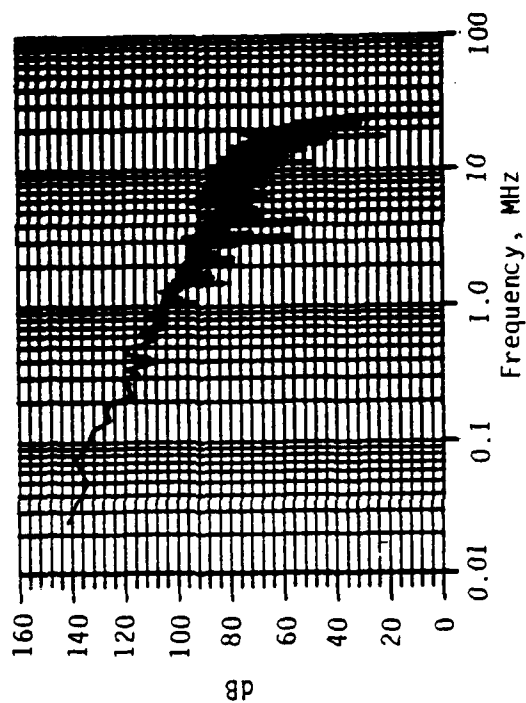
Figure 30. FFTs of Two 1979 and Two 1980 Electric Field Waveforms

70
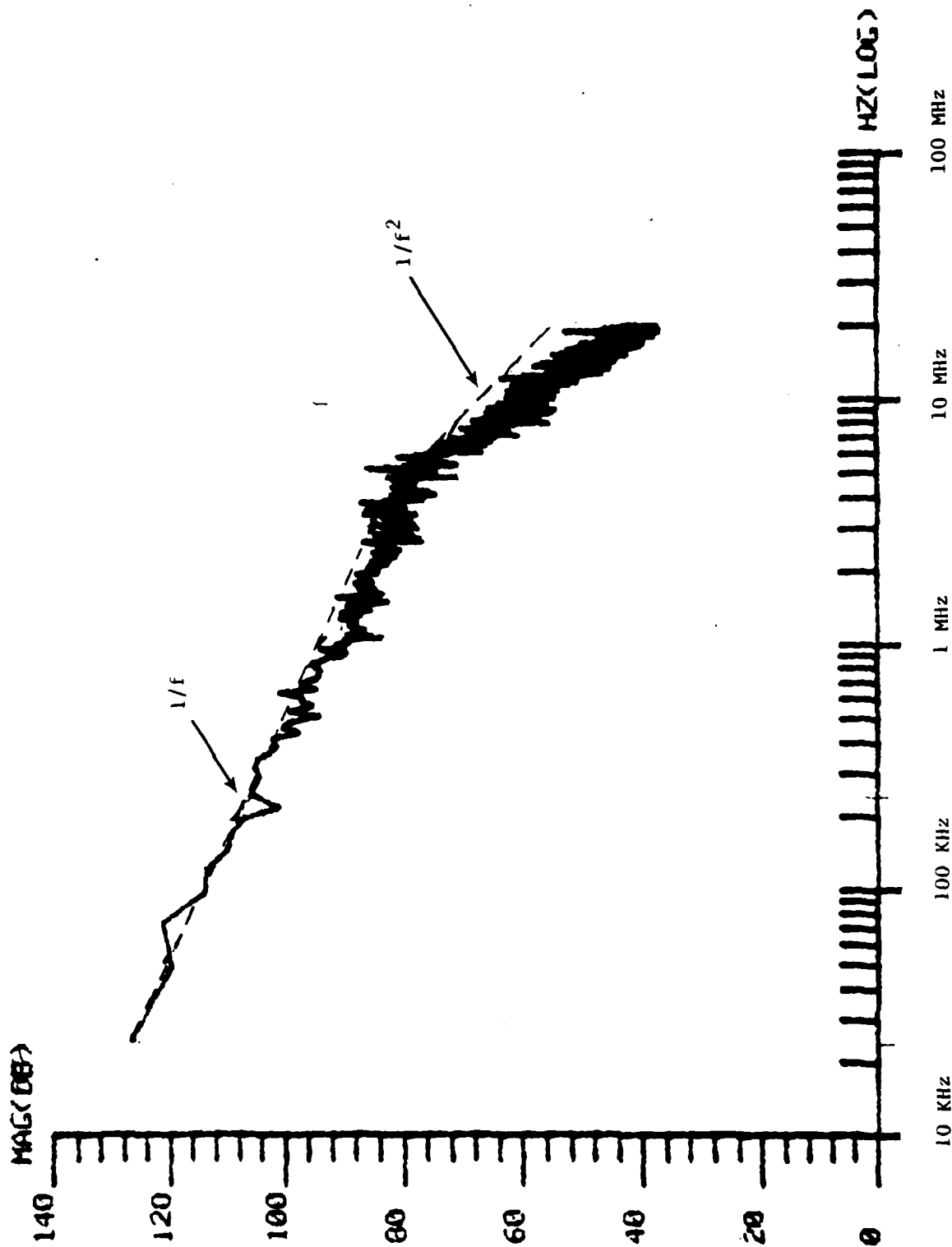
Figure 31. Comparison of Average Frequency Spectrum From Four 1979-1980 Events with 1/f and 1/f² Approximation Curves.

71

from airborne data with the $1/f$ spectrum lower frequency range and the $1/f^2$ spectrum for the higher frequency range. This figure indicates that the spectrum of return strokes for airborne measurements decays faster than $1/f^2$ above 2 MHz.

2. PARTIAL RESULTS OF THE 1981 TEST

During the summer of 1981, many simultaneous electric fields between the ground and the aircraft were recorded. Most of the correlated data is for lightning between 10 and 35 km from the Cowpens station (Figs 15a and 17) with the aircraft located within the outer perimeter of the remote stations. Correlated data were obtained on July 15, 16, 22, 23, and 31 and on August 25 and 27. In addition, airborne data were obtained on July 9 and 17 and on August 26 and 27. For some of the correlated data there were four or five ground stations recording VHF, one ground analog electric field station and airborne digital and analog data recorded in the aircraft. Correlated airborne data were obtained at different altitudes. On August 27th the aircraft made seven passes over the Cowpens site at 1500 feet altitude (MSL) with lightning between 10 and 20 km from the site. On August 25th the aircraft made three passes at an altitude of 8000 feet and two passes at 5000 feet with lightning between 5 and 20 km from the site. All the remaining data were collected at an altitude of about 15000 feet.

There were two confirmed direct attachments to the aircraft. Those occurred at 17:21:44 EDT on July 17th and at 17:09:45 EDT on August 26th. Both of these direct strikes will be fully analyzed in Section V of this report.

Including all 12 flights, 5193 data windows of 164 μsec with 20 MHz frequency response were recorded in the Digital Transient Recorder (DTR). To analyze these high resolution data windows and to determine the correlation of these events with the continuous recording of analog data in the aircraft and on the ground, several events were chosen for each storm day for which simultaneous data existed. The selected events had to meet at least one of the conditions enumerated below:

1. Aircraft location was within 20 km of the Cowpens site -and a digital data window was obtained in the aircraft for a flash within about 25 km of the Cowpens station.

2. The corresponding electric field analog data during a DTR event at the ground site, the aircraft, or both, exceeded 100 V/m.

3. The DTR data for the electric field exceeded 100 V/m.

a. Analysis of the Correlated Airborne/Ground Data for 5 Flashes

(1) The 174731 Flash, 27 Aug 81

Data obtained for a flash where the aircraft was located right over the Cowpens station at an altitude of 1500 ft on August 27th at 17:47:31 are first presented. Figure 32 shows the electric field waveform for the entire flash as recorded in the aircraft (Fig 32a) and on the ground (Fig 32b). Since the low frequency response for the ground E-field is about 0.2 Hz versus about 0.5 Hz in the aircraft, the airborne waveform decays slightly faster than the corresponding ground data. The overall structure of the lightning flash was quite complex. Figure 33
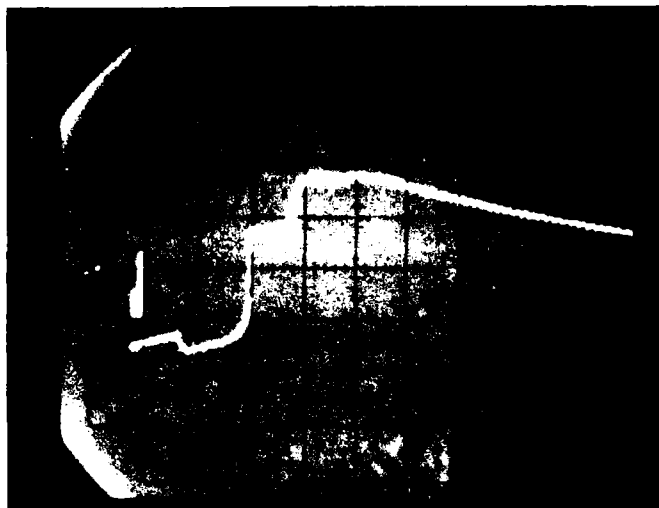
a. Waveform Recorded on the Aircraft (Horizontal Scale is 100 ms/div. Vertical Scale is 110 V/m/div.)
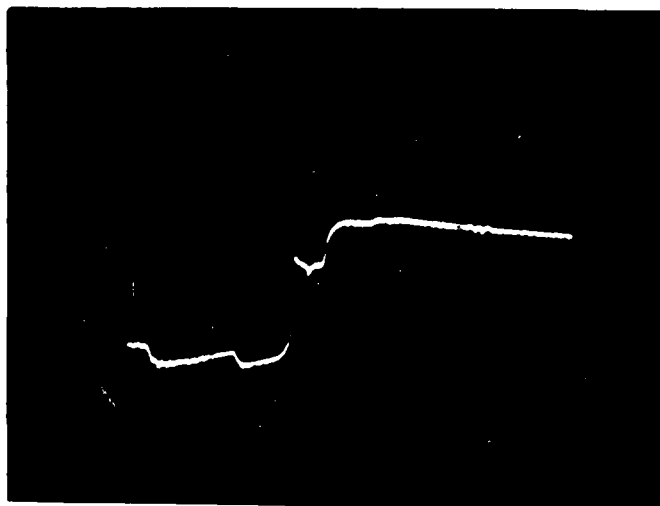
b. Waveform Recorded on the Ground (Horizontal Scale is 100 ms/div. Vertical Scale is 30 V/m/div.)

Figure 32   Airborne and Ground Electric Field Waveforms Recorded on 27 Aug 81 at 17:47:31.
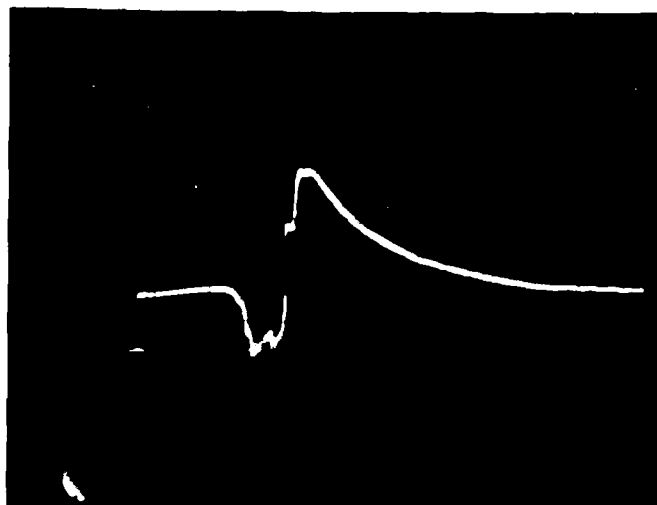
Figure 33. Five Second Window Showing the Electric Field
Waveform Recorded on the Aircraft at 17:47:31
on 27 Aug 81. (Horizontal Scale - 500 ms/div.
Vertical Scale - 112 V/m/div.)

shows a five second window including the waveform as recorded on the aircraft. For the first 400 ms the structure of the E-field appears to indicate an intracloud discharge which is followed by a cloud-to-ground discharge. The different polarity of the intracloud and cloud-to-ground discharge indicates the flash occurred at a distance greater than about 8 to 10 km from the measuring point (Ref 33), which is consistent with the low magnitude of the field. The last 400 ms of the discharge are characterized by a return stroke preceded by a stepped leader and what appeared to be another intracloud discharge about 80 ms after the return stroke. The polarity of the stepped leader prior to the return stroke also indicates that the horizontal distance from the measuring location is greater than the height of the point charge neutralized by the discharge. Figure 34 shows correlated pictures of the electric field and the VHF radiation as recorded simultaneously at the Cowpens station. Figure 34a shows a one ms/div scale comparison of these waveforms and Figure 34b shows the same comparison with a scale of 50 μsec/div. A large VHF pulse occurs 20 to 40 μsec after the beginning of the return stroke. Similar time differences between the beginning of the E-field and for the VHF pulse for the return stroke have been observed by other investigators (Refs 12, 28 and 34). This is probably because the VHF radiation originates at the cloud level and it takes this much time before the near ground return stroke pulse propagates to the originating region in the cloud.

The magnitude of the electric field change in Figure 32a is about 360 V/m and the total magnitude change in Figure 32b is only about 100 V/m. That is, the electric field measured in the
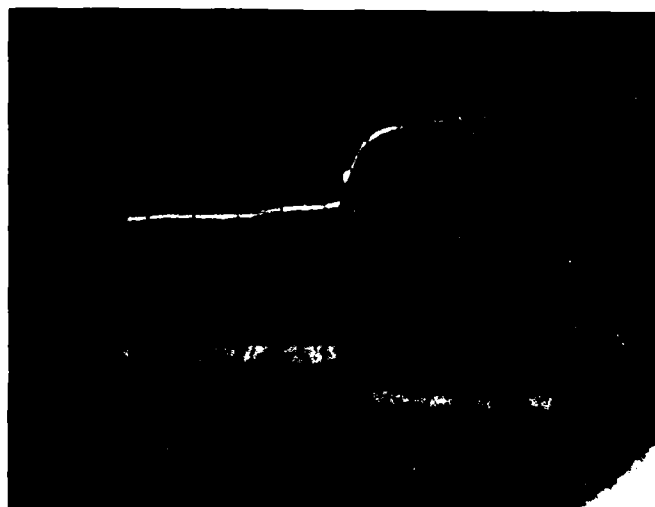
a. One msec/div Time Resolution
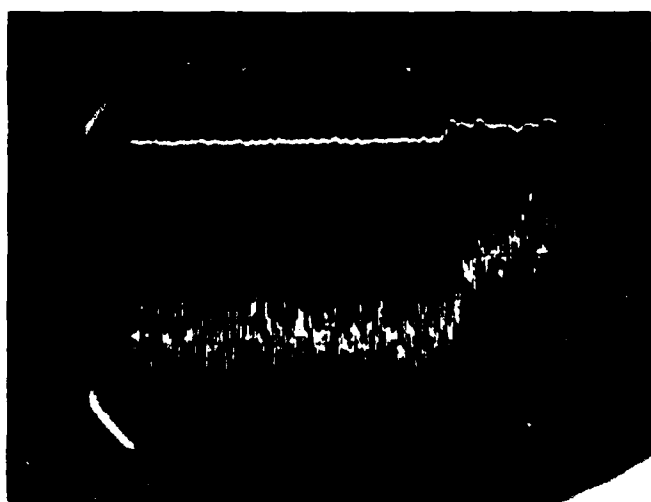
b. Fifty μsec/div Time Resolution

Figure 34. Correlated Electric Field and VHF Radiation as
Recorded on the Ground in the Vicinity of a Return
Stroke at Two Different Time Resolutions (Vertical
Scale is 30 V/m/div.)

77

aircraft FUF is about 3.6 times the ground measurement. A similar relationship was observed when an expansion of the first return stroke was taken. Figures 35a and b show simultaneous waveforms for the first return stroke at the aircraft and on the ground, respectively. The electric field change for the first return stroke was about 42 V/m in the aircraft and about 15 V/m on the ground which gives a ratio of 2.8 between aircraft and ground measurements. That is, the aircraft upper fuselage surface field is enhanced by a factor of about 3 when compared to the ground incident field. The airborne analog data were obtained using two different channels with an overall range from about 20 V/m to about 10,000 V/m. Since 42 V/m is near the lowest detectable level of about 10 V/m, the signal-to-noise ratio in Figure 35a is low and it is difficult to study the fine structure of the airborne return stroke. However, since four different channels were used for the electric field on the ground, a better signal-to-noise ratio can be achieved for lower magnitudes. The ground return stroke waveform in Figure 35b exhibits properties similar to those previously reported in the literature (Refs 6, 7, and 8) and in Figure 25. However, the fast front is about 2 μsec instead of the hundred nanosecond range presented earlier in this report for the high resolution data of 1979 and 1980. It should also be noted that the 500 kHz bandwidth did not limit the risetime for these waveforms. Another important comparison is presented in Figure 36. Figure 36a shows correlated traces of the electric and magnetic field (top and bottom traces, respectively). A wider window of the trace in Figure 35a is shown on the top trace of Figure 36a and

78
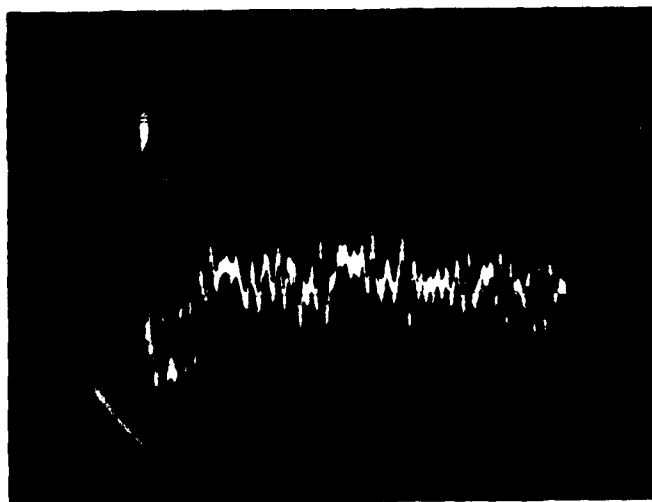
a. Electric Field at the Aircraft
    Vertical Scale: 14 V/m/div
    Horizontal Scale: 10 µs/div
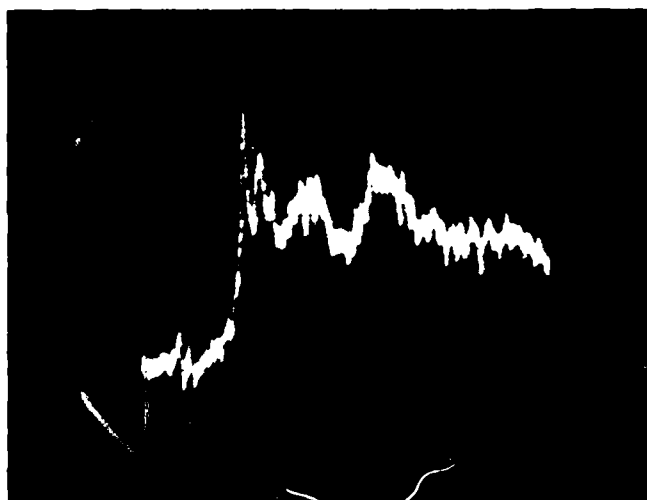
b. Electric Field on the Ground
    Vertical Scale: 3 V/m/div
    Horizontal Scale: 10 µs/div

Figure 35. First Return Stroke as Recorded Analog FM
           Channels with 500 kHz Bandwidth.
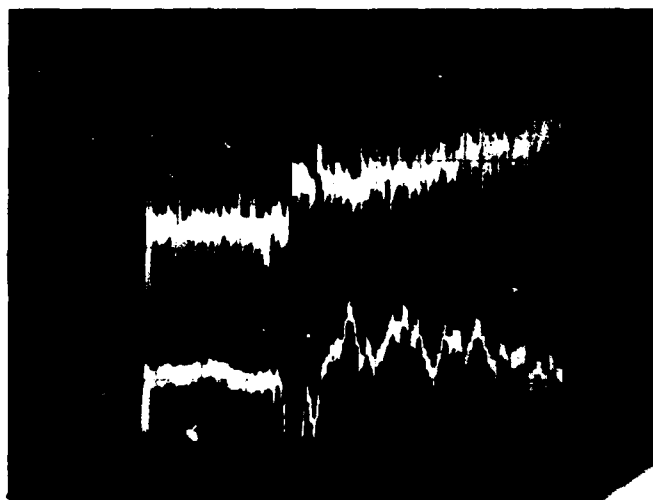
a. Electric (Top Trace) and Magnetic (Bottom Trace) Fields
at 50 μsec/div Resolution. The display of the Magnetic
Field is Saturated at the Time of the Return Stroke.
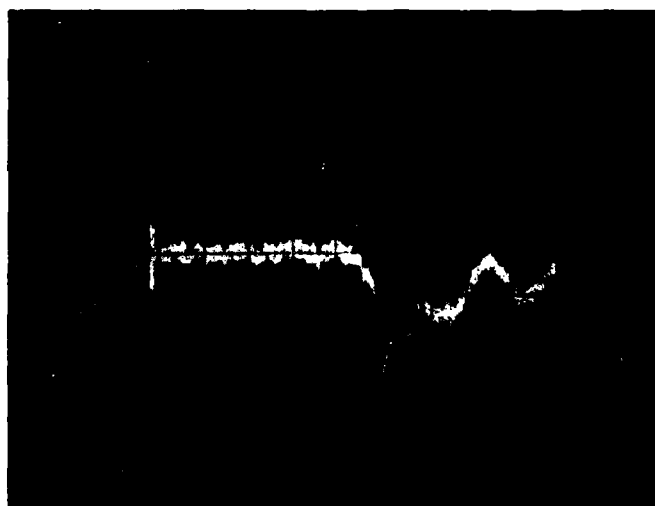
b. Expansion of Magnetic Field Trace (Bottom of a above).
Horizontal Scale is 10 μsec/div.

Figure 36. Correlated Airborne Electric and Magnetic Fields for a
Return Stroke.

80
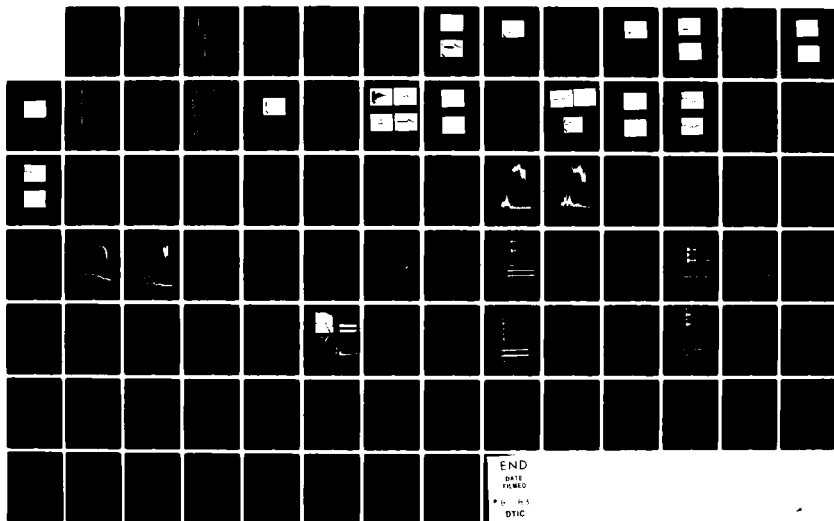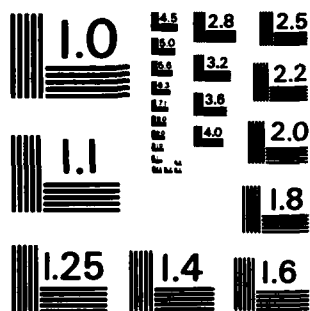
MICROCOPY RESOLUTION TEST CHART

NATIONAL BUREAU OF STANDARDS-1963-A

the corresponding magnetic field recorded on a direct record channel with 1.5 MHz frequency response of an analog tape recorder is shown on the bottom trace. An expansion of the magnetic field is shown in Figure 36b. The return stroke characteristic of the airborne magnetic field with a window of 10 μsec per division in Figure 36b correlates well with the ground electric field in Figure 35b. At 1500 feet it is expected that the incident electric field in the air will be the same as the incident field on the ground for lightning flashes over 20 km away (Ref 35). Indeed, this is the case for these data, except for the relative magnitude of the field. The fact that the airborne readings are about 3 times larger than the ground is because the actual measured field is the surface field on the aircraft which is being enhanced by a factor of about 2.8 with respect to the incident field at the location of the aircraft. The actual aircraft measurements of the field could be corrected by this enhancement factor. However, all the measured airborne quantities in this report represent the surface fields and they are not corrected by the enhancement factor. This enhancement factor of nearly 3 was also verified for two other flashes when simultaneous measurements were taken right over the Cowpens station with the aircraft flying at 5,000 and 8,000 ft MSL.

A high resolution DTR data window was recorded for this flash at about 185 ms prior to the return stroke. Figures 37a and b show correlated waveforms of the electric field and the trigger pulse, respectively. The corresponding electric field pulse at the time of the trigger event is shown with an arrow in
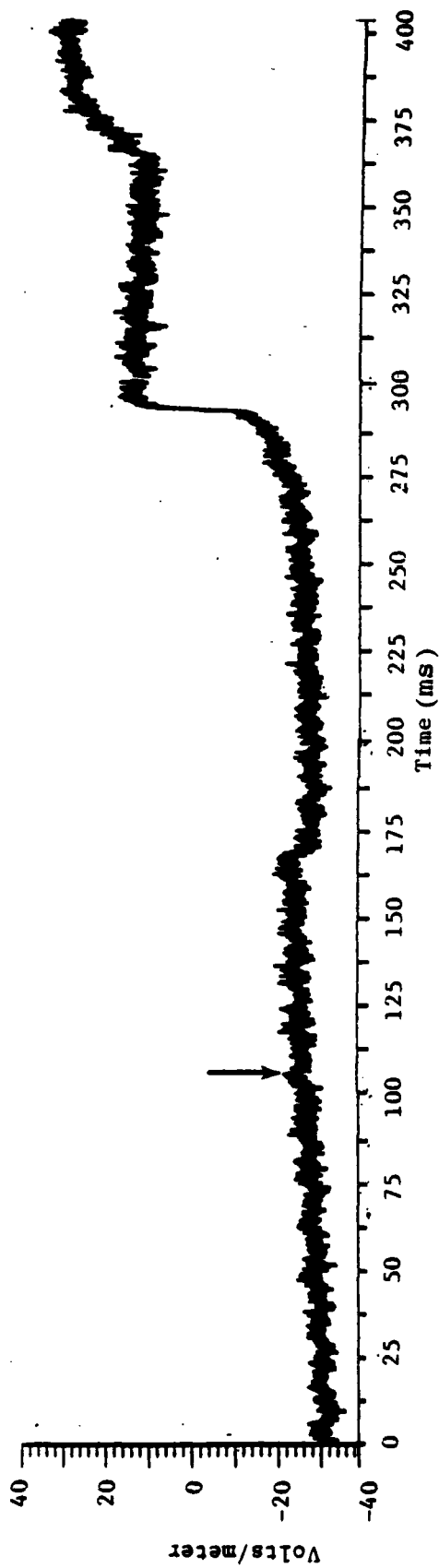
a. Electric Field
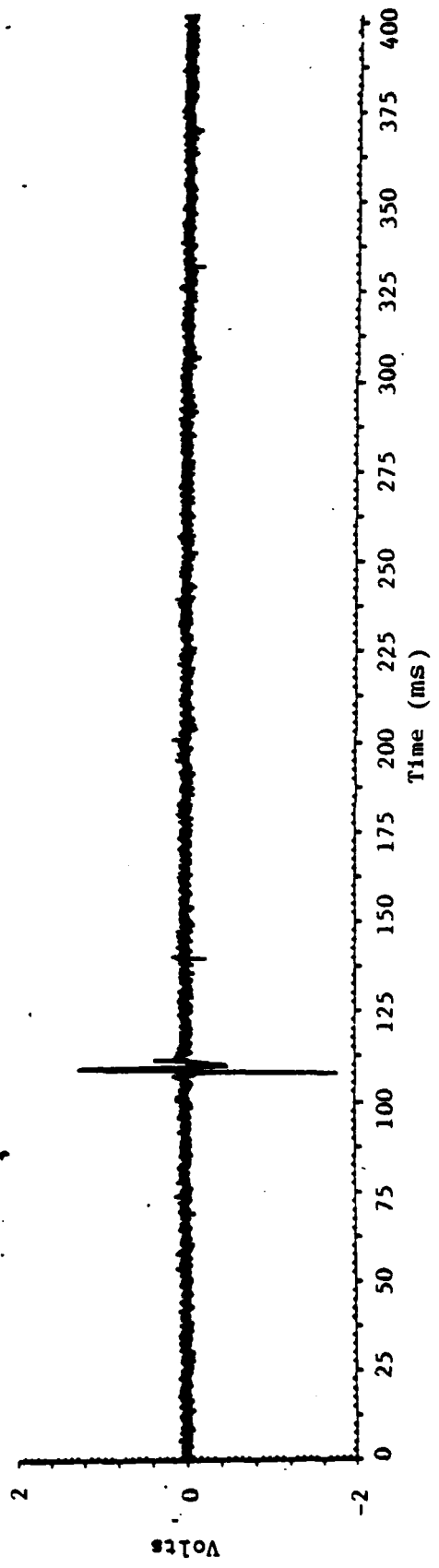
b. Trigger Pulse

Figure 37. Correlated Waveforms for a Flash at 17:47:31 of the Electric Field in the Forward Upper Fuselage and the Trigger Pulse Used by the DTR to Obtain a High Resolution Data Window. Time in Microseconds.

82

Figure 37a. The sensor signal used to trigger the DTR during August 27th was the derivative signal of the Q-Dot sensor located at the aft upper fuselage. Even though the derivative trigger threshold of the DTR detected a pulse on the Q-Dot sensor, no significant change was detected in the electric field at the forward upper fuselage (see Figure 37a at the arrow). The low level of the correlated pulse in the electric field record may be due to different aircraft sensitivity to the various sensors and their respective locations. To ensure that high frequency resolution was available from all the electric and magnetic field sensors, the choice of the trigger signal was varied after each flight to fully study each sensor response.

Three 164 μsec data windows at the time of the trigger are shown in Figure 38. Figure 38a shows the trigger signal from the Q-Dot sensor whereas 38b and c show the same event on the magnetic field sensors oriented physically in the nose-to-tail direction and wing-to-wing direction, respectively. Arrows indicate the actual pulse that triggered the DTR. The first 43 μsec of the data is the amount of time used in the pre-trigger mode. Analysis of the data in Figure 38 shows that the very fast pulse had a risetime of about 200 nsec while the magnitudes of the electric and magnetic fields were on the order of a few V/m and hundredths of A/m, respectively. Since this pulse is of such a small magnitude, it is unlikely that it will produce a hazard to any instrumentation during flight. Similar pulses have been observed by Weidman and Krider (Ref 36). More data have to be analyzed before any conclusion on these pulses can be obtained.

83
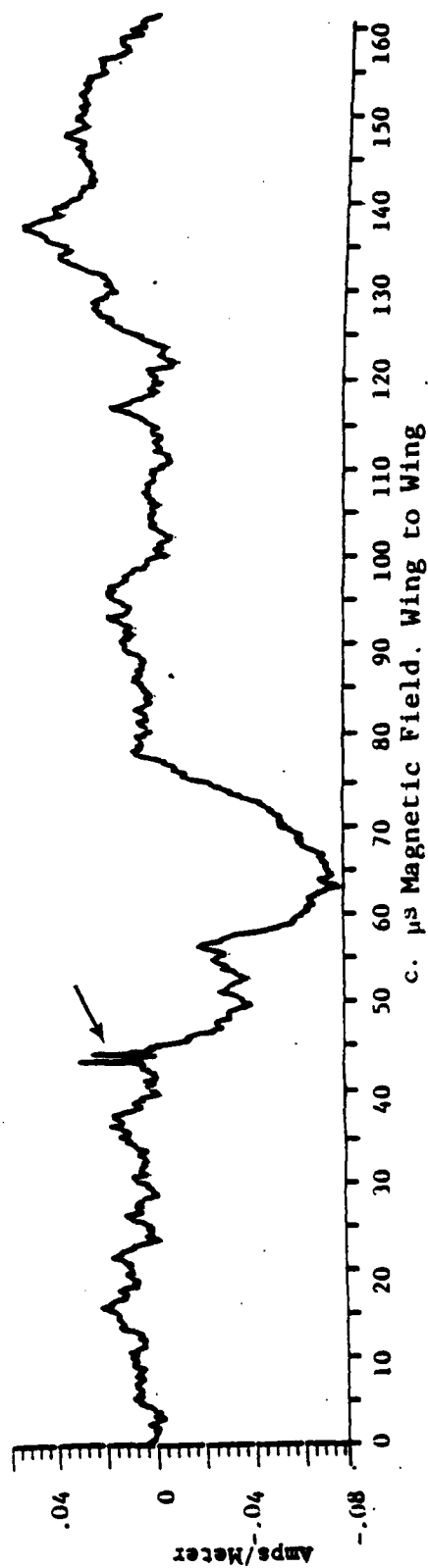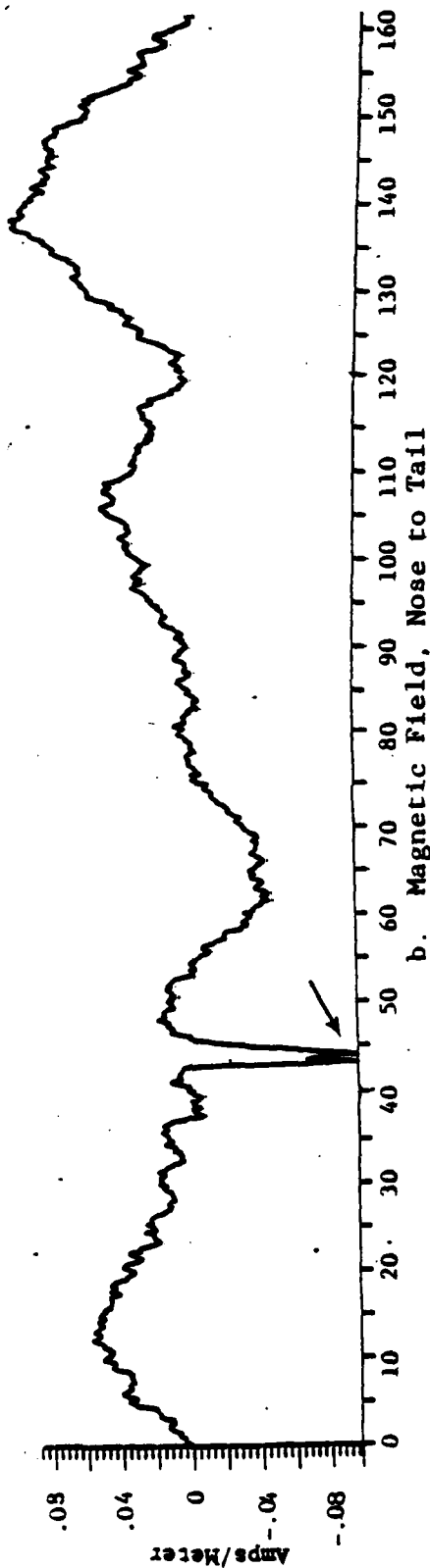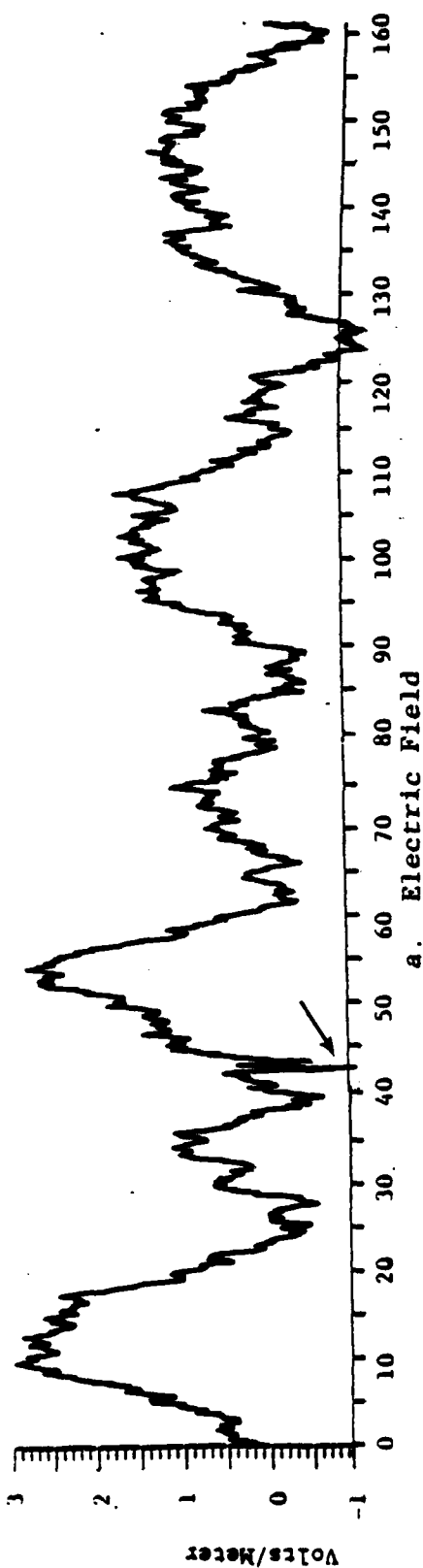
Figure 38. Correlated 164 μsec Data Windows from Three Sensors Obtained in the DTR with 20 MHz Frequency Response at 17:47:32 on 27 Aug 81.

a. Electric Field

b. Magnetic Field, Nose to Tail

c. μ³ Magnetic Field, Wing to Wing

(2) The 174616 Flash, 27 Aug 81

Data analysis was also performed for a flash where the aircraft was located 7 km from the Cowpens site on a heading of 358° degrees at an altitude of 1500 ft. This flash occurred on 27 Aug at 17:46:16. Figure 39 shows the electric field waveform for the entire flash which lasted for about one second and consisted of an intracloud discharge followed by a three stroke cloud-to-ground discharge. From the magnitude of the first stroke of the cloud-to-ground flash, it is apparent that the flash was about 10 km from the Cowpens site. Since the aircraft was 7 km from the ground site, it is impossible to make any magnitude comparison between the electric field recorded on the aircraft, Fig 39a, and on the ground, Fig 39b. It appears that the flash was much closer to the ground site. However, the structure of the waveform can be correlated. It is noted that for several seconds prior to the beginning of the intracloud discharge, halfway through the trace in Figure 39a, there are some variations in the electric field record detected by the aircraft. This electric field change has to be produced by variation of the charge in the vicinity of the aircraft but probably is not related to the flash being analyzed. A strong implication that this is the case can be made by noting that this field change is not detected at the ground site. An expansion of Figure 39a is given in Figure 40 where the variation in the electric field is observed for two seconds prior to the discharge. The total field change during this time exceeds 10%

a. Electric Field Recorded at the Aircraft.

b. Electric Field Recorded on the Ground.

Figure 39. Airborne and Ground Electric Fields Recorded on 27 Aug 81 at 17:46:10. (Vertical Scale - 110 V/m/div., Horizontal Scale - 500 ms/div.)

Figure 40. Expanded Magnitude Scale of the Airborne Electric
Field Record of Figure 39(a). Horizontal Scale -
500 msec/div. Vertical Scale - 30 V/m/div.

of the field change (about 15 V/m) during the first stroke and is probably caused by static electrification of the aircraft. Since this flash was probably located about 10 km away from the aircraft, the field change of 15 V/m due to charge transfer in the neighborhood of the aircraft surface had nothing to do with the occurrence of the flash. It would be important to determine how high the field change in the vicinity of the aircraft must be before it can trigger a lightning flash which will transfer charge with the surrounding medium. This question is discussed later in this report. An answer to this question might be obtained experimentally in this program by analyzing a large amount of data.

Figure 41 shows correlated waveforms of the ground electric field and VHF radiation in the neighborhood of the first return stroke. The total duration of the fast discontinuity during the return stroke is about 2 ms. However, the sharp part of the waveform which has a discontinuous trace on Figure 41 only represents about 20% of the total field change. A sharp discontinuity in the electric field record is also observed about 50 ms after the first return stroke. This discontinuity is referred to in the literature as a K change (Ref 37). Both the return stroke and the K-change have correlated VHF pulses. More details on the correlation for the first return stroke are shown in Figure 42. Charge appears to be transferred through the channel for more than one millisecond after the sharp discontinuity of the return stroke. The VHF radiation starts tens of microseconds before the return stroke and continues for about 1.5 ms, ending with
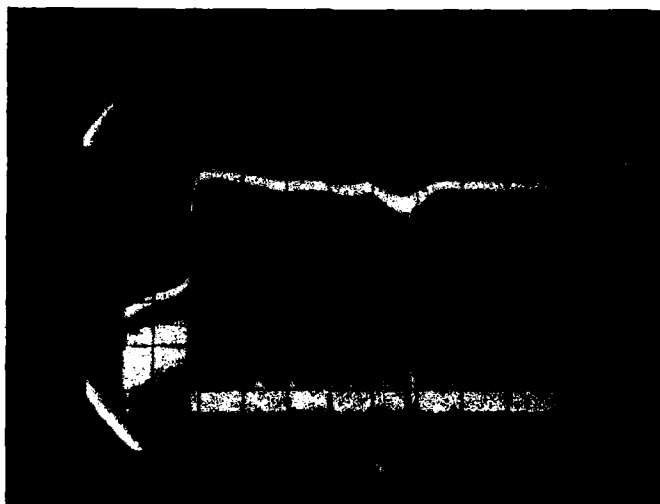
Figure 41. Expanded View of the Electric Field and the Correlated VHF Radiation in the Neighborhood of the First Return Stroke. The Time Scale is 10 ms/div. The Magnitude Scale for the Electric Field is 30 V/m per Division.
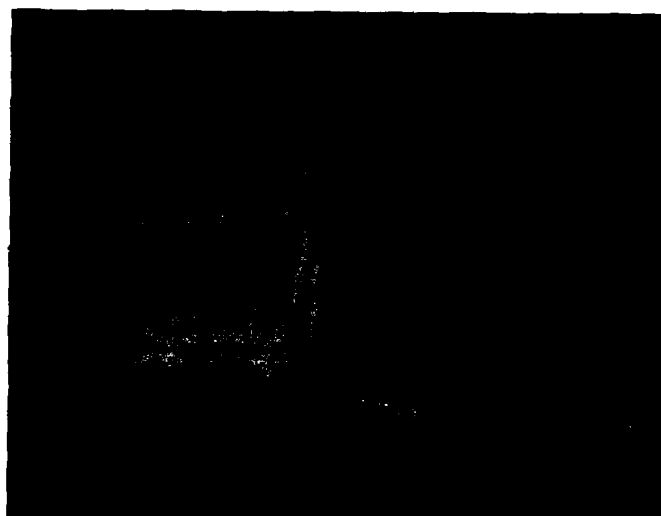
a. Vertical Scale: 30 V/m/div.
   Horizontal Scale: 0.5 ms/div.
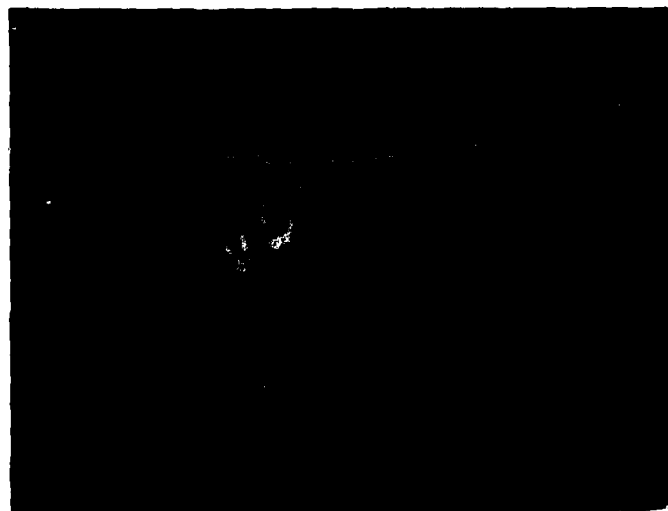
b. Expanded View of (a).
   Vertical Scale: 30 V/m/div.
   Horizontal Scale: 50 μsec/div.

Figure ⁴² Co⁻ ...ated Electric Field and VHF Radiation in
         th. Vicinity of the First Return Stroke.

another VHF pulse. This large pulse is probably caused by expansion of the return stroke channel into virgin air above the stepped leader-return stroke charge location.

Figure 43 shows correlated waveforms for the return stroke for the airborne (a) and ground systems (b). The magnitude of field change and structure of the waveform during the field change is very similar for both systems. Since the aircraft was located about 7 km from the Cowpens site, it is suspected that the lightning channel was about equal distance from both sides. The risetime for these waveforms is about two microseconds and their properties are similar to those reported for first return strokes (Refs 6 and 8). Figure 44 shows correlated waveforms of the airborne electric and magnetic field in a window of 100 μsec per division. The magnetic field fast field change cannot be fully observed but it has a similar risetime to the electric field. After this first fast magnetic field change there is a large pulse with a risetime of about 50 msec. This pulse does not correlate with the electric field record or the ground VHF radiation.

Figure 45 shows the correlation between the airborne electric field record (a) and the trigger pulse (b). The DTR recorded an event about 10 msec prior to the return stroke. There does not appear to be a significant pulse in the electric field record which can be correlated to the triggered event but the risetime of the triggered pulse is less than 100 nsec. An arrow is drawn in Figure 45a at the time of the triggered event. However, the trigger was obtained based on the Q-Dot sensors. Figure 46 (a), (b) and (c) shows an expanded view of the DTR data

91
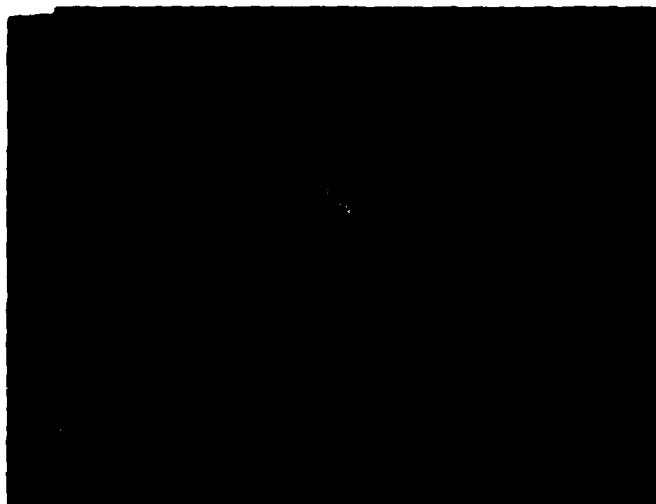
a. Electric Field at the Aircraft

b. Electric Field on the Ground

Figure 43. Correlated Ground and Airborne Electric Fields During the
Sharpest Discontinuities of the First Return Stroke
Vertical Scale - 14 V/m/div. Horizontal Scale -
10 µsec/div.

Figure 44. Correlated Waveforms of the Electric and
Magnetic Field Recorded at the Aircraft
during the First Return Stroke. Vertical
Electric Field Scale: 28 V/m/div. Horizontal
Scale: 100 μsec/div.

40

20

0

−20

−40

volts/meter

0 25 50 75 100 125 150 175 200 225 250 275 300 325 350 375 400

Time, Milliseconds

a. Electric Field

2

1.6

0.8

0

−0.8

−1.6

−2

volts

0 25 50 75 100 125 150 175 200 225 250 275 300 325 350 375 400

Time, milliseconds

b. DTR Trigger Pulse
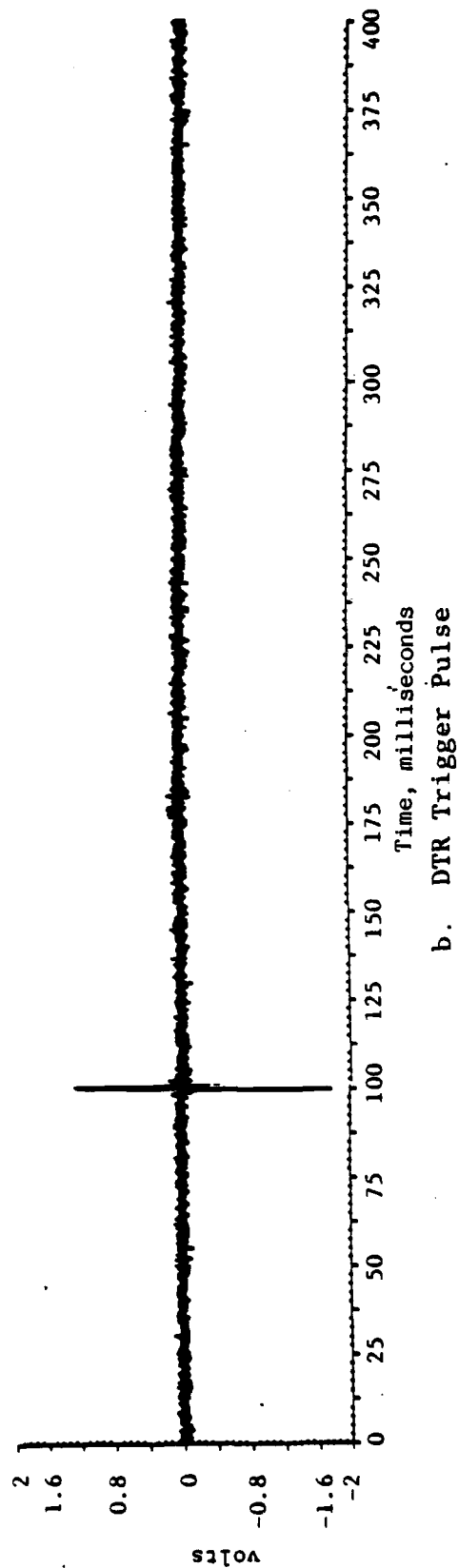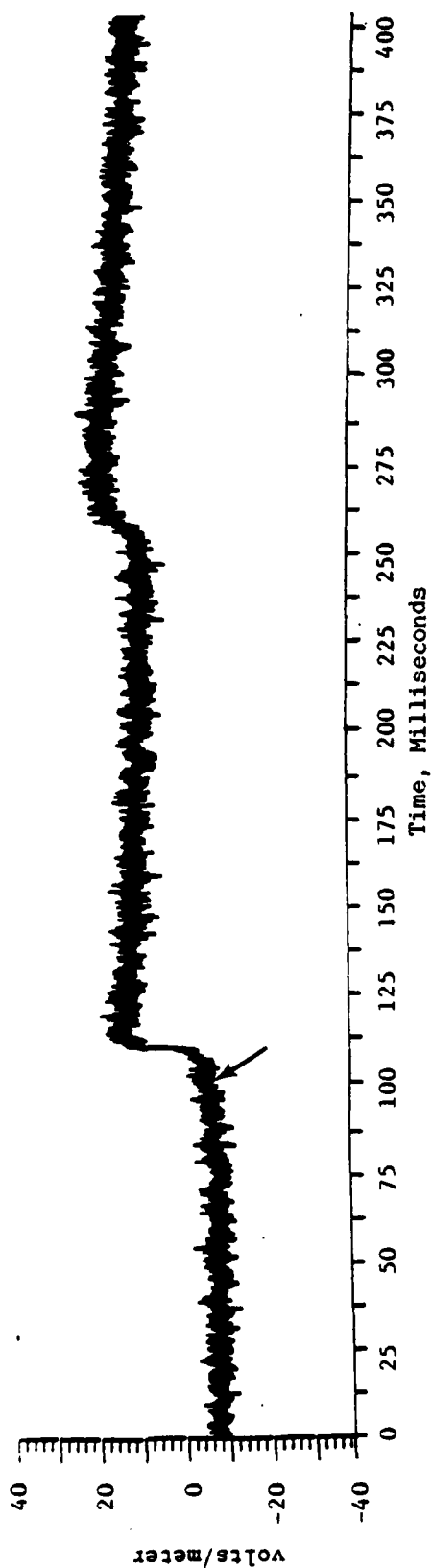
Figure 45. Correlated Waveforms of the Electric Field on the
Forward Upper Fuselage (Top) and the Triggered
Pulse (Bottom) used by the DTR to Obtain a High
Resolution Window for a Flash at 17:46:16 on 27 Aug 81.

94

window at the time of the trigger for this flash. An arrow drawn at 43.8 μsec after the beginning of the record shows the pulse that triggered the DTR system. The electric field record from the aft upper fuselage in Figure 46a shows a ten to twenty microsecond wide pulse with superimposed pulses ranging from fractions of microseconds to about five microseconds. Since most of the pulses observed in Figure 46a through c are within the noise level, no conclusions are made about their possible significance. However, this technique illustrates some of the pulses that can be recorded in a derivative triggered system.

Next, an analysis is presented for some of the correlated data collected on August 25, 1981. During this flight the aircraft flew at its normal altitude of about 15,000 feet but some data were collected at 8000 and 5000 feet. Some results for the data collected for flashes at the lower two altitudes are presented and discussed.

(3)   The 164048 Flash, 25 Aug 81

At 16:40:48, a lightning flash was recorded when the aircraft was right over the Cowpens station at an altitude of 5000 feet. The airborne electric field record for this flash is shown in Figure 47. From this figure it appears that the lightning was a cloud-to-ground flash with four return strokes. However, the time between the return strokes was almost 200 msec. This interval is generally too large for the return stroke channel to have stayed ionized (Ref. 37), and each return stroke is likely to have its own stepped leader (see flash at 18:18:07, Ref. 12). The airborne and ground analog records near the first
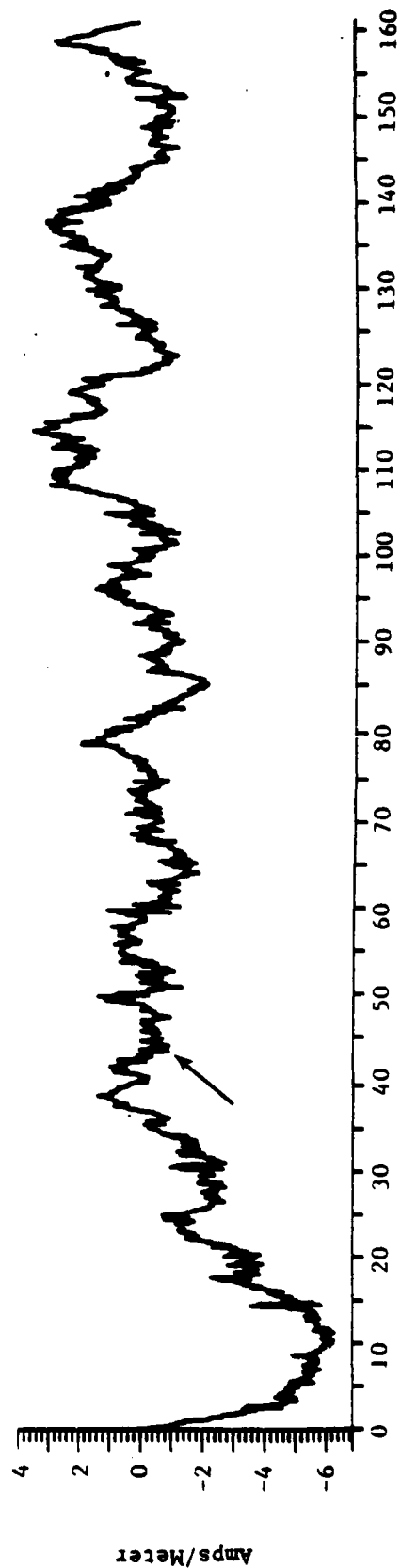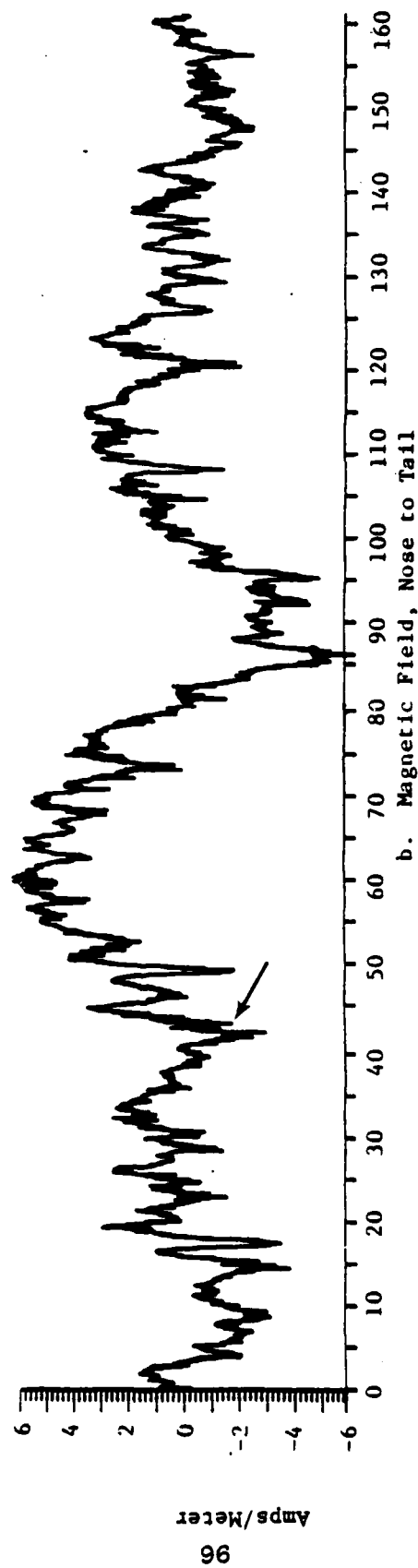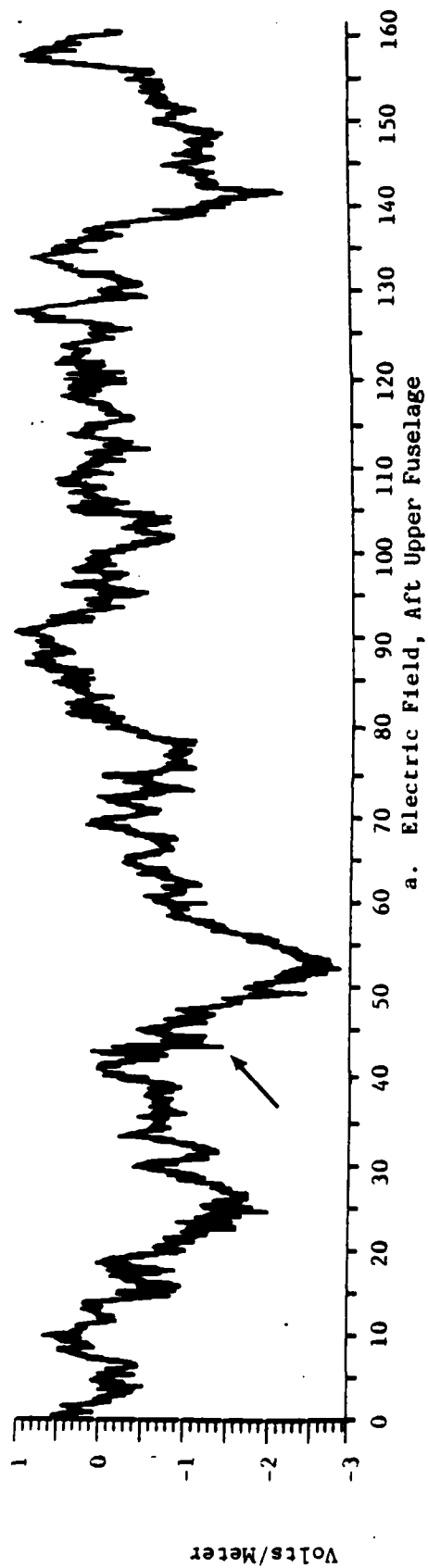
Figure 46. Correlated 164 Microsecond Data Window from Three Sensors Obtained at 17:46:16 on August 27, 1981

a. Electric Field, Aft Upper Fuselage

b. Magnetic Field, Nose to Tail

c. Magnetic Field, Wing to Wing

Volts/Meter

Amps/Meter

Amps/Meter

96
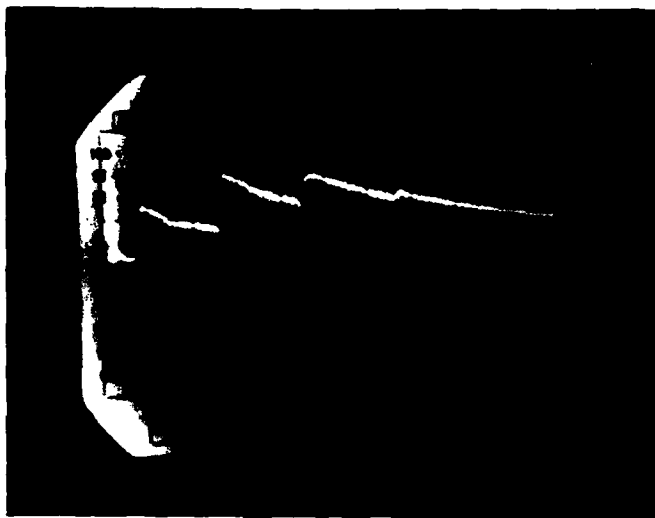
Figure 47. Airborne Electric Field for a Flash at
16:40:48 on 25 Aug 81. Horizontal
Scale is 200 msec/div.

97

return stroke were expanded to observe the electric field record. Figure 48 compares correlated airborne and ground analog records during the first return stroke. The fast transition of the electric field record corresponded to less than 50% of the overall field change which is similar to the two flashes previously discussed. The actual risetime of the fast transition in the airborne record of Figure 48 is in the order of a few microseconds. These results were also obtained in the ground electric field, as shown in Figure 48 (d).

(4) The 165414 Flash, 25 Aug 81

At 16:54:14, when the aircraft was at 7 km from the Cowpens site at an altitude of 8300 feet, a lightning flash was recorded. Figure 49 shows correlated electric field records with 100 msec/div as recorded in the aircraft (a) and at the ground station (b). The upper trace in Figure 49(a) is the trigger pulse which occurred during the first return stroke. From observation of the electric field record it appears that the flash consisted of an intracloud discharge which lasted for about 300 msec followed by a cloud-to-ground flash with three return strokes. The intracloud portion of the discharge has a negative going discontinuity in contrast with positive going discontinuities due to the return strokes which lower negative charge to ground. Expanding the electric field record in the area of this discontinuity, it was observed that this discontinuity lasted tens of milliseconds. Therefore, it was concluded that this discontinuity was not related to a positive return stroke to ground but to a process inside the cloud. An expansion was made of the ground electric field record with 500 kHz bandwidth in the
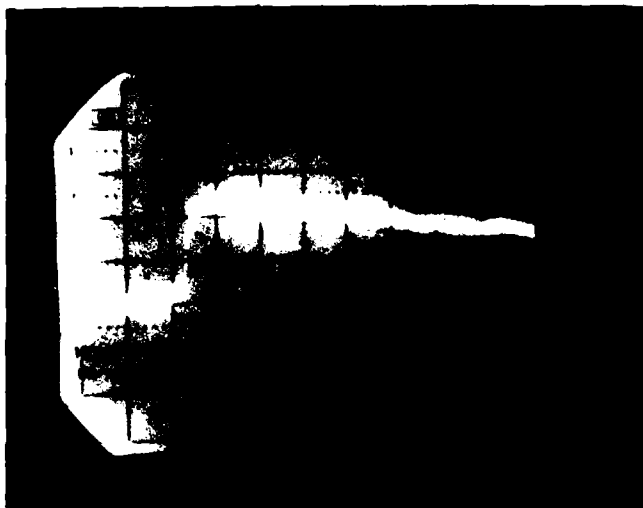
a. Airborne Electric Field
   Horizontal Scale: 10 msec/div
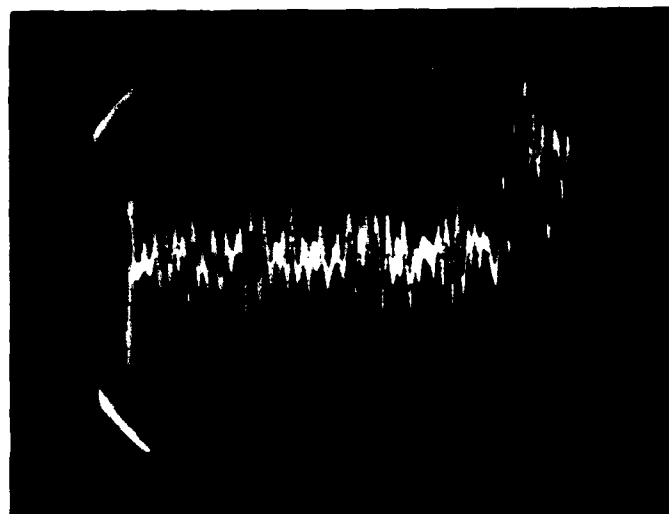
c. Airborne Electric Field
   Horizontal Scale: 10 µsec/div

b. Ground Electric Field (Top Trace)
   and Correlated VHF Radiation
   Horizontal Scale: 10 msec/div.

d. Ground Electric Field
   Horizontal Scale: 100 µsec/div

Figure 48.   Comparison of Airborne and Ground Records for a First
             Return Stroke at 16:40:48 on 25 Aug 81
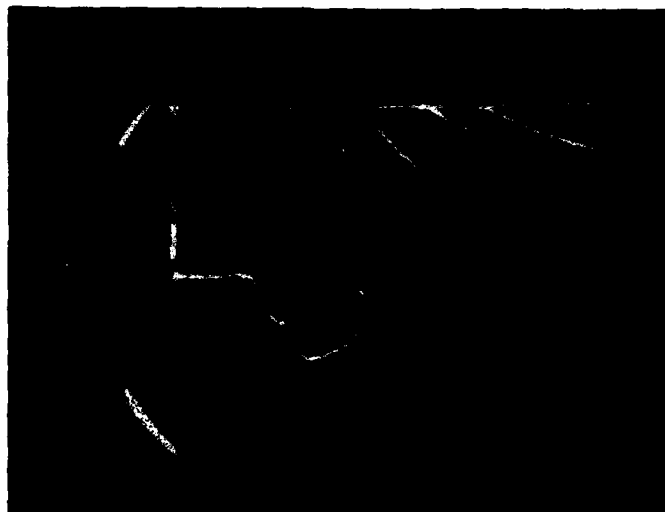
a. Airborne Electric Field. The Top Trace with a Discontinuity at the Time of the Return Stroke Shows the Trigger Pulse. Vertical Scale:120 V/m/div.

b. Ground Electric Field. Vertical Scale: 80 V/m/div.

Figure 49. Comparison of Electric Field at 8300 Ft Altitude and Ground Electric Field at 16:54:14 on 25 Aug 81. Horizontal Scale - 100 ms/div.

100

FM channel and the airborne DTR record with 20 MHz bandwidth. The first return stroke is compared in Figures 50(a), (b), and (c) using a scale of 80 μsec and 8 μsec per division for the airborne data and 50 μsec per division for the ground data. The characteristics of the return stroke recorded in the aircraft with 20 MHz bandwidth are comparable to the ground recording with 500 kHz bandwidth. The risetime for this event was calculated using the technique previously explained for the 1979 and 1980 DTR data. The risetime for the return stroke was about one microsecond, which is longer than those summarized in Figure 27.

(5)   The 162855 Flash, 25 Aug 81

At 16:28:55, a seven stroke cloud-to-ground lightning flash was recorded simultaneously at the aircraft and ground stations. The aircraft was located 20 km away from the Cowpens site at an altitude of 11,000 ft. Figure 51 shows the electric field record of the entire flash as recorded in the continuous recording analog tapes with 2 MHz response in the aircraft and at the ground sites. The first three return strokes in the flash were preceded by stepped leaders. These return strokes had risetimes of 400 nsec, 500 nsec, and 2 μsec. The first two return stroke risetimes might have been bandlimited by the 2 MHz frequency response. The fifth return stroke in the flash was captured by the 20 MHz Digital Transient Recorder (DTR). Looking at all the analog records, it appears that the fifth return stroke has the fastest risetime. The risetime of the fastest part of the fifth return stroke is about 100 nsec. Figure 52 shows correlated records of the electric and magnetic fields in

101
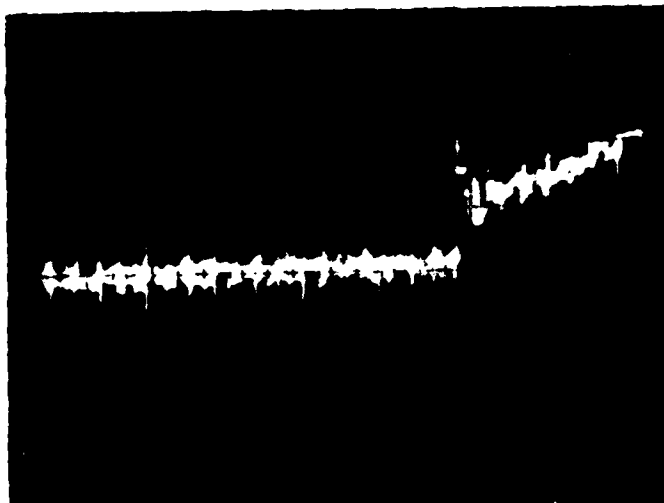
a. Airborne Electric Field DTR Record
   Vertical Scale: 30 V/m/div.
   Horizontal Scale: 80 μsec/div.
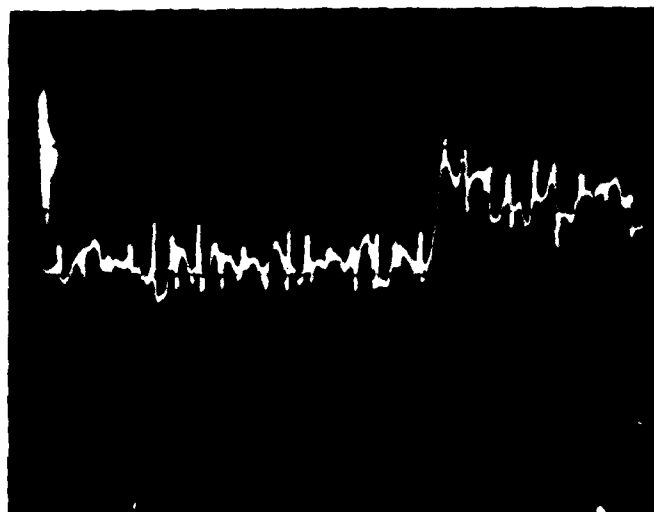
b. Airborne Electric Field DTR Record
   Vertical Scale: 30 V/m/div.
   Horizontal Scale: 8 μsec/div.

C. Ground Electric Field Analog Record
   Veritcal Scale: 20 V/m/div.
   Horizontal Scale: 50 μsec/div.

Figure 50.   Comparison of an Airborne Electric Field DTR Record
to the Corresponding Ground Electric Field Analog Record.

102
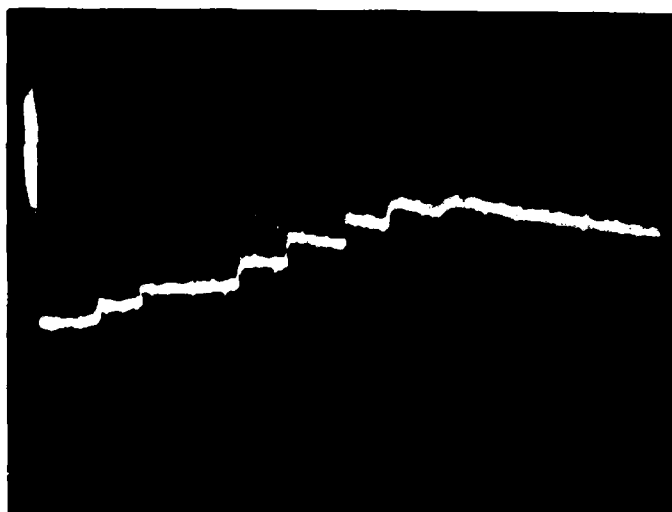
a. Airborne Electric Field
   Horizontal Scale 82 ms/div
   Vertical Scale 600 V/m
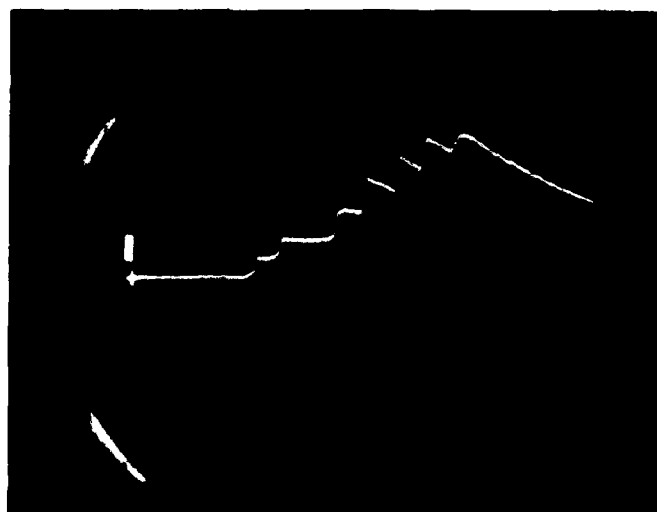
b. Ground Electric Field
   Horizontal Scale 100 ms/div
   Vertical Scale 30 V/m

Figure 51. Comparison of Airborne and Ground Records for
the 162855 Flash on 25 Aug 81.

103
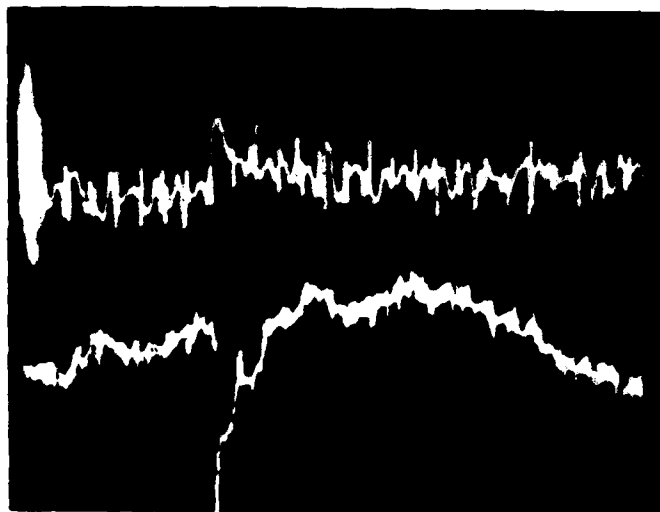
a. Airborne Electric Field Record (Top)
    and Airborne Magnetic Field Record
    (Bottom). Horizontal Scale 16 μsec/div
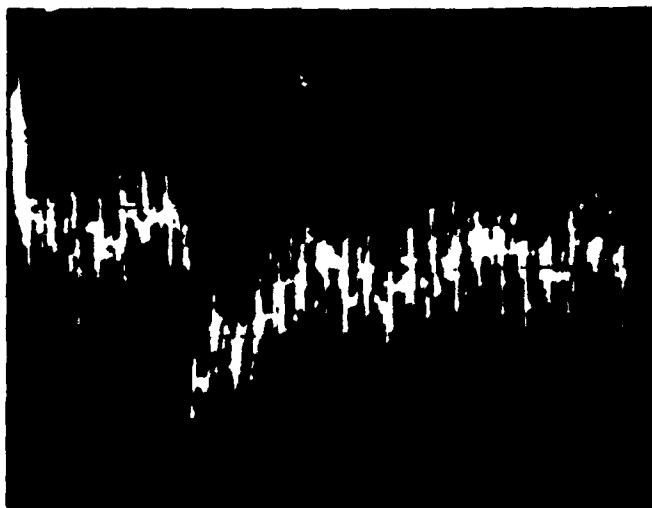
b. Ground Electric Field
    Horizontal Scale 16 μsec/div

Figure 52. Comparison of Airborne Electric and Magnetic
            Fields (a) and Ground Electric Field (b) for
            the Fifth Return Stroke at 16:28:55 on
            25 Aug 81.

the aircraft (Fig 52a) and the electric field on the ground for the fifth return stroke with a scale of 16 μsec/div. An expansion of the magnetic field for the fifth return stroke obtained from the 20 MHz digital recorder is shown in Figure 53 with scales of 4 μsec/div and 400 nsec/div.

We also compared the correlated return stroke electric fields for all the other return strokes in the flash based on the data obtained in the analog records. The airborne and ground electric field records are very similar as observed in Figure 52. This is the expected result in the far field.

Figure 54 shows a comparison of the ground electric field and the correlated airborne magnetic field for the second return stroke. As may often be the case due to the relative location of the flash, the B-field waveform is inverted with respect to the E-field but the structure of the waveforms is the same.

(6) Summary of the Correlated Ground/Airborne Electric and Magnetic Field Records

In the previous sections correlated electric and magnetic field records were presented for five lightning flashes that occurred when the flash was within 35 km of the aircraft and the Cowpens site. It was shown experimentally that the ground and airborne electric and magnetic field waveforms produced by lightning had similar characteristics. However, the magnitude of the surface field in the air is usually two or three times larger than the incident field recorded on the ground. It was shown that the risetime observed in the airborne and ground electric field records during return strokes varies from about 100 nsec to several microseconds. Even though the return stroke pulses are

105
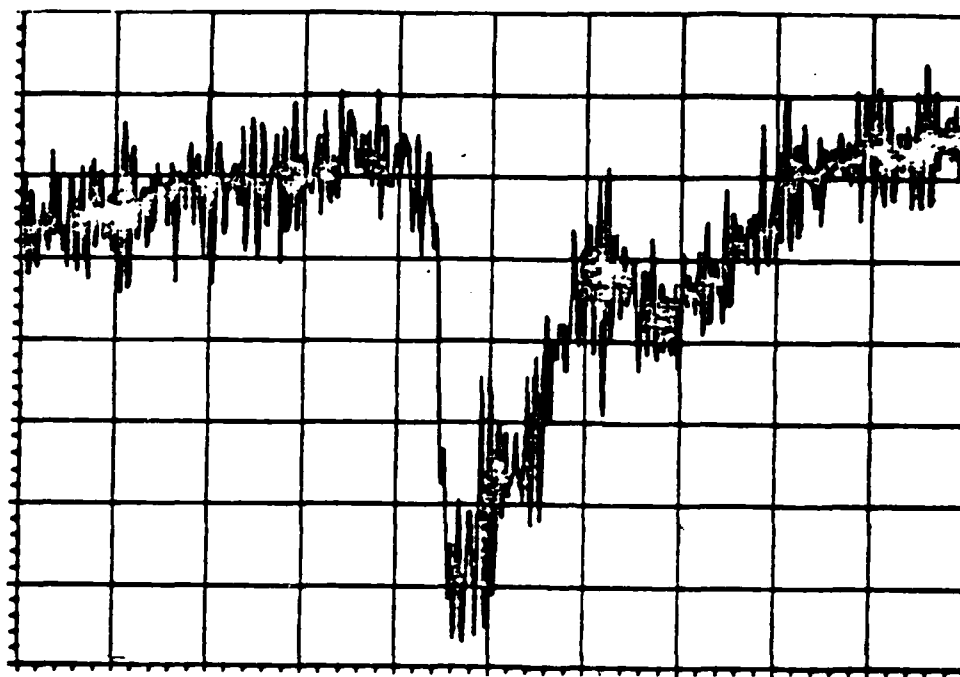
(a)
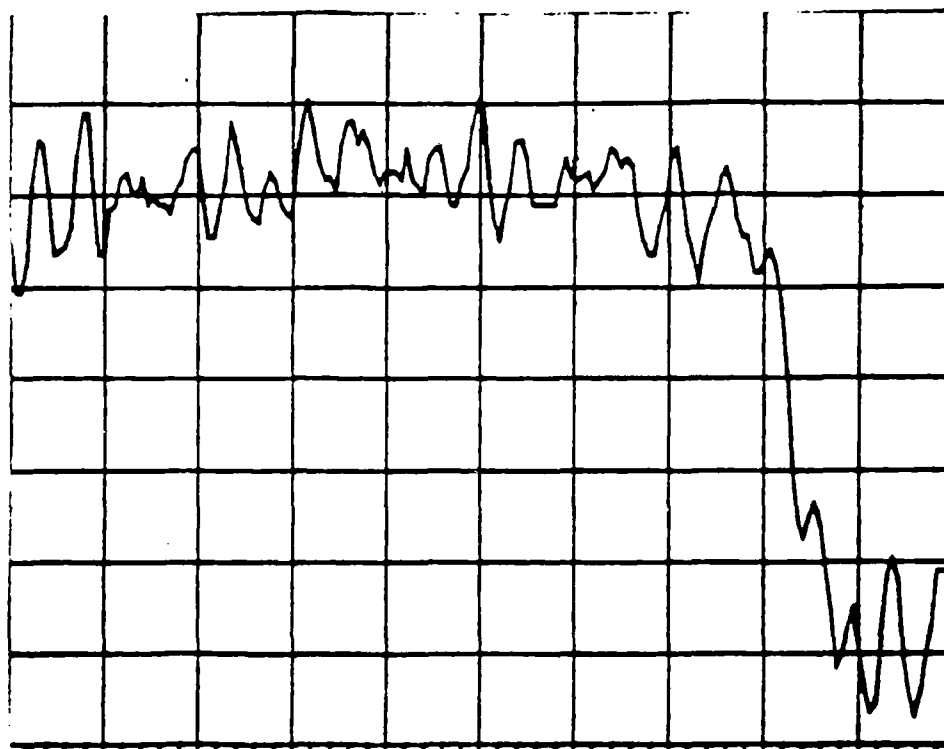
(b)

Figure 53. Magnetic Field Recorded in the Airborne DTR during
the Fifth Return Stroke (a) Scale: 4 usec/div
(b) Scale: 400 nsec/div.

-->|div ↓--
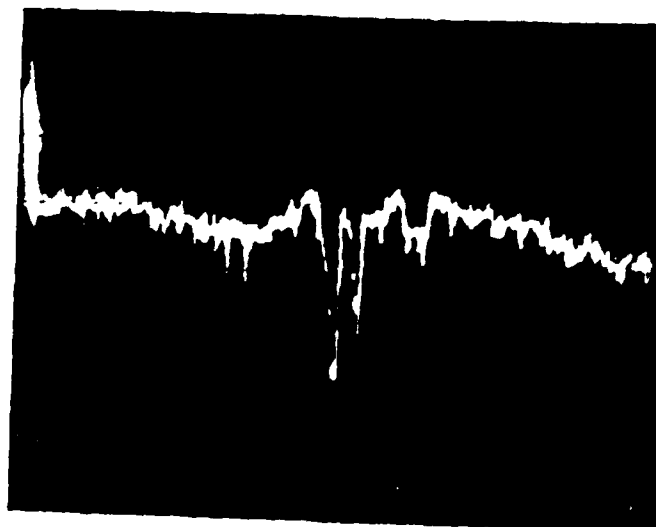
a. Airborne Magnetic Field.
   Scale 15 μsec/div
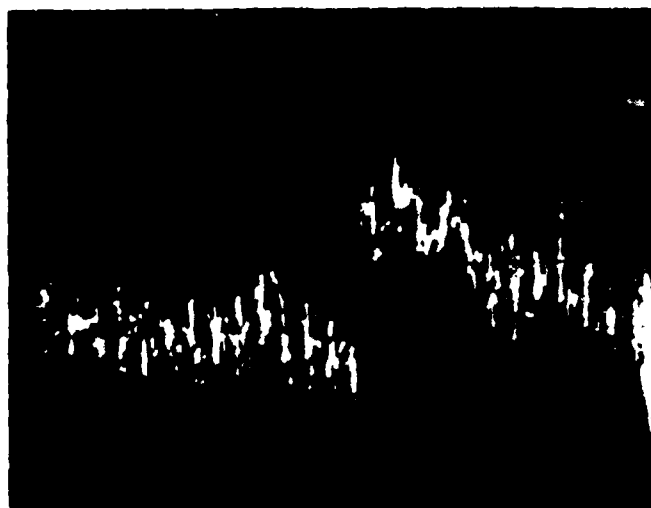
-->|div |←-

b. Ground Electric Field
   Scale 16 μsec/div

Figure 54.   Correlated Airborne Magnetic Field and Ground
             Electric Field for the Second Return Stroke
             in Flash at 16:28:55 on 25 Aug 81.

107

the largest pulses encountered in the electromagnetic field records, they are not necessarily the fastest pulses. We have observed many pulses faster than return strokes during the preliminary breakdown, the leader phase, the J-change process, and the intracloud discharge. The risetimes of these pulses are on the order of tens of nanoseconds. Derivative trigger devices used to capture a time domain window with a larger bandwidth will often trigger on events other than return strokes. For two of the five flashes previously discussed the 20 MHz data window was obtained 185 msec and 10 msec prior to the return stroke (174731 and 174616). Digital data were shown also for the first return stroke in flash 165414 and for the fifth return stroke in flash 162855. Flash 164048 did not have any DTR window during the duration of the event. In 1981 about 1200 of the 5193 data windows displayed in the ten channel DTR were return strokes. Next, an analysis is presented for some return strokes measured when the aircraft was not close enough to the ground station to permit collection of simultaneous ground and airborne data.

   c.   Analysis of Airborne Electric and Magnetic Field Records

It was not always possible to predict at what time thunderstorms would develop around the Cowpens ground site and to have the aircraft collecting data at that time. Once the aircraft was airborne and if no thunderstorms were found near the ground site, the aircraft was directed to find a thunderstorm within 300 km of the Miami airport and collect data at an altitude of 16,000 ft. In this section a discussion of some of the data is presented for two of these days: 16 July and 26 Aug,

1981. The DTR was set to trigger only on very large values so that most of the data obtained in the·20 MHz, 8192 sample data windows were return strokes.

(1) First Return Stokes

Figures 55 and 56 represent typical electric and magnetic field data during first return strokes. From the airborne radar, the thunderstorm cell was estimated to be about 20 km from the aircraft in Figure 55 and about 5 km in Figure 56. The risetimes were measured in the fastest portion of the return stroke waveforms, which is to the right of the marks shown in the graphs. In Figure 55 the risetimes were 287 nsec for the E-field and 352 nsec for the H-field. In Figure 56 the risetimes were 162 nsec for the E-field and 304 nsec for the H-field. As is the case for all first return strokes when a pre-trigger period can be observed, the last few stepped leaders pulses can be observed prior to the return stroke. The last stepped leader pulse in Figures 55 and 56 were 6 and 7 µsec prior to the return stroke, respectively. The previous stepped leader pulses observed in Figure 55 were between 5 to 7 µsec apart but in Figure 56 were about 12 µsec apart.

Fifty-five first return strokes captured in digital windows on 16 July and 26 Aug have been analyzed for risetime. Risetimes for the electric and magnetic fields of the 26 strokes collected on 16 July are displayed in a histogram in Figure 57. They average 355 nsec and 372 nsec, respectively. Similar data for the 29 strokes collected on 26 Aug are shown in Figure 58. Average risetime for these electric fields is 170 nsec and for the magnetic fields, 218 nsec. The fact that the data for 26 Aug

FIGURE 55. TYPICAL FIRST RETURN STROKE MAGNETIC FIELD (TOP) AND ELECTRIC FIELD (BOTTOM) WAVEFORMS FROM A FLASH AT A DISTANCE OF ABOUT 20 KM.

FIGURE 56. TYPICAL FIRST RETURN STROKE MAGNETIC FIELD (TOP) AND ELECTRIC FIELD (BOTTOM) WAVEFORMS FROM A FLASH AT A DISTANCE OF ABOUT 5 KM.

Number

Microseconds Risetime
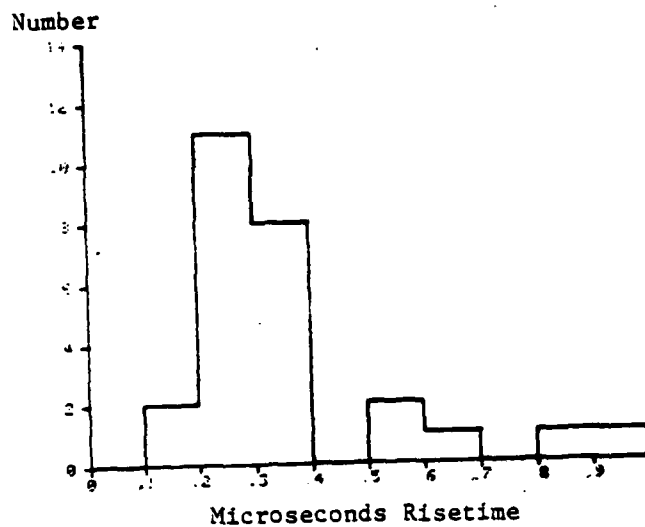
Figure 57a. Risetimes of E-Field Waveforms from 26
First Return Strokes During a Florida
Thunderstorm on 16 Jul 81.

Number

Microseconds Risetime
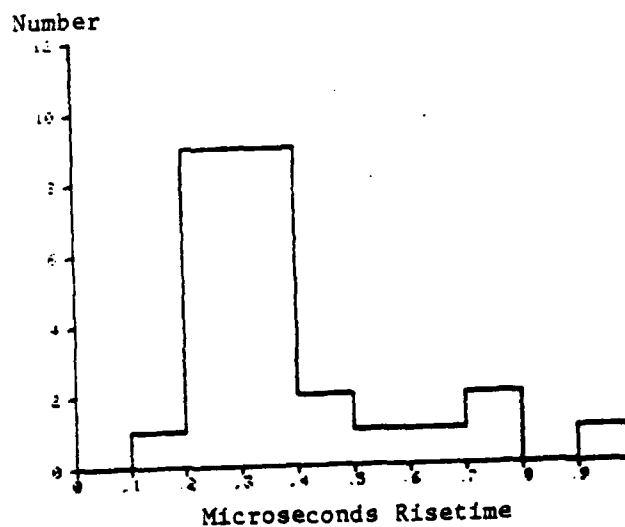
Figure 57b. Risetimes of H-Field Waveforms from 26
First Return Strokes During a Florida
Thunderstorm on 16 Jul 81.

Number

Microseconds Risetime
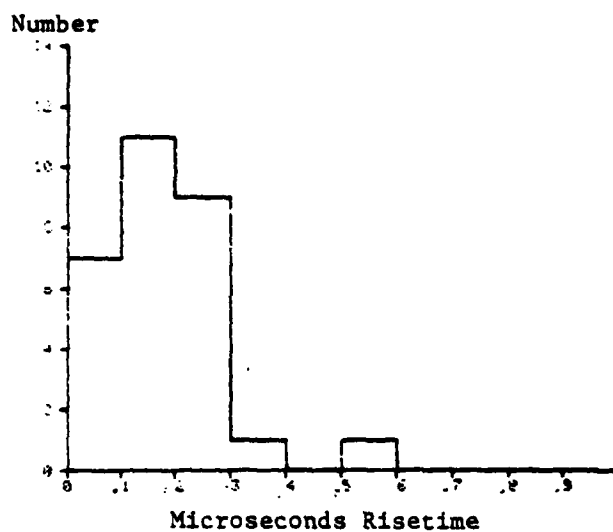
Figure 58a.   Risetimes of E-Field Waveforms from 29
First Return Strokes During a Florida
Thunderstorm on 26 Aug   81.

Number

Microseconds Risetime
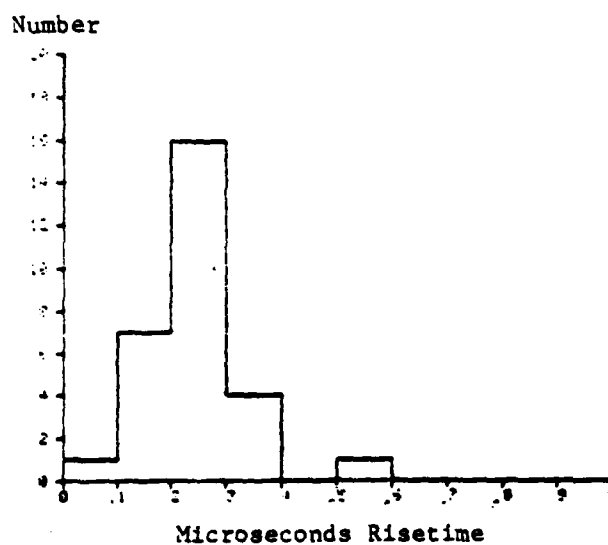
Figure 58b.   Risetimes of H-Field Waveforms from 29
First Return Strokes During a Florida
Thunderstorm on 26 Aug   1981.

113

has considerably faster risetimes probably indicates a degree of variability in the intensity of Florida thunderstorms.

Figures 59 and 60 show the FFTs of the electric and magnetic field data displayed in Figure 56. The flash occurred at a distance of about 5 km from the aircraft. Figures 59(a) and 60(a) were obtained using the technique described in Section IV except that the FFTs were determined directly from the derivative data. The data in Figures 59 and 60 are typical representation of many FFT's obtained for return strokes between 3 to 7 km from the aircraft. Since this is derivative data, to be comparable to Figure 31 the spectrum should be constant up to about 2 MHz and decay as $1/f$ from 2 MHz to 25 MHz. This is very much the case in Figure 59 and 60 except that a resonance in the frequency spectrum occurs between 2 and 5 MHz. Comparable to Figure 31, above 5 MHz the spectrum decreases at a rate faster than $1/f$. The variation in the frequency spectrum from 1 to 14 MHz are expanded in linear plots in Figures 59(b) and 60(b). Before an interpretation of this pattern is provided, it is important to indicate that the FFTs of all the electromagnetic fields produced by return strokes measured in the aircraft at distances greater than about 10 km during the 1981 program showed similar characteristics to those described in Section IV and summarized in Figure 31.

A possible interpretation of the behavior of the FFT as a function of distance can be provided by the aircraft resonances. Assume that the aircraft can be modeled as an RLC circuit with transfer function

114
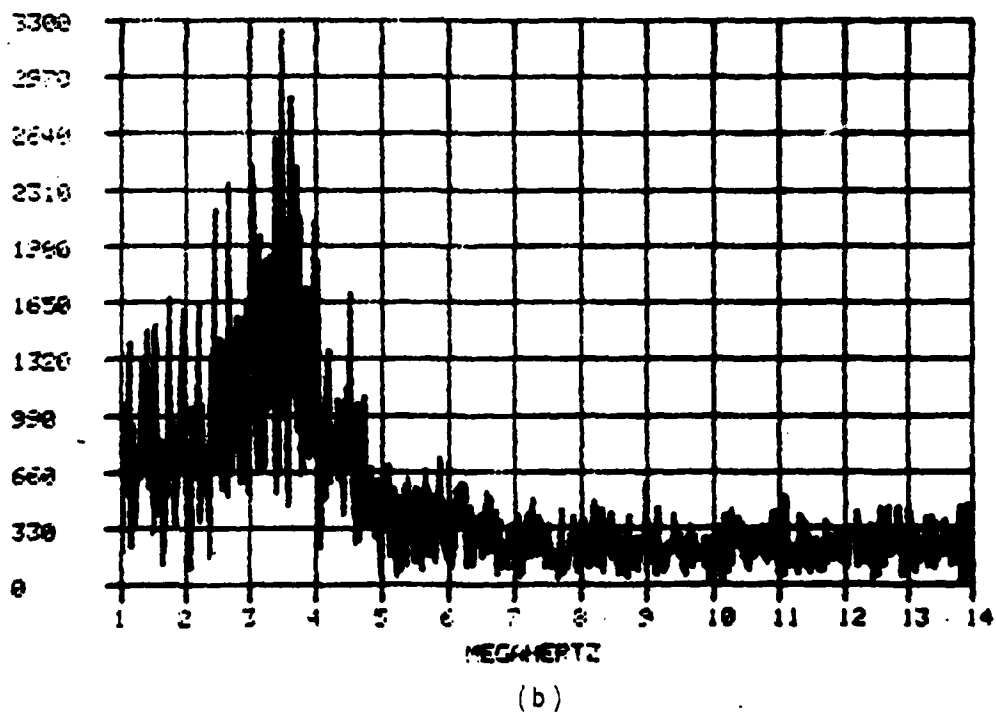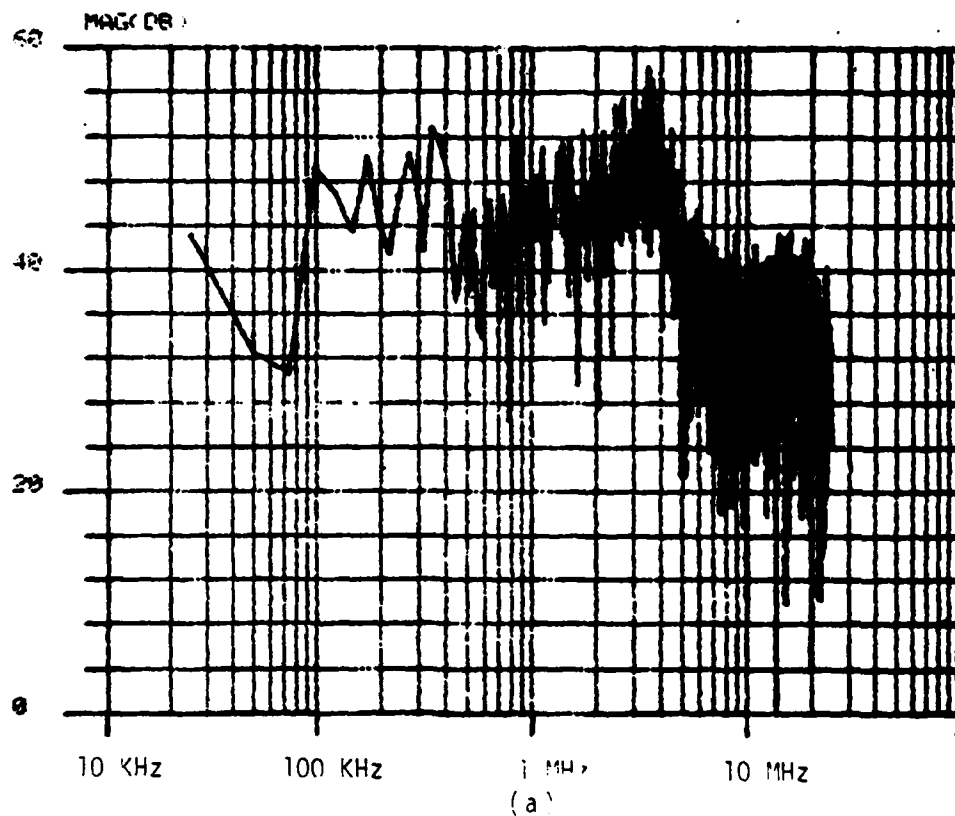
FIG 59. FFT OF THE RESPONSE OF THE ELECTRIC FIELD ON THE
AFT LOWER FUSELAGE TO A FIRST RETURN STROKE
(LOG-LOG PLOT, TOP; 1-14 MHZ EXPANSION, BOTTOM)
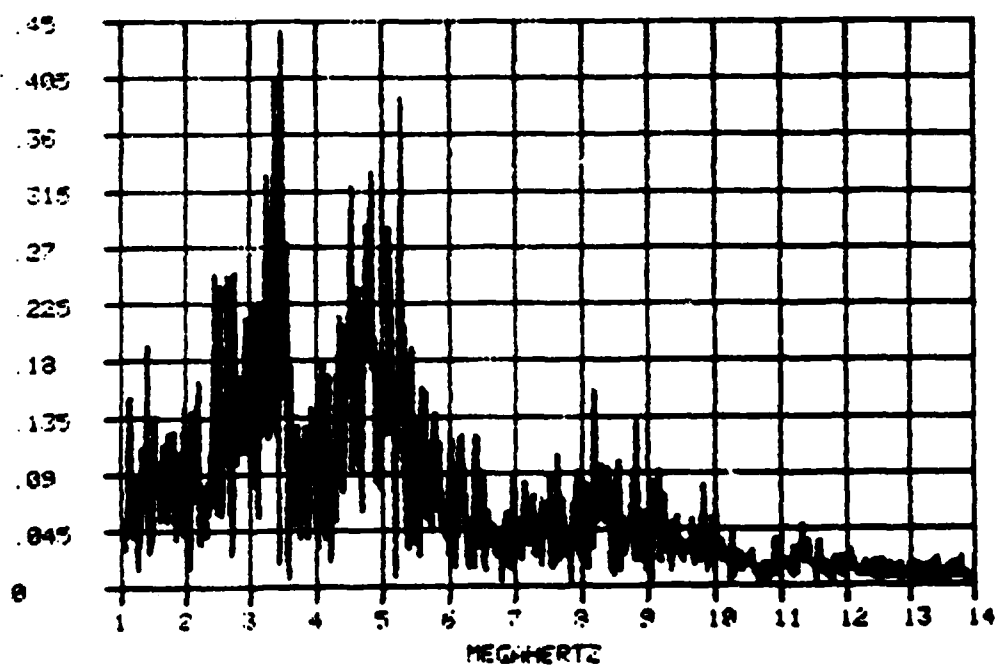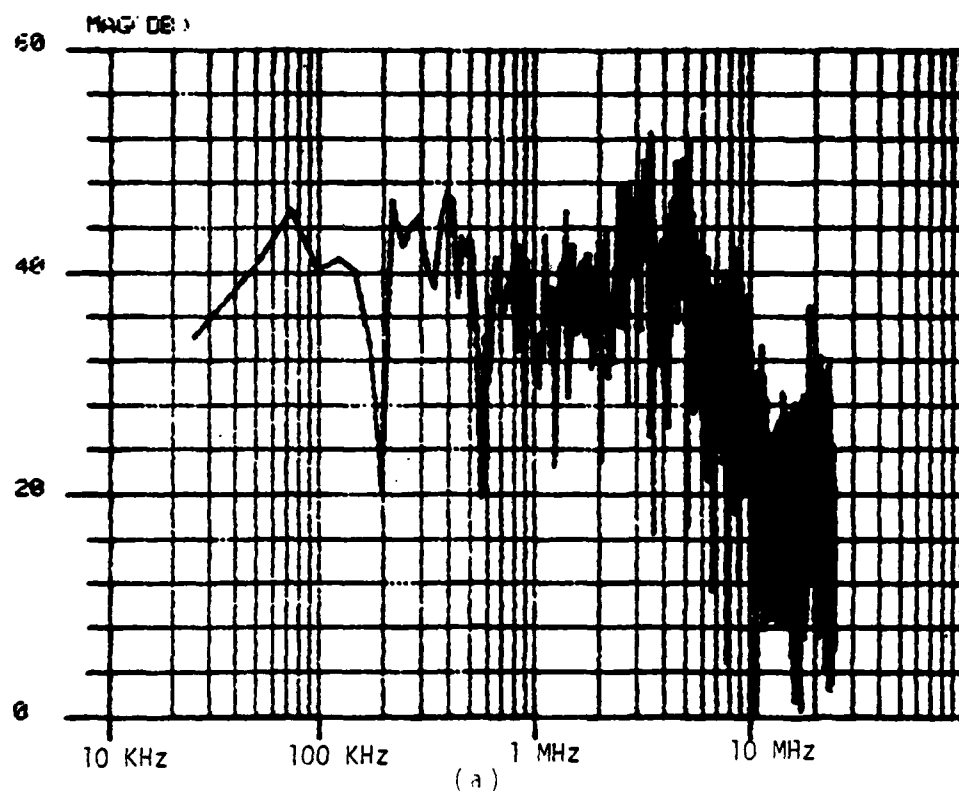
FIG 60. FFT OF THE RESPONSE OF THE MAGNETIC FIELD ON THE
FORWARD UPPER FUSELAGE TO A FIRST RETURN STROKE.

116

$$H(s) = \frac{Ks}{s^2 + Bs + \omega_o^2} \qquad (25)$$

Then the quality factor is $Q = \omega_o/B$, where ω_o is the center frequency and B the bandwidth. The center frequency, ω_o, should correspond to the resonant frequency of the aircraft, and, as discussed in Section II, is probably determined by the half wavelengths of nose-to-tail and wing-to-wing dimensions. These frequencies, 3.7 and 5 MHz respectively, are in the 2-5 MHz bandwidth shown in Figures 59 and 60.

When the aircraft is more than 10 km from the cloud-to-ground discharge, the high frequency electromagnetic fields equal to greater than the resonant frequency of the aircraft might be sufficiently attenuated by ground propagation to produce no significant effect on the overall frequency response. This might be the case in the FFT of Figure 31. However, as the aircraft gets closer to the discharge there is a much larger high frequency content in the electromagnetic fields impinging on the aircraft. These arguments justify the resonant frequencies found in the FFT in Figures 59 and 60.

(2) Subsequent Return Strokes

Twenty-six subsequent return strokes collected by the DTR on 26 August also have been analyzed. Figures 61 and 62 show typical electric and magnetic field waveforms for two of these subsequent strokes. The distances to the thunderstorm cell estimated from the airborne radar were 5 km in Fig 61 and about 10 km in Fig 62. The risetimes measured from the places marked in Figure 61 were 111 nsec for the electric field and 250 nsec for
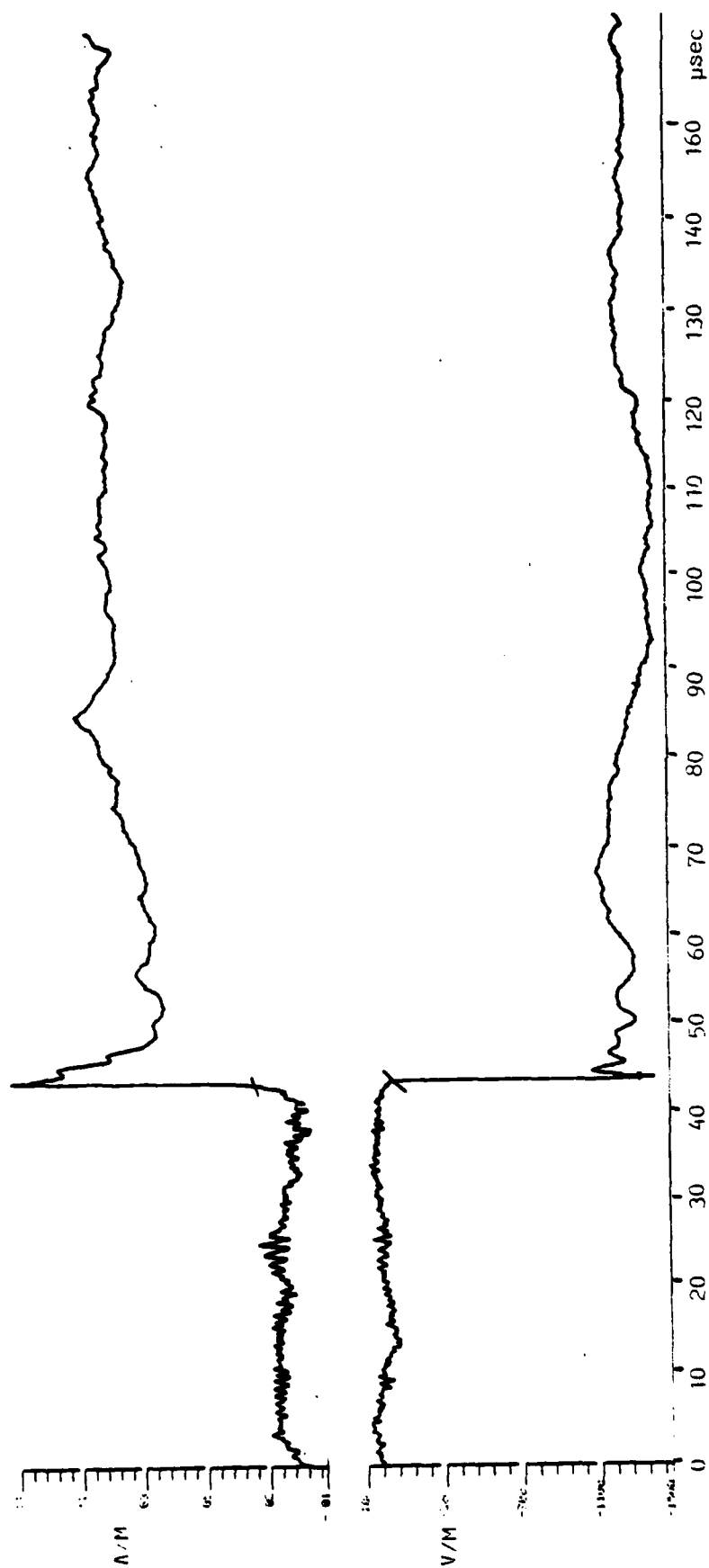
Fig 61. TYPICAL SUBSEQUENT STROKE MAGNETIC FIELD (TOP) AND ELECTRIC FIELD (BOTTOM) WAVEFORMS FROM A FLASH AT A DISTANCE OF ABOUT 5 KM.
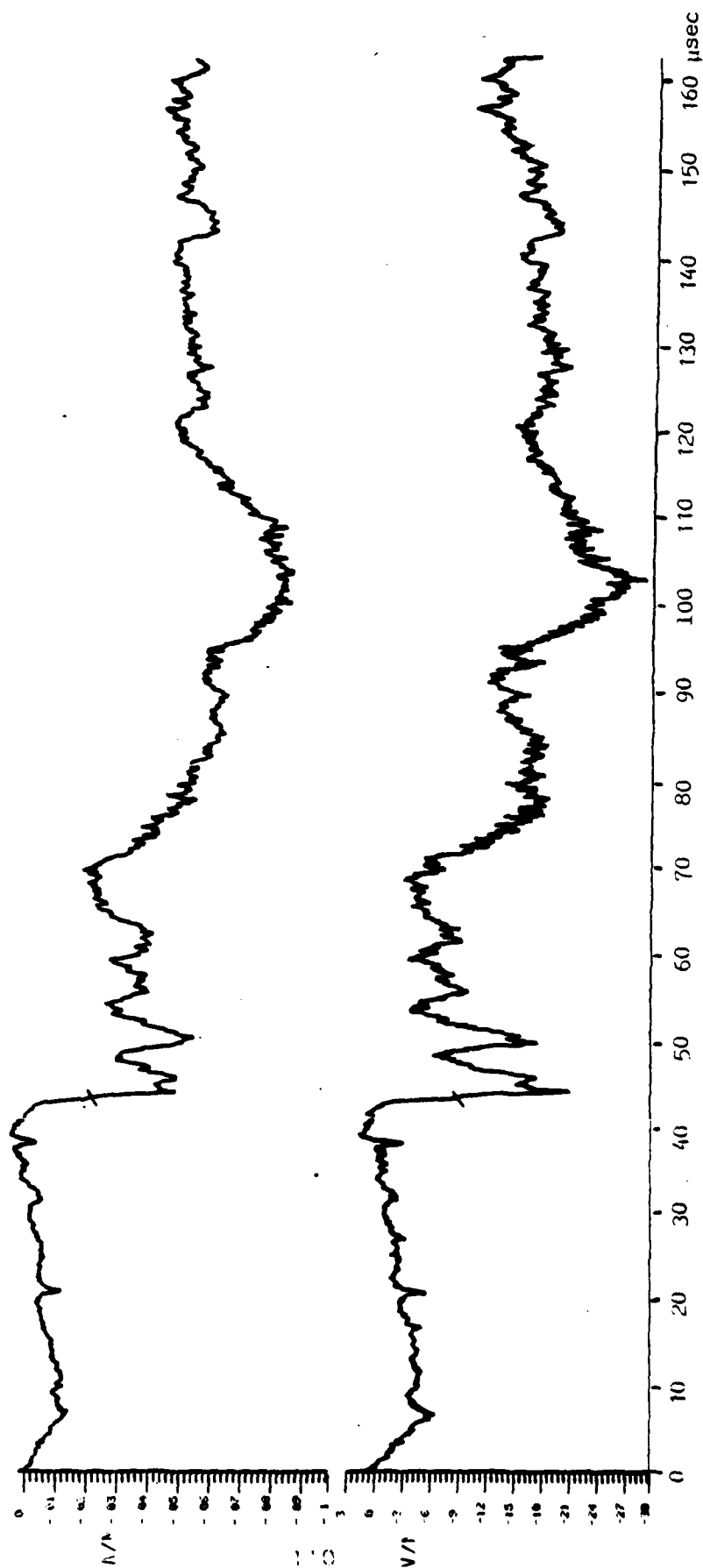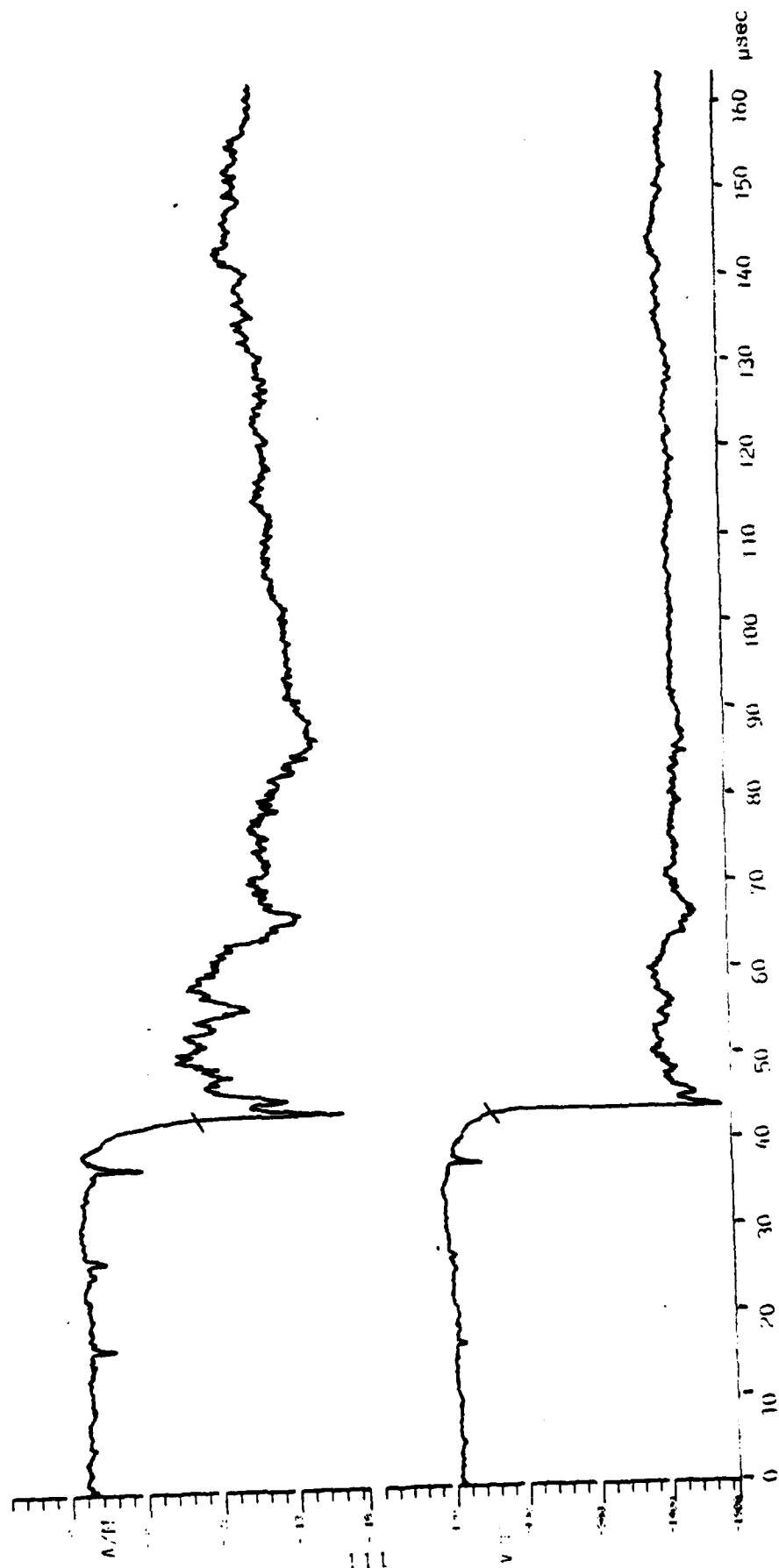
118
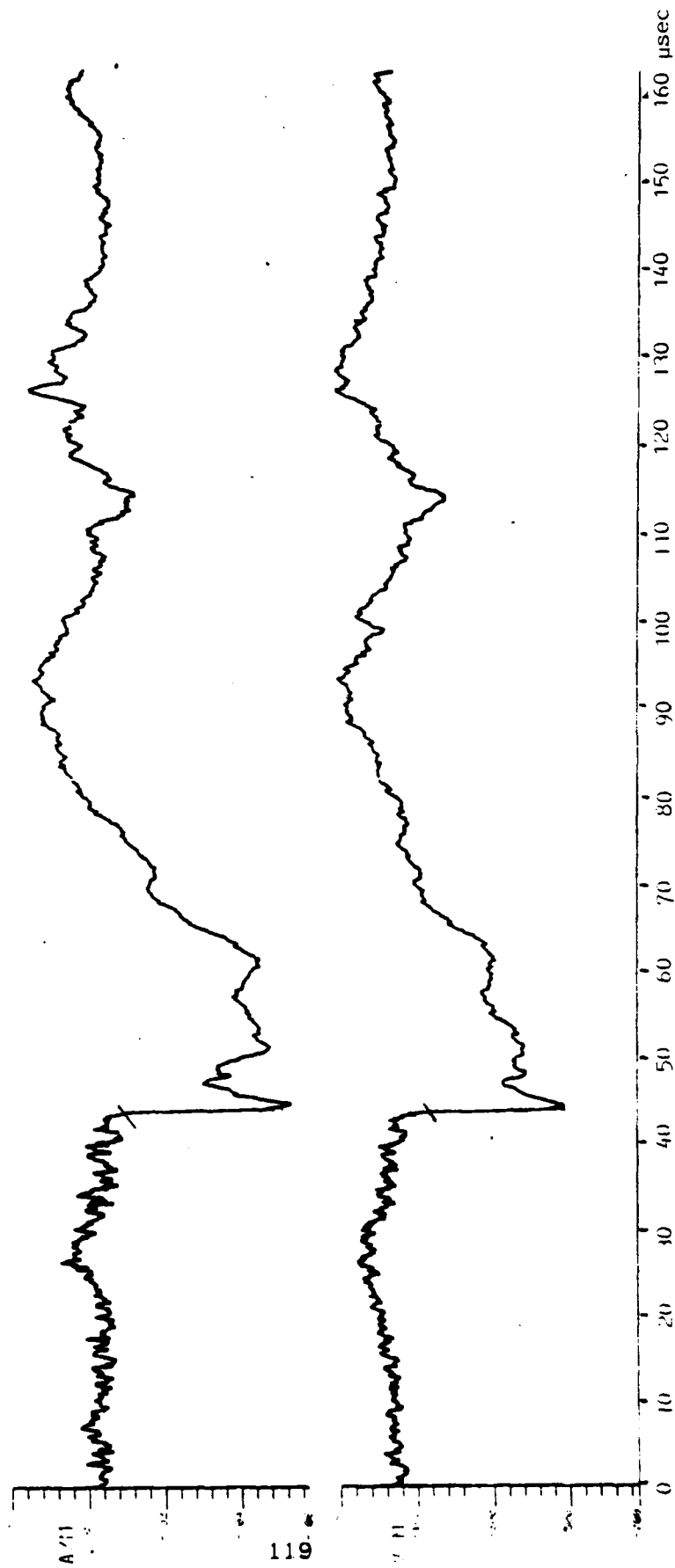
FIG 62. TYPICAL SUBSEQUENT STROKE MAGNETIC FIELD (TOP) AND ELECTRIC FIELD (BOTTOM) WAVEFORMS FROM A FLASH AT A DISTANCE OF ABOUT 10 KM.

119

the magnetic field. In Figure 62 the risetimes shown were 183 nsec for the electric field and 266 nsec for the magnetic field. None of these waveforms exhibit the initial slow rise or the isolated stepped leader pulses which are characteristic of first return strokes.

The histograms of the risetime for the electric and magnetic fields of these 26 subsequent return strokes are shown in Figures 63(a) and (b). The average risetime for the 26 events was 260 nsec for the electric field and 215 nsec for the magnetic field. As in the case of the first return strokes, none of the measured risetimes were band-limited by the 20 MHz recorder bandwidth. With this bandwidth, risetimes can be measured without equipment limitation to at least 40 nsec.

Figures 64 and 65 show the FFT of the response of the electric and magnetic field sensors to a subsequent return stroke about 5 km away from the aircraft. These FFT responses are fairly similar to those displayed in Figures 58 and 59 for first return strokes at the same distance from the aircraft. Therefore, the previous discussion about the interpretation of the frequency response will also apply to subsequent return strokes.

(3) Summary of the Analysis of the Airborne Electric and Magnetic Field Return Stroke Records

In Section IV, an analysis of 55 first return strokes and 26 subsequent return strokes recorded in the aircraft DTR with a 20 MHz frequency response has been presented. The first return strokes were obtained from two different days. The average risetime of the electric field waveforms for 26 first

Number

Microseconds Risetime
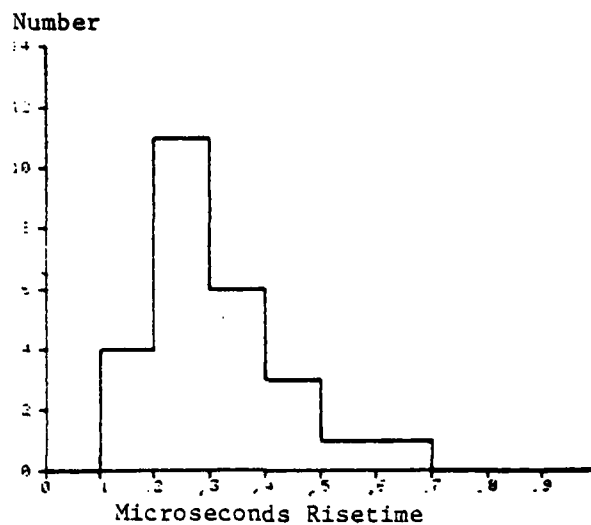
Figure 63a. Risetimes of E-Field Waveforms from 26
Subsequent Return Strokes During a Florida
Thunderstorm on 26 Aug 81.

Number

Microseconds Risetime
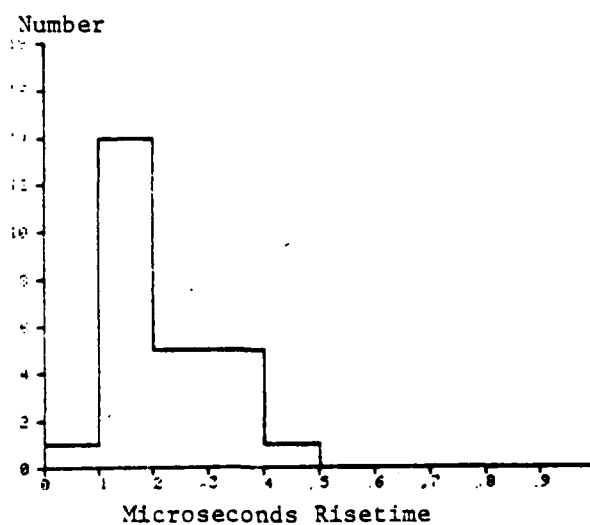
Figure 63b. Risetimes of H-Field Waveforms from 26
Subsequent Return Strokes During a Florida
Thunderstorm on 26 Aug 81.

121
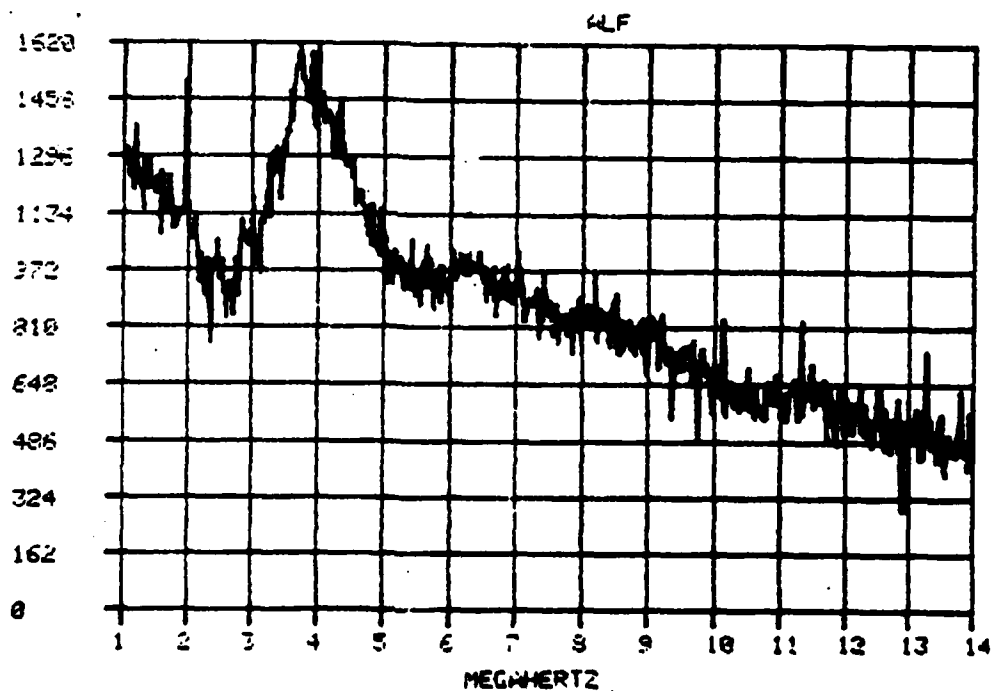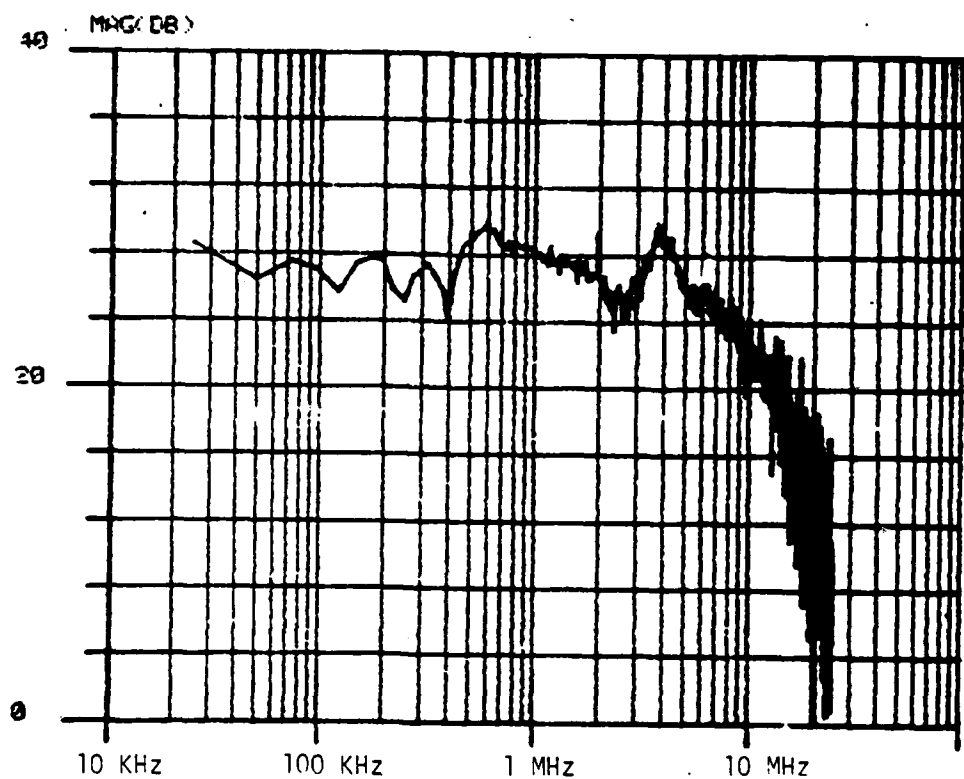
FIG 64. FFT OF THE RESPONSE OF THE ELECTRIC FIELD ON THE AFT LOWER FUSELAGE TO A SUBSEQUENT STROKE ABOUT 5 KM AWAY FROM THE AIRCRAFT.
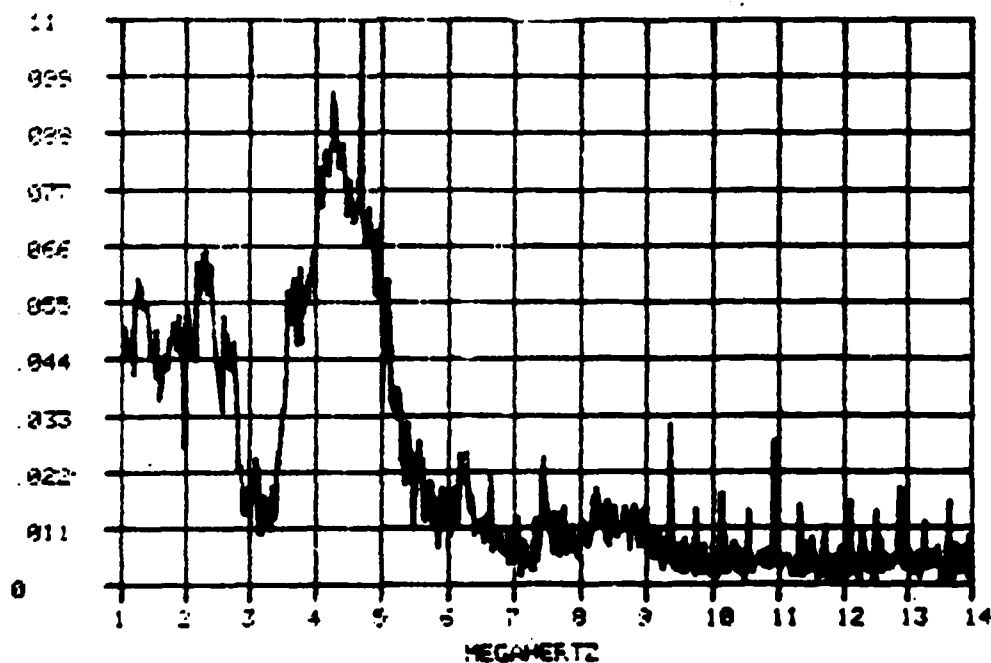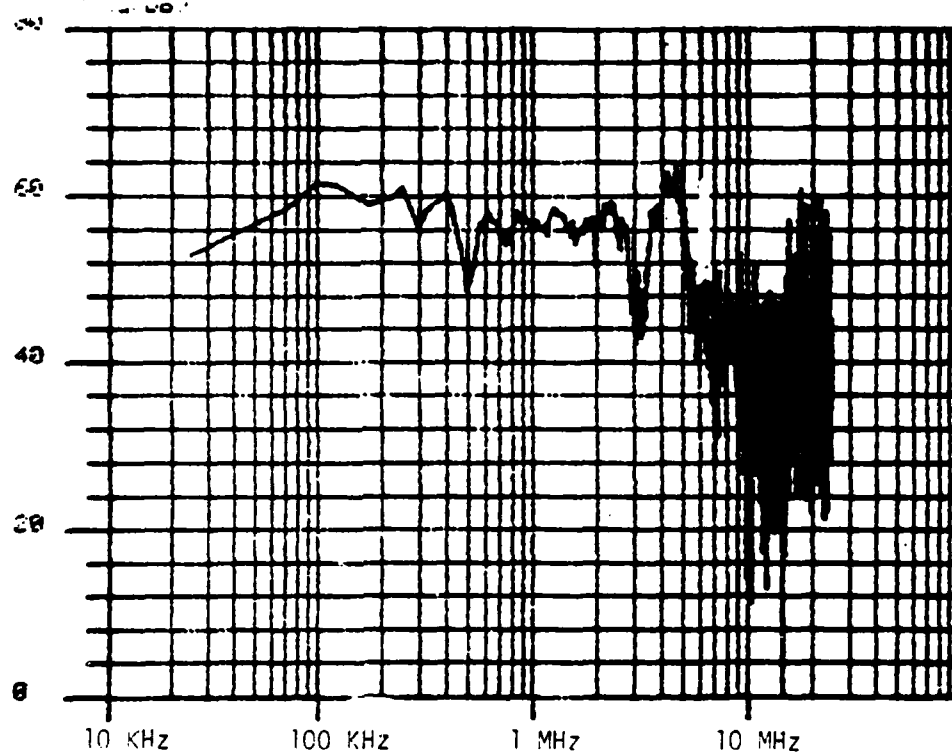
FIG 65. FFT OF THE RESPONSE OF THE MAGNETIC FIELD ON THE FORWARD UPPER FUSELAGE TO A SUBSEQUENT STROKE ABOUT 5 KM AWAY FROM THE AIRCRAFT.

return strokes on the first day was 355 nsec and for the 29 events on the second day was 170 nsec. The differences in these risetimes for a comparable number of events were attributed to the relative intensity of the thunderstorm. The risetime in the electric field records for 26 subsequent return strokes recorded on the second day was 260 nsec. The shape of the electromagnetic field waveforms for first and subsequent return strokes based on airborne measurements 2 to 35 km from the discharge was found to be similar to but faster than those reported from ground measurements (Refs 6 to 12). However, most of the reported ground measurements were performed with a limited frequency response of 2 MHz.

An important effect of the aircraft on the measurements of the electromagnetic field due to return strokes when the aircraft is less than about 10 km from the discharge has been observed. At these short distances, there is an increase in the frequency components of the electromagnetic fields at the resonant frequencies of the aircraft (2 to 5 Mhz). The aircraft resonant frequencies can then be observed in an FFT of the data.

SECTION V

DIRECT LIGHTNING ATTACHMENTS

TO THE AIRCRAFT

During the 1981 flight test program, the WC-130 received two direct strikes which caused minor damage to the aircraft. These strikes occurred on 17 July at 17:21:44 and on 26 August at 17:09:45. In this section, the electromagnetic surface fields measured on the aircraft and the location of the thunderstorm activity near the aircraft for these two flashes will be described.

1. The Direct Strike on 17 Jul 81

On 17 July at 17:21:44, the air crew reported a direct strike to the aircraft which was characterized by a loud noise and a small boom. The aircraft was flying inside the cloud in an area of light precipitation at 405 km/hour at an altitude of 17,000 ft with an outside air temperature of -0.7°C. There was no anvil above the aircraft and the cloud tops were estimated at 22,000 ft.

Figures 66 and 67 show the ground weather radar data obtained from the National Weather Service (NWS) Office at Miami, Florida superimposed with the airborne radar and Stormscope data around the time of the direct strike. The contours with continuous lines correspond to the NWS data which are associated with areas of rain or clutter. Crosses are shown to surround those areas of heavy precipitation observed in the airborne radar. The

SOUTHERN
FLORIDA

ATLANTIC OCEAN

Miami

Ground
Site

Aircraft

Date: 17 July 1981 Time: 1716 EDT

—— Rain or Clutter Contour
xxx Regions of Highest Percipitation from
     Airborne Radar
--- Locations of Return Strokes from
     Stormscope Data

20 Km
Scale

Fig 66. Weather Radar and Stormscope Data 5 Minutes before the Lightning Attachment on 17 Jul 81

SOUTHERN
FLORIDA

ATLANTIC OCEAN

Ground
Site

Aircraft

Miami
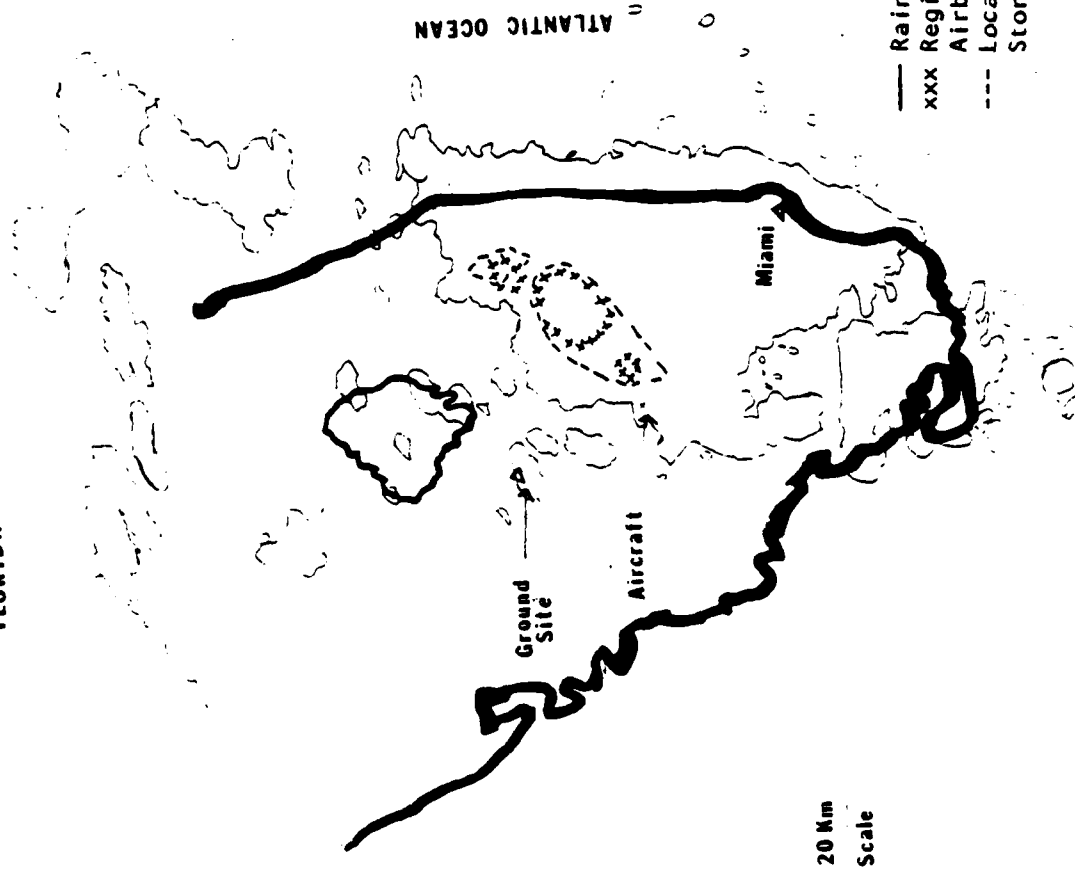
—— Rain or Clutter Contour
xxx Regions of Highest Precipitation from
Airborne Radar
--- Locations of Return Strokes from
Stormscope Data

Date: 17 July 1981   Time: 1722 EDT

20 Nm
Scale

Fig 67. Weather Radar and Stormscope Data 1 Minute after the Lightning Attachment on 17 Jul 81

dashed lines are used to enclose the regions for which the Storm-scope indicated lightning flashes in the five minutes prior to the time of the figures. The locations of the aircraft and ground station are shown in both maps. From these data it appears that the aircraft was near the edge of the cloud in an area of weak precipitation when the lightning attachment occurred.

Time windows of 400 msec, 82 msec, 4 msec, and 164 μsec are used to display this strike. The event was not recorded in the DTR; therefore, all the electromagnetic field data presented here were obtained by displaying the continuous analog data which are limited by a frequency response of 2 MHz. The sensor outputs presented here are from the electric field forward upper fuselage (E FUF), electric field aft lower fuselage (E ALF), magnetic field loops oriented to measure the current in the nose-to-tail and wing-to-wing directions (H NT and H WW) and the derivative of the current sensors on the aft upper fuselage (J AUF), left upper wing (LUW), left lower wing (J LLW) and right upper wing (J RUW). The measurements from the magnetic field and current sensors were converted to uniform current flow using an absolute calibration of the aircraft model as given by Burrows (Ref 38).

a.   The 400 msec Data Windows

Figure 68 shows the data collected from all the sensors during the flash. The flash lasted about 300 msec and consisted of two phases. The first phase of about 76 msec consisted of pulses tens of microseconds apart with a duration of several microseconds. The second phase consisted of three large solitary pulses and five smaller pulses spread out over 224 msec.

128
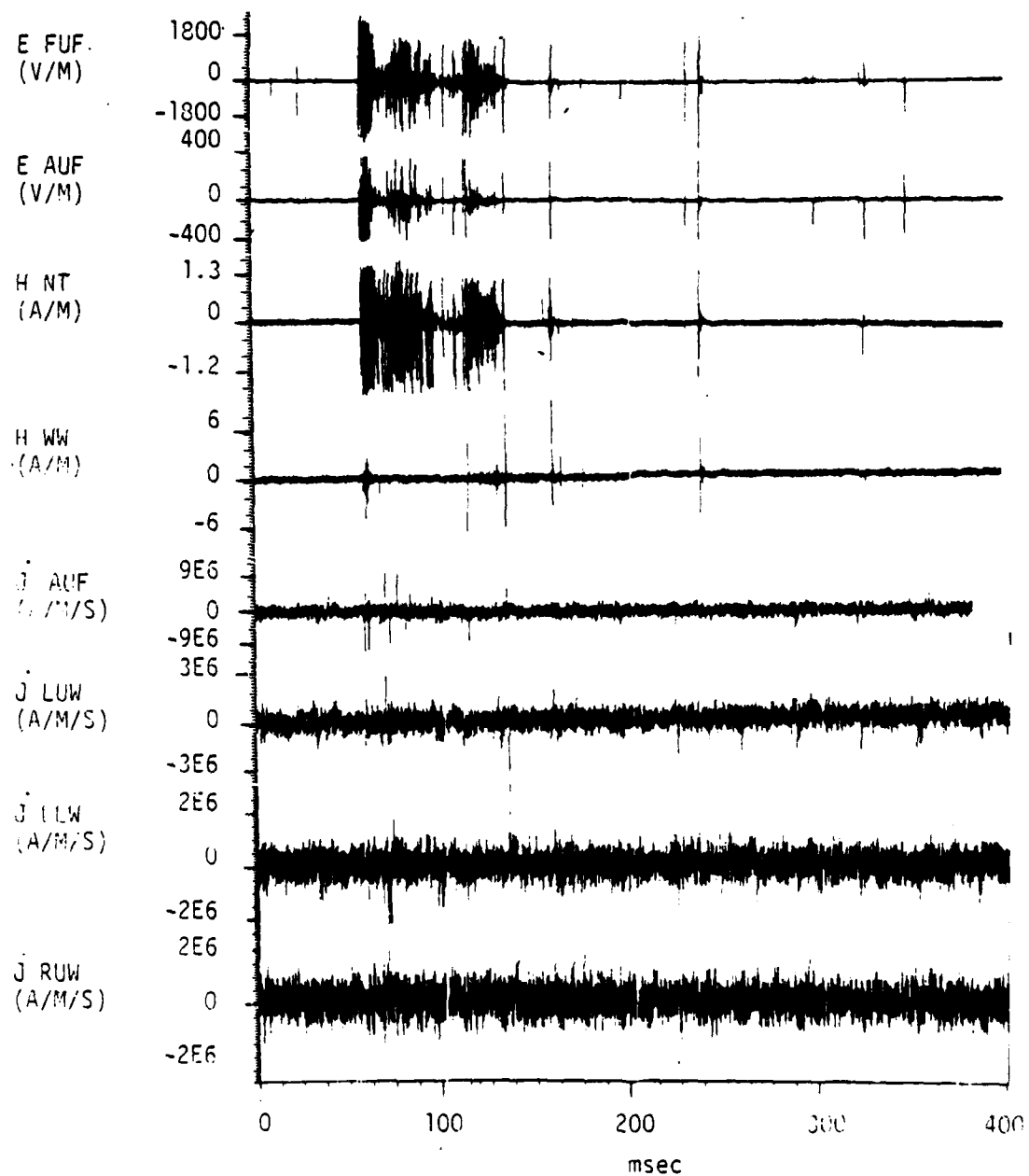
Fig 68. Electric, Magnetic, and Current Density Fields
for the Entire Flash on 17 Jul 81.

The electric field in the E FUF and E AUF sensors saturated at ±2500 V/m and ±500 V/m, respectively. The magnetic field sensor oriented to measure maximum current flow in the nose-to-tail direction saturated at about ±1.6 A/m, but the magnetic field sensor to measure maximum current flow in the wing direction and the J sensors did not saturate. The maximum value of the magnetic field in the wing direction was about 1 A/m. The maximum uniform current value corresponding to any of the pulses was 650 A, which was obtained from one of the pulses recorded by the J AUF sensor. A review of the data for the E FUF, H NT, H WW, and J AUF in Figure 67 shows that most of the current flow occurred across the fuselage. This is easily seen because the E FUF and H NT have the largest number of pulses of maximum relative magnitude and they are well correlated. However, only a few of these pulses are correlated with the H WW sensor. In addition, the corresponding values for the J sensor on the aft upper fuselage are larger than the J current value in the wing.

The J sensors are calibrated for a range between 100 A and 30 kA. These sensors are always within the noise level for nearby flashes and are primarily intended for direct strike cases. By correlating the pulses in the four J sensors outputs in Figure 68, the time and relative location of the largest current flow in the aircraft can be determined. Even though most of the current flow in the aircraft was along the fuselage as shown by comparing the H NT and H WW readings in Figure 68, there were some pulses which showed correlated magnetic field in the wing-to-wing direction.

b.   The 82 msec Data Window

Figure 69 shows the first 82 msec data window for the
flash.   The train of pulses that occurs in the initial active
period on the E-field sensors starts to decrease in magnitude for
several milliseconds after the first 10-15 msec then increases
again for 10-15 msec. This data window contains most of the
very active portion of the flash and the different pulse repeti-
tion rates can be observed. The beginning of the flash has a
high pulse repetition rate of 10 pulses per millisecond for about
43 msec and the following 25 msec has a slower rate of about 2
pulses per millisecond. The readings of the three electric field
sensors and the magnetic field sensors in the nose-to-tail direc-
tion were saturated at the beginning of the flash. At least one
large pulse is correlated on all the sensor outputs during the
first 5 msec of the flash.

c.   The 4 msec Data Window

The two four millisecond windows shown in Figures 70 and
71 cover the first 8 msec of the flash. The first 4 msec window
begins with the activity just prior to the start of the flash and
the second 4 msec window begins about the time the first 4 msec
window ends.

Figure 70 shows the first evidence of the flash. A slow
field change of about -1800 V/m occurred on the E FUF sensor
during a period of about 42 μsec. Also, during this period the E
AUF sensor output increased to about 200 V/m. These low
frequency pulses suggest a leader propagation. Since the E FUF
sensor recorded a greater field change, it can be assumed that the

131

Fig 69. Display of the Electric, Magnetic and Current
Density Data for First 32 msec of the Lightning
Attachment on 17 Jul 81.

Fig 70. Display of the Electric, Magnetic, and Current Density Data for the First 4 msec of the Lightning Attachment on 17 Jul 81

133

leader was closest to the nose and extended to higher altitude. Also, there is some activity in the H NT sensor during this period, indicating current flow along the fuselage. This may indicate that the leader was propagating from the aircraft to the cloud charge center or that a streamer was leaving the aircraft to meet the leader which was propagating down from the cloud. The apparent leader propagation lasts less than 200 μsec. This short duration of the leader field change may be due to instrument limitation. The frequency response of the sensors only goes down to about 5 kHz and a typical leader steady field change would not be detected.

The first fast field change of the sensors shown as "1" in Figure 70 occurred about 190 μsec after the initial field change and it reached 3200 V/m in the E FUF. Also, the E AUF and H NT recorded correlated pulses with a field change of 1000 V/m on the E AUF and 3.25 A/m on the H NT. The second correlated pulse ("2" in Figure 70) was correlated on all the sensors and was the first fast field change seen on the H WW and all of the J AUF sensors. This was one of the highest amplitude pulses on the H WW at about .7 A/m. The J AUF sensor measured a current of about 300 A while the J LUW, J LLW and J RUW measured about 250 A, 100 A, and 150 A, respectively. Since the current flow in the LUW is greater than in the LLW, the lightning channel probably first attached to the upper part of the aircraft. The remainder of the J sensor readings seem to correlate well with one another. The J AUF recording had the highest readings with four pulses over 500 A and one pulse near 800 A.

Pulses 3 through 6 in Figure 70 are correlated on all the

134

sensors and represent current flow along the fuselage and the wing. Figure 70 also shows a fast train of pulses for about 125 μsec on the E FUF, E AUF, and H NT sensors about 600 μsec after the first fast field change (pulse 1).

The second 4 msec window, shown in Figure 71, has several features that cannot be seen in the first 4 msec window. The H WW sensor shows little activity after 2.1 msec. The LUW sensor pulse repetition rate is higher than the RUW sensor indicating non-symmetrical current flow. There is a large current pulse on the J AUF which will be discussed later for the 164 μsec window.

There are several features that can be seen when looking at both 4 msec windows together. First, the total number of pulses can be estimated. There are around 70 discrete pulses during the 7.5 msec after the initial fast field change or a little less than 10 pulses per millisecond. However, these pulses do not occur on a repetition basis which could suggest that they are related to any of the aircraft resonant frequencies.

The total number of pulses for the flash was estimated at 180 to 200 pulses by looking at the display in Figures 69, 70 and 71.

d. The 164 μsec Data Window

A 164 μsec data window is shown in Figure 72 around the time of pulse 6 in Figure 70. This time includes one of the largest pulses in the flash. As previously discussed, the E FUF, E AUF and H NT pulses are saturated. The bottom four waveforms represent the result of using the computer integration routine discussed in Section 3 to integrate the J data. Calculation of charge transfer can be done by first determining the uniform

135

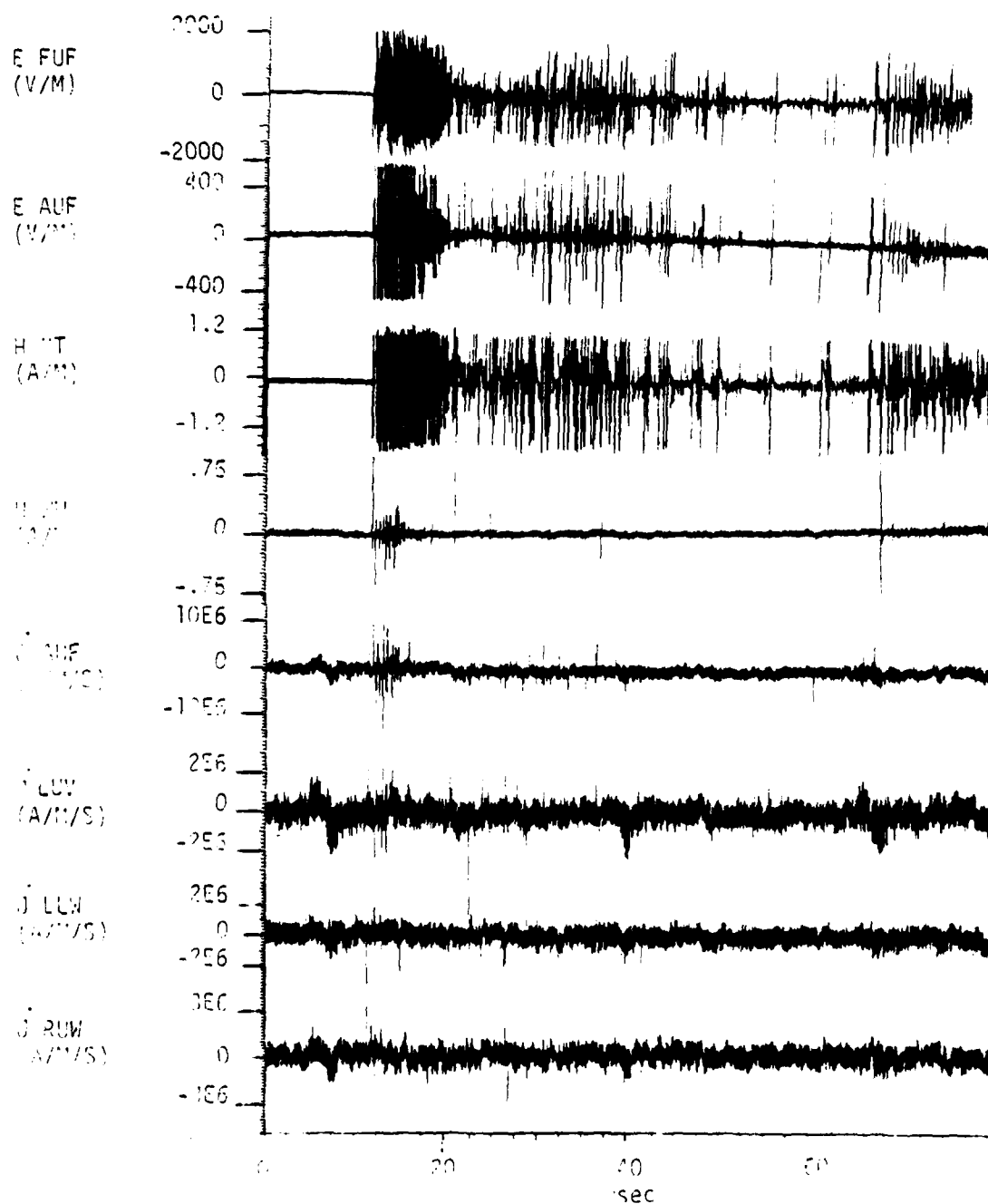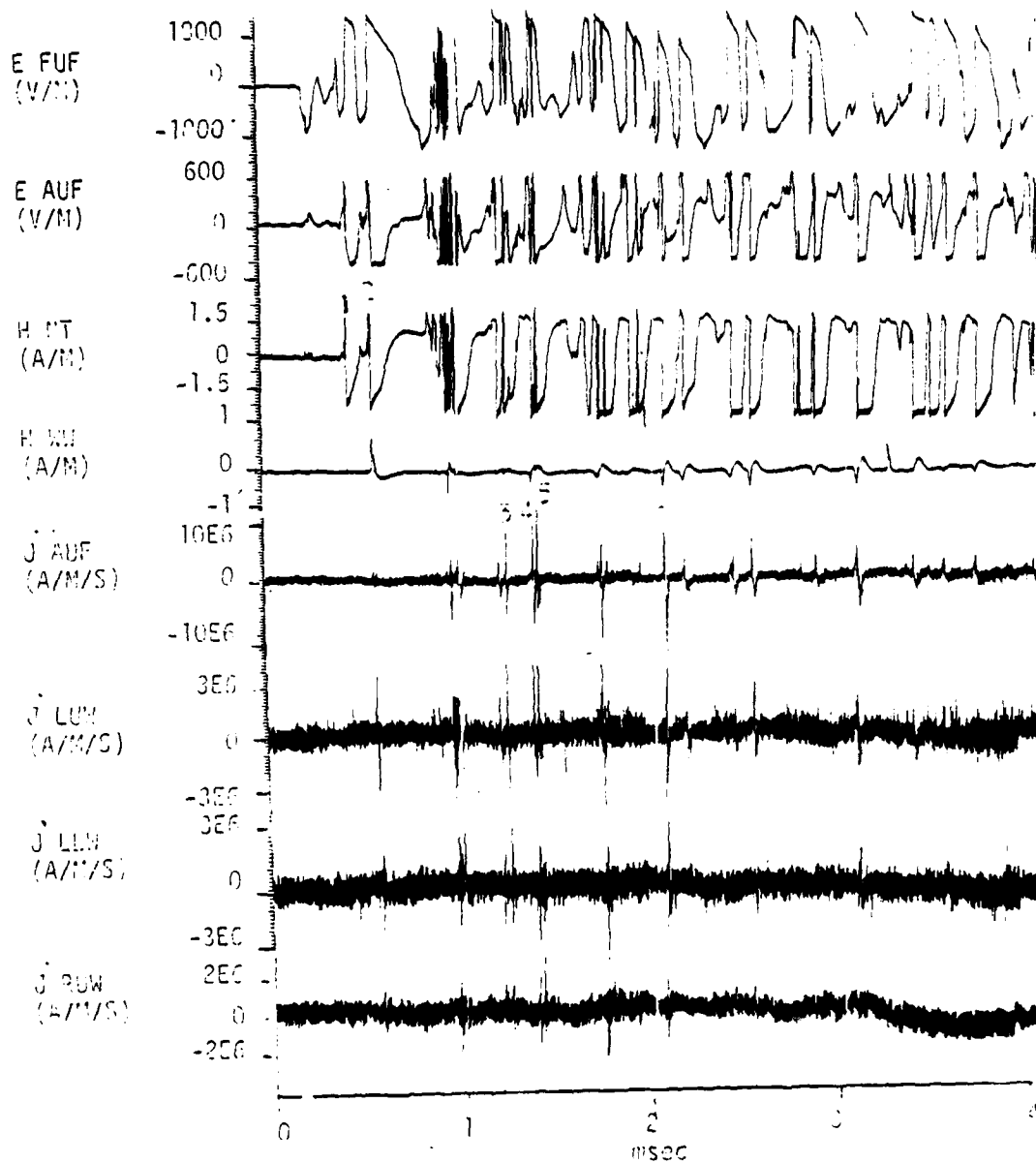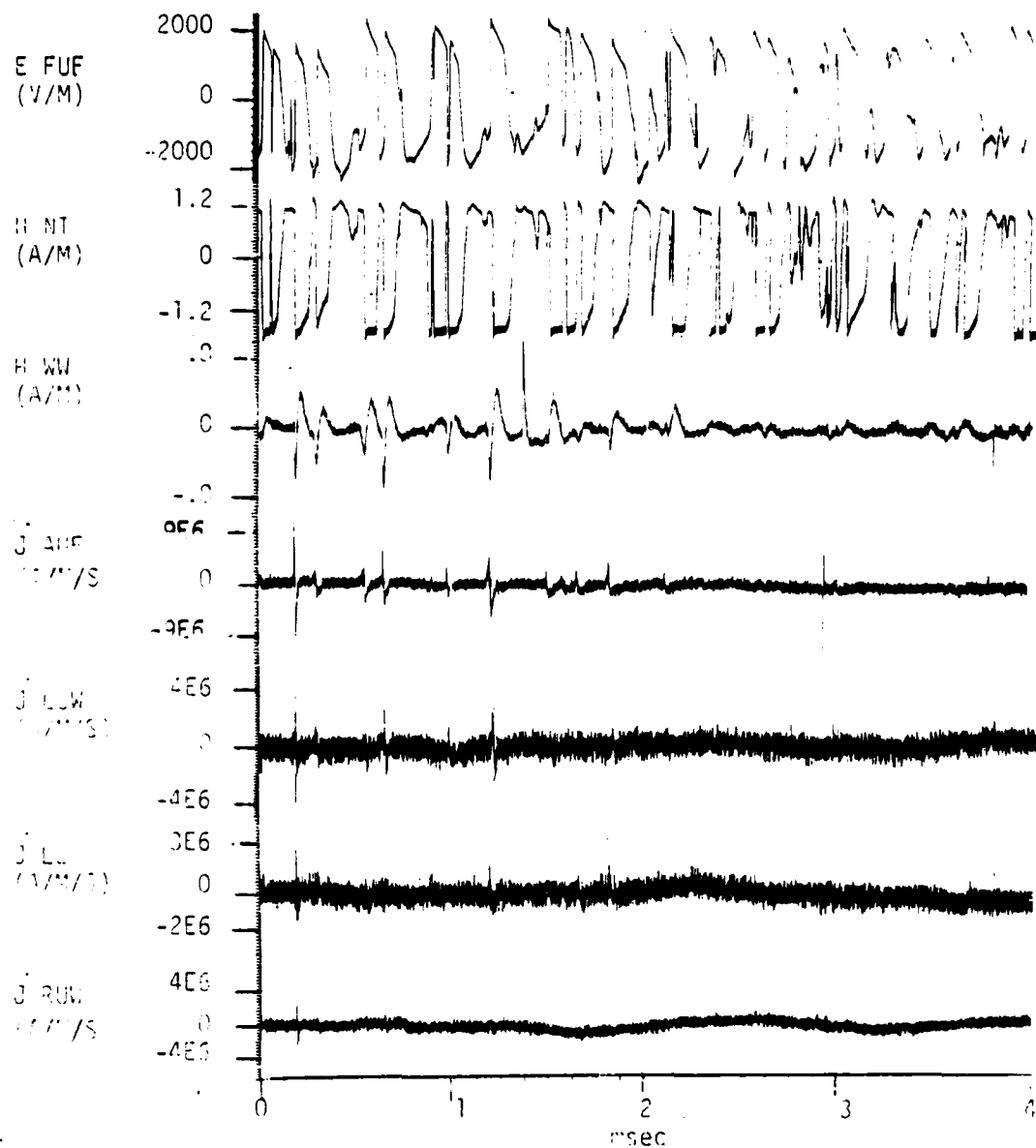Fig 71. Display of the Electric, Magnetic, and Current
Density Data for the Second 4 msec of the Lightning
Attachment on 17 Jul 81.

136
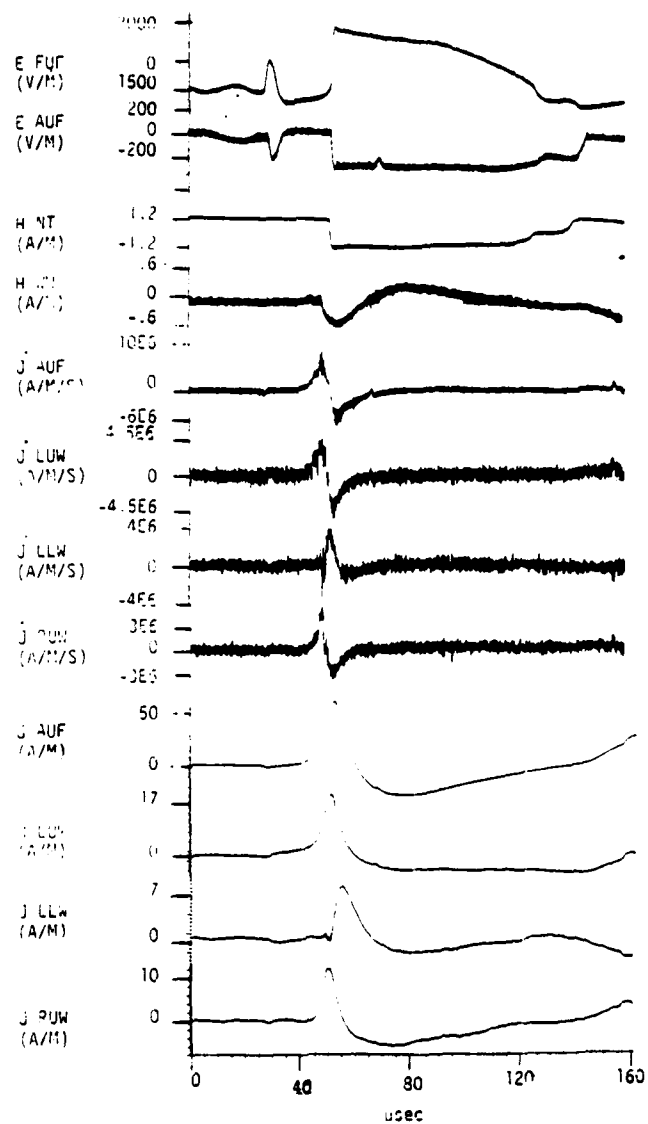
Fig 72.   A 164 usec Detailed Expansion of Pulse 6
          in Figure 70 .

137

current by using the Burrows computer calibration for the aircraft (Ref 38) and then measuring the risetime of the pulse to calculate the charge. The estimated charge in the J AUF by using this technique was 8.15 millicoulombs. This value is in the order of magnitude of several millicoulombs suggested by Shaeffer (Ref 36) as the maximum charge an aircraft can hold.

The risetimes of most of the unsaturated pulses in the flash were analyzed from data windows of 164 μsec. Table 6 shows the risetimes for ten of the largest unsaturated pulses for four of the sensors. The term BL is used to indicate that the pulse was band-limited due to the 2 MHz upper frequency response of the analog recorder. The fastest risetime that can be accurately measured with this recorder is about 350 nsec. Any pulse with risetime around 350 nsec is considered band-limited and shown as BL. A dashed line in Table 6 indicates that the pulse was too small on that sensor for an accurate risetime measurement.

e. Damage and Continuing Current Calculation

Damage to the aircraft was caused by a continuing current stroke as it swept across nine fastening screws spread along the upper fuselage from a spot outside the copilot's window to a spot near the wing. Figure 73 shows some of the pits produced during the attachment. Also, one of the two antenna wires mounted between the upper fuselage and the stabilizer was burned in half.

A laboratory test was performed to estimate the continuing current necessary to produce the same amount of damage as seen on the aircraft. The distance between the nine burned rivets ranged

Pulse Number	1	2	3	4	5	6	7	8	9	10
J AUF	BL*	1.1	BL	.63	BL	3.8	6.0	BL	1.0	.38
J LUW	.5	.99	BL	-	.4	2.9	5.0	BL	.9	BL
H WW	1.0	2.0	-	.71	-	6.0	3.5	-	-	1.4
E AUF	-	-	-	-	-	-	-	.95	1.4	1.0

*Risetime is band limited due to equipment limitations.

Table 6. Measurements of Risetimes (in μsec) for the Ten Largest Unsaturated Pulses during the Lightning Attachment on 17 Jul 81.

139

(a)
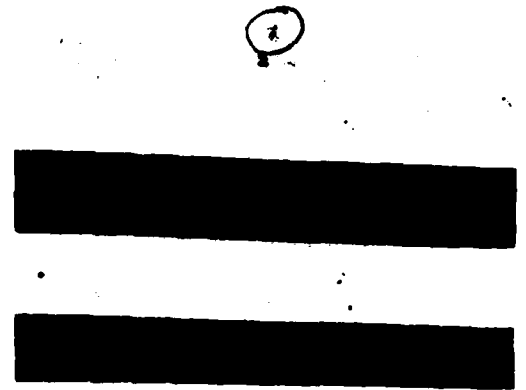
(b)
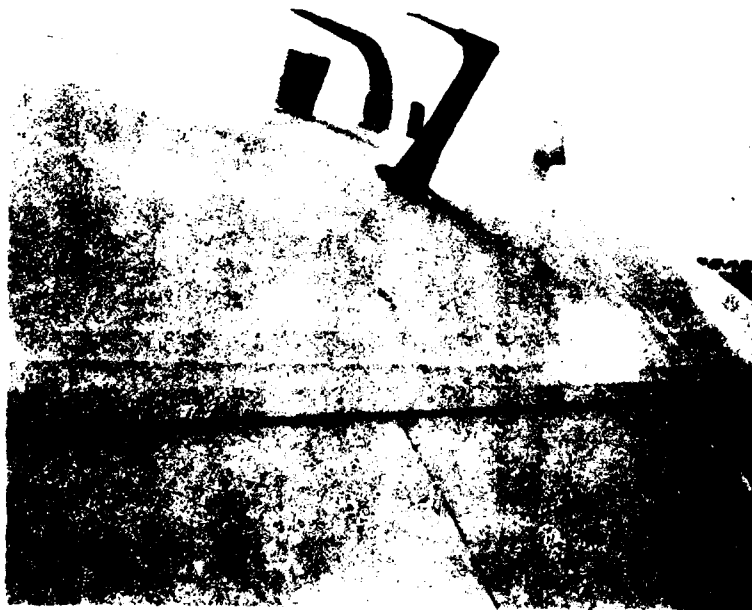
(c)

(d)

Fig 73. Burn Spots Produced by the Continuing Current
during the Lightning Attachment on 17 Jul 81.

140

from 33 cm to 158 cm for a total length of 5.4 meters. The total duration of the swept stroke can be estimated by dividing this distance by the aircraft speed of 405 km/hr or 112 m/sec. This results in a total attachment of 48.2 msec and an average dwell time of 47.7/8 = 5.96 msec. The charge transfer to produce a burn in a rivet which is comparable to the one in the aircraft was estimated by increasing the current in a simple (source voltage)/(resistor)/(aircraft rivet) circuit. A current of 35 A for a duration of 9 msec was needed to produce the same burn in the rivet. Therefore, the charge transfer was estimated as $35 \times 9 = .315$ coul and the continuing current as $.315/5.96 = 52.9$ A.

This value of continuing current in the flash could have been measured directly from the magnetic field recordings if the sensors had a frequency response down to near DC. But since the frequency response was limited to a few kilohertz, the continuing current level had to be estimated by using this method.

2. The Direct Strike on 26 Aug 81

On 26 August at 17:09:45, the aircrew reported a second direct strike to the aircraft, again characterized by a loud noise and a small boom. The aircraft was flying at 333 km/hr at an altitude of 16,000 ft. with an outside air temperature of +5°C. It was inside a cloud in an area of slushy precipitation in a rapidly building part of the cloud formation. There was a large anvil above the aircraft and the cloud tops were estimated as 30,000 ft. Prior to this strike, no lightning had been seen on the Stormscope within 5 km of the aircraft. The crew, which has experience flying under adverse weather conditions, estimated that the attachment was made across the fuselage.

141

All the sensors except the E LWT were kept at the same magnitude saturation levels as in the 17 July flash. The saturation level of the E LWT sensor was changed to 320,000 V/m. This sensor did not saturate during this direct lightning strike. With the exception of the E FUF, the frequency response of all the sensors also remained the same. The E FUF sensor was recalibrated to give a low frequency response of less than 1 Hz. Two new experiments were also implemented. Wires were placed along the left wing and their induced voltage was monitored in the instrumentation recorder. Wires were also run along the fuselage from near the cockpit area to the tail of the fuselage. The signals recorded on these induced wires will be referred to as wing wire and fuselage wire data.

The only damage produced by the strike was to two of the computer systems on board the aircraft. Memory dumps occurred to these two computers which were located in the forward fuselage behind the cockpit area. These computers operated properly once they were re-initialized after completion of the flight. This strike did not produce any burn marks. The aircraft was searched extensively especially along the fuselage but no new burns could be found. This implies that the flash had low or nonexistent continuing current. The low frequency response of the E FUF sensor would have normally detected any continuing current, but this sensor drifted into saturation prior to the strike due to the rain in the external plate.

Time windows of 800 msec, 82 msec, 4 msec, 1.6 msec, and two 164 usec were used to analyze this data. As in the 17 July

142
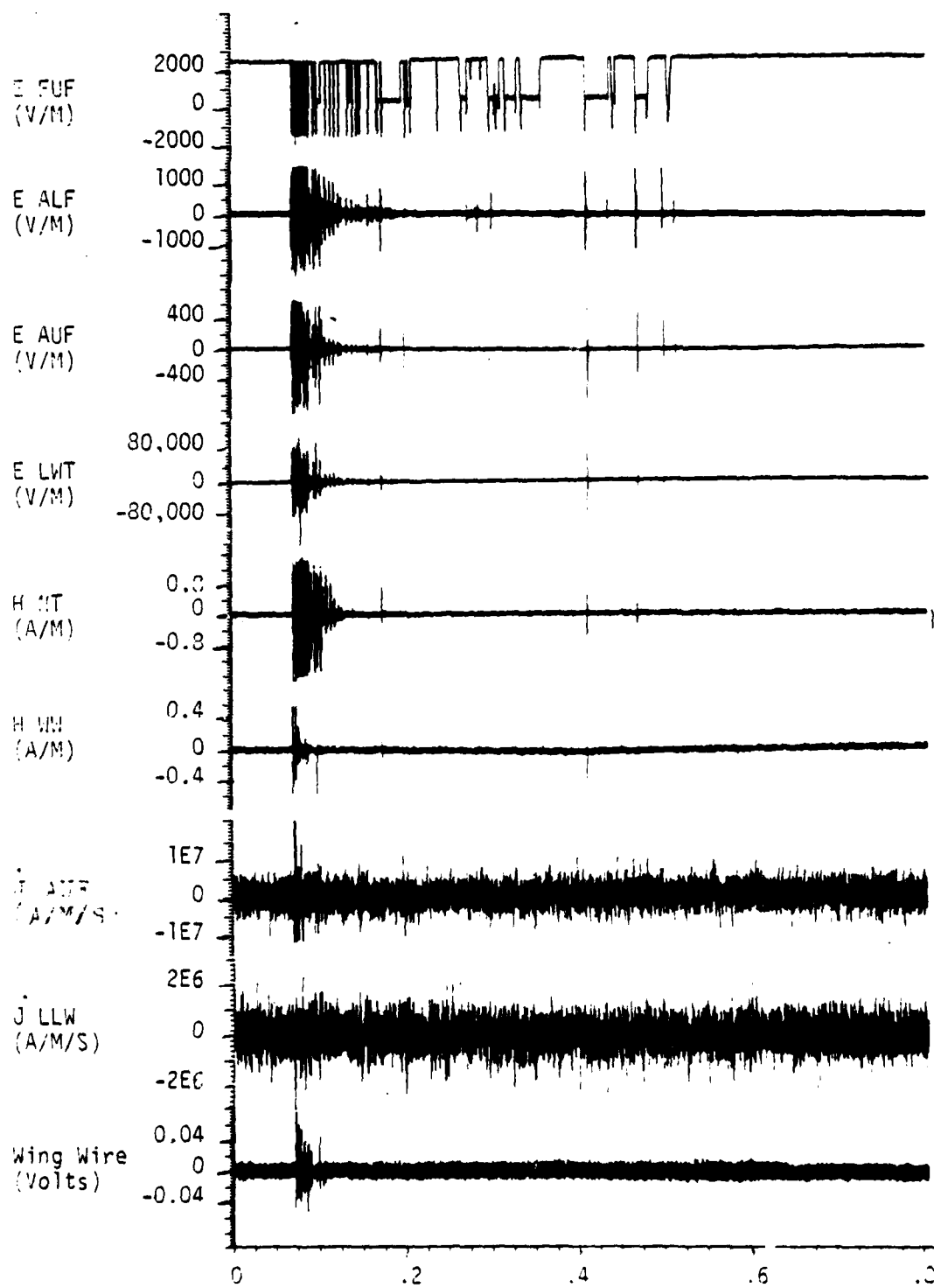
Fig 74. An 800 msec Window of the Lightning Attachment on 21 Aug 81.

flash, we also calculated the uniform current from the Burroughs (Ref 38) computer program for the two magnetic fields and the three displays of current density sensors.

a. The 800 msec Time Window

Figure 74 shows all four electric field sensors, the two magnetic field sensors, two of the current density sensors and the voltage in the wing wire during the entire duration of the flash. The top trace is the E FUF. Because of the low frequency response, this sensor drifted into a saturation level of over 2000 V/m prior to the flash. During the flash this sensor oscillated between the positive and the negative saturation level and zero. The second trace is the E ALF which saturated at a reading of about ±2000 V/m. The third trace is the E AUF, normally referred to as the Q sensor. This sensor was calibrated for a saturation level of ±800 V/m. The fourth trace is the E LWT which ranged between 120,000 and -160,000 V/m. These maximum values occurred near the beginning of the flash but a large pulse with magnitude in the range from 80,000 V/m to -10,000 V/m occurred 350 msec after the initial large pulse. The fifth and sixth traces are the magnetic field sensors. The magnetic field sensors were calibrated for ±1.5 A/m. The H NT became saturated but the H WW remained below the saturation level. From the amount of activity shown on the H NT sensor it is clear that most of the current flow was along the fuselage. The next two traces for the J AUF and J LLW sensors were not saturated. The bottom trace of the wing wire had a maximum induced voltage of about 80 mv.

The flash lasted 460 msec and probably consisted of an

active phase followed by few isolated pulses. The initial active phase lasted about 110 msec with most of the activity occurring in the first 30 msec. The pulse repetition rate during the first 30 msec reached a maximum of 10^4 pulses/sec and then decreased. As can be observed in Figure 73, the magnitude of these pulses also decreased after the first 30 msec. After this initial phase there was a quiet period which lasted 240 msec where only three pulses on the order of a few hundred V/m were observed on the E ALF sensor.

The largest of the isolated pulses occurred after a 300 msec quiet period and was followed by a few other pulses between 25 and 60 msec apart. The largest of these pulses is 20% lower than the largest pulse in the initial active phase.

b. The 82 msec Time Window

Figure 75 shows the first 82 msec time window of the flash. The electric field pulses during the active period of the first phase of the flash correlated well with the H NT indicating that most of the current flow was along the fuselage. The J AUF shows several large amplitude pulses at the beginning of the flash. Since the J AUF sensor will measure current flow along the fuselage but is scaled to measure thousands of amperes instead of tens of amperes as in the H NT, it is possible to determine the relative level of the H NT saturated pulses by looking at the J AUF record. The largest current flow in the J AUF, nearly 3 kA, occurred at the beginning of the flash. The activity in all the sensors decreased nearly exponentially during

Fig 75. First 32 msec of the Lightning Attachment on 26 Aug 31

-146
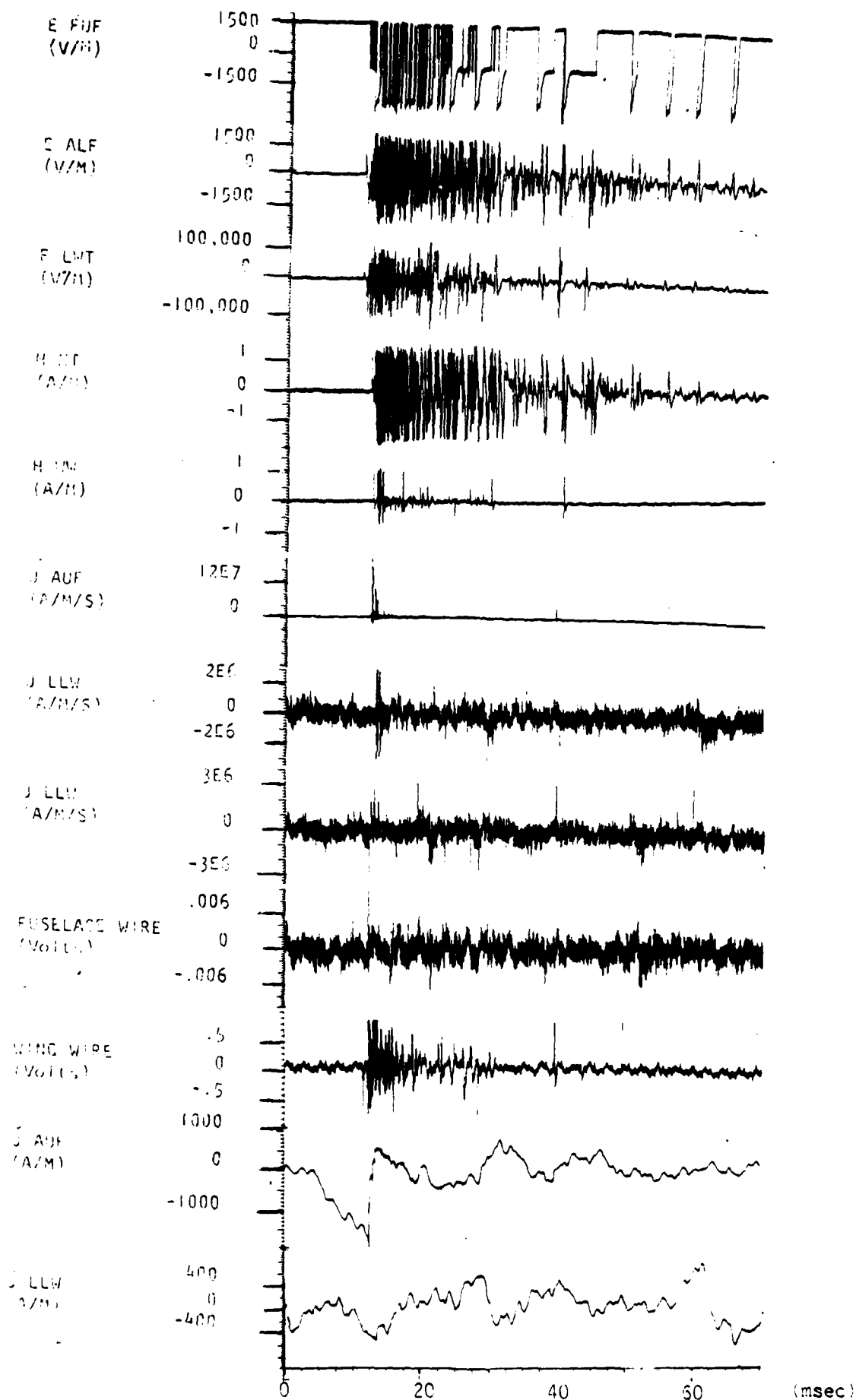
the first attachment. The bottom two traces in Figure 75 are the software integrated results of the $\dot{J}$ AUF and $\dot{J}$ LLW displays.

c.   The 4 msec Time Window

The first indication of the flash can be observed in the slow electric field change obtained on all four electric field sensors. Figure 76 shows the first four millisecond window for the four electric field sensors, the two magnetic field sensors, and the derivative and integrated data from the current density sensor.

The electric field change in the left wing tip first rises to 24,000 V/m over a 125 μsec period and starts to decrease slowly. About 350 μsec after the initial field change, the first fast field change occurs on the left wing tip. There were three fast field changes on the left wing tip, each lasting a few microseconds and about 50 μsec apart. The first two pulses caused a field change of -24,000 V/m and the third was -60,000 V/m. The slow field change at the beginning of the discharge is an indication of a leader propagation; however, its short duration of 350 usec before an abrupt discontinuity might indicate that pockets of charge were neutralized just a few hundred meters after the leader initiation. Also, since no activity is seen in the magnetic field sensors during the slow electric field change, it can be assumed that the leader propagated from the cloud to the aircraft. If the leader had propagated from aircraft to cloud there should be some earlier evidence of current flow on the H-field sensors that would be necessary to support leader propagation. Two points should be made about this observed

147
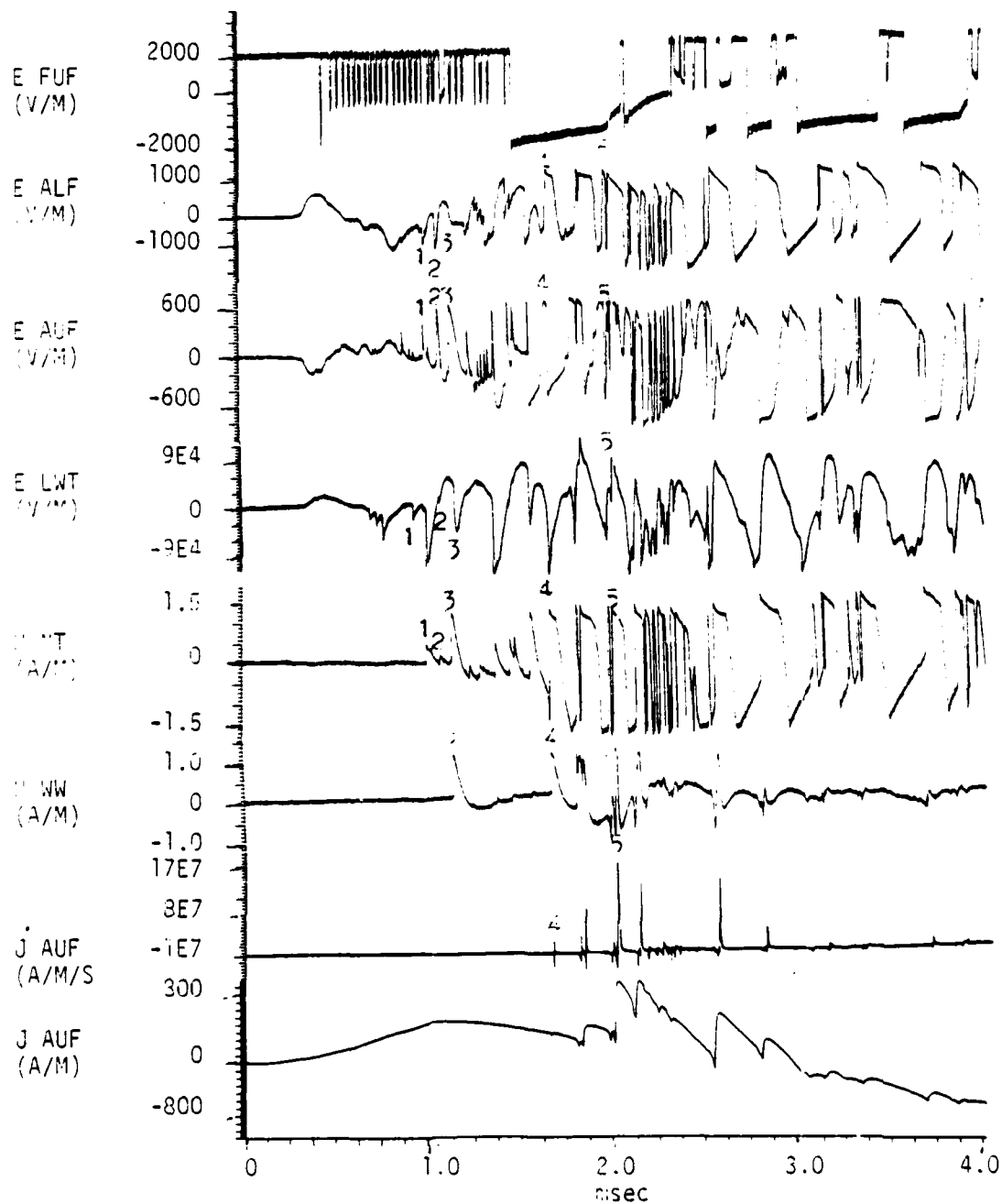
Figure 76. First 4 msec of the Attachment on 26 Aug 81.

148

leader. First, leader propagation from cloud to aircraft does not necessarily mean a natural lightning flash. There is no other evidence of leader propagation past the aircraft, indicating that no natural cloud-to-ground or intracloud lightning took place. Second, the length of the leader indicates that the charge center of the cloud and the aircraft were within 175 m of one another. Apparently the cloud charge center coming in contact via the leader with the aircraft did not produce a high enough field to propagate streamers between the aircraft and another charge center or the aircraft and ground. It seems reasonable to assume that this was a triggered cloud-to-aircraft flash and not a natural lightning flash.

The other electric field sensors during the initial 125 usec period reached only -200 V/m on the aft upper fuselage and 1000 V/m at the aft lower fuselage with very small correlated fast field change for the first three sharp pulses which were observed on the left wing tip. This fact might indicate that field enhancement is larger on the aircraft wing tips. The first correlated fast field change in the first millisecond of the flash was observed about 680 usec after the initial change. The field change at this time reached 100,000 V/m at the left wing tip, 400 V/m at the aft upper fuselage, and 800 V/m at the aft lower fuselage. This field change shown as pulse (1) in Figure 76 is the first magnetic field change detected and occurred in the magnetic field sensor oriented to read a maximum value for current flow along the fuselage. The magnitude of pulse (1) was 0.5 A/m or about 8 A of uniform current, but there was no correlated field change in the other magnetic field sensor. Since the

149

magnetic field sensor oriented to measure maximum current flow perpendicular to the fuselage was not located in the fuselage intersection with the wing but about three meters forward of the wing, therefore the H WW sensor is not a true representation of the wing current. The next fast field change, shown as pulse (2) in Figure 76, is mainly observed in the fuselage electric field sensor and in the magnetic field sensor sensitive to fuselage current. Pulse (3) in Figure 76 is the first correlated pulse for both magnetic fields with readings of 1.4 A/m in the wing-to-wing direction and 1.3 A/m in the nose-to-tail direction. The actual magnitude of this pulse on the magnetic field sensors might have been slightly larger than these values because these readings are about the saturation level. Pulse (3) correlates well with a pulse on the order of 600 V/m in the aft upper fuselage but the corresponding field change at the left wing tip and aft lower fuselage have a slower risetime. Pulse (4) in Figure 76 shows an important correlation. This is the first pulse which shows a correlated change in the J-Dot AUF sensor. The reading on the H NT sensor can be compared with the J-Dot AUF sensor. The J-Dot AUF sensor provides a reading for larger values of current flow along the fuselage which will saturate the H NT sensor. The reading in Pulse (4) is equivalent to about 400 A of uniform current flow along the fuselage. The readings on the AUF and ALF electric field sensors are saturated and the left wing tip shows a correlated pulse of -150,000 V/m. This pulse occurred about 1.8 msec after the leader initiation. All the pulses in Figure 76 correlate quite well on all the sensors.

130

Pulse (5) shows the largest current flow along the fuselage which corresponds to about 3000 A. The channel between the aircraft and cloud probably takes some time to become fully established after contact is made, thus delaying the time before maximum current flow is seen. The time between the current bursts on the J-Dot AUF sensors is from tens of microseconds to several hundred microseconds. The four largest $\dot{J}$ AUF pulses, by using the average risetime technique and applying Burroughs model described earlier, correspond to currents of 1.2 ka, 3.0 ka, 2 ka, and 2.2 ka, respectively. They are separated from other pulses by 125 usec 80 usec, 50 usec, and 200 usec. Given the shape of the current pulses, the charge on the aircraft for each isolated pulse discharge can be calculated. This was done for two of the pulses for the 164 usec analysis and will be described later.

There appears to be about 5-10 pulses per msec on the E-field and H-field sensors. If this can be considered an average value over the most active period of the flash (30 msec), then 150-300 pulses occurred during the most active period. Only about 10 to 20 additional pulses occurred in the flash after the initial active period. There are three important features of the E and H-field pulses. First, they are variable in duration. Some pulses are as short as several microseconds while others last up to 300 microseconds. Second, about 1.1 msec after the start of the first fast field change, a 375 usec period of rapid pulse repetitions occurs. Since the start of this period coincides with the largest pulse on the $\dot{J}$ AUF sensor, this 375 usec period represents the majority of the energy transfer during the flash. There are about 14 pulses during this period on the E ALF, E AUF,

151

E LWT, and H NT sensors.

d. The 1.6 msec Time Window

Figure 77 shows a 1.6 msec expansion of Figure 76. This expansion starts about 1.25 msec after the beginning of the record in Figure 75. In addition, the J LLW data and the induced fuselage and wing wire voltage during this time period are included in the display. The same pulses (4) and (5) in Figure 76 are now shown with the new time scale. Pulse (4) produced the largest current value on the left lower wing sensor at over 1000 A and the largest induced voltage on the fuselage wire of over 5 mV. Pulse (5) produced the largest value on the aft upper fuselage of nearly 3000 A. During these pulses the wing wire showed induced voltages of -120 mV to 140 mV but the 140 mV voltage appears to have reached a saturated level. Table 7 shows the maximum values of current, electric and magnetic fields and their derivatives during the direct strike. This table was made by taking the maximum nonsaturated pulses. Since the magnetic field and the induced wing wire voltage were saturated at 1.5 A/m and 140 mV, respectively, their maximum values in Table 7 are quite small.

e. The 164 μsec Time Window

Time windows of 164 μsec for the 10 largest pulses in the flash were displayed. Figures 78 and 79 show two of these data windows. Figure 78 corresponds to the largest pulse on the $\dot{J}$ AUF during the first attachment. This is pulse (5) in Figure 77. Figure 79 contains the largest pulse in the $\dot{J}$ AUF after the

152
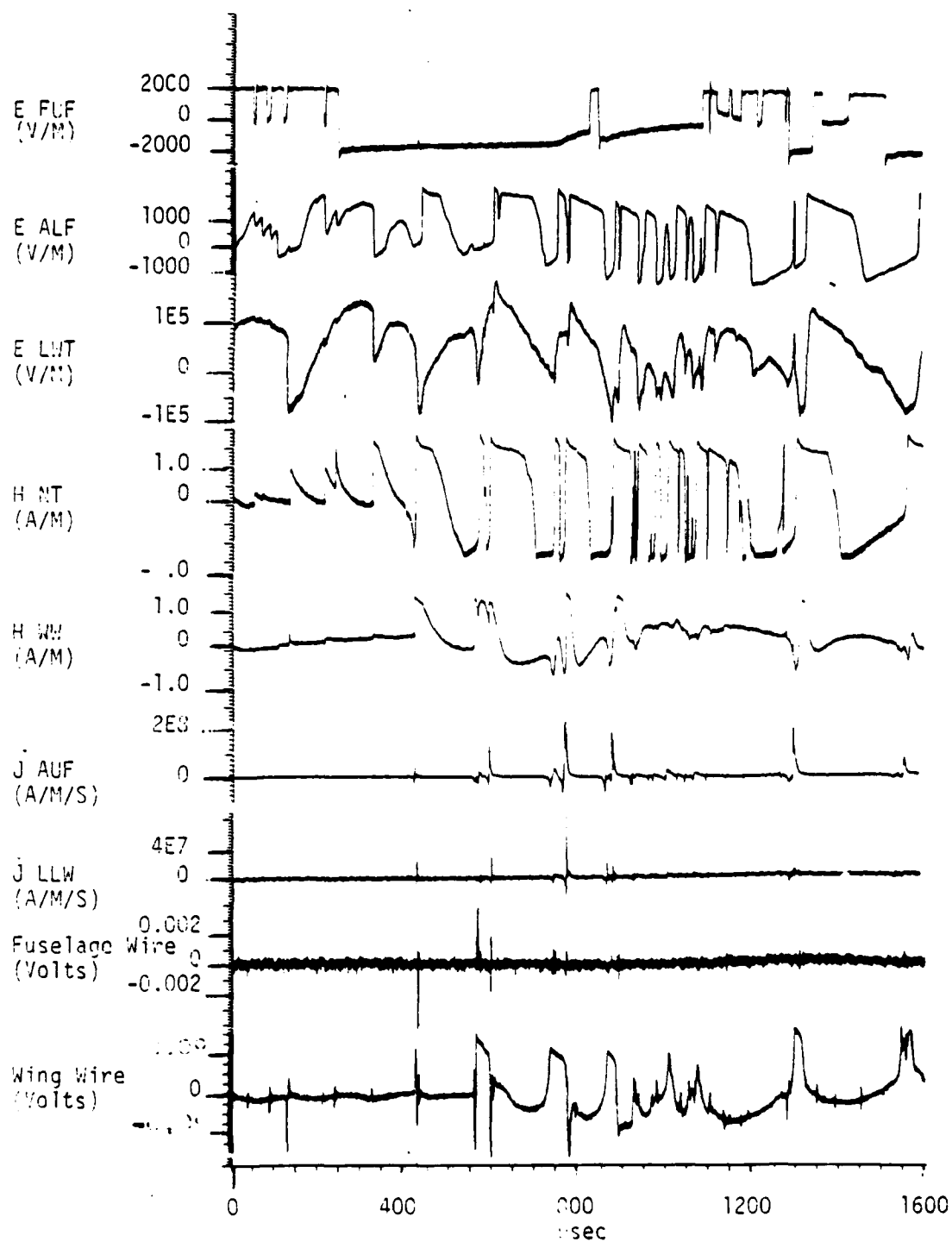
Figure 77. A 1.6 msec Expansion at the Time of the Largest Individual Pulses during the First Attachment of the Lightning Strike on 26 Aug 81

153

Figure 78. A 164 µsec Data Window that Includes the Largest Pulse in the J AUF during the First Attachment.

154
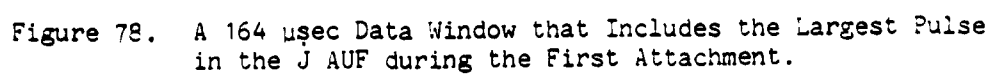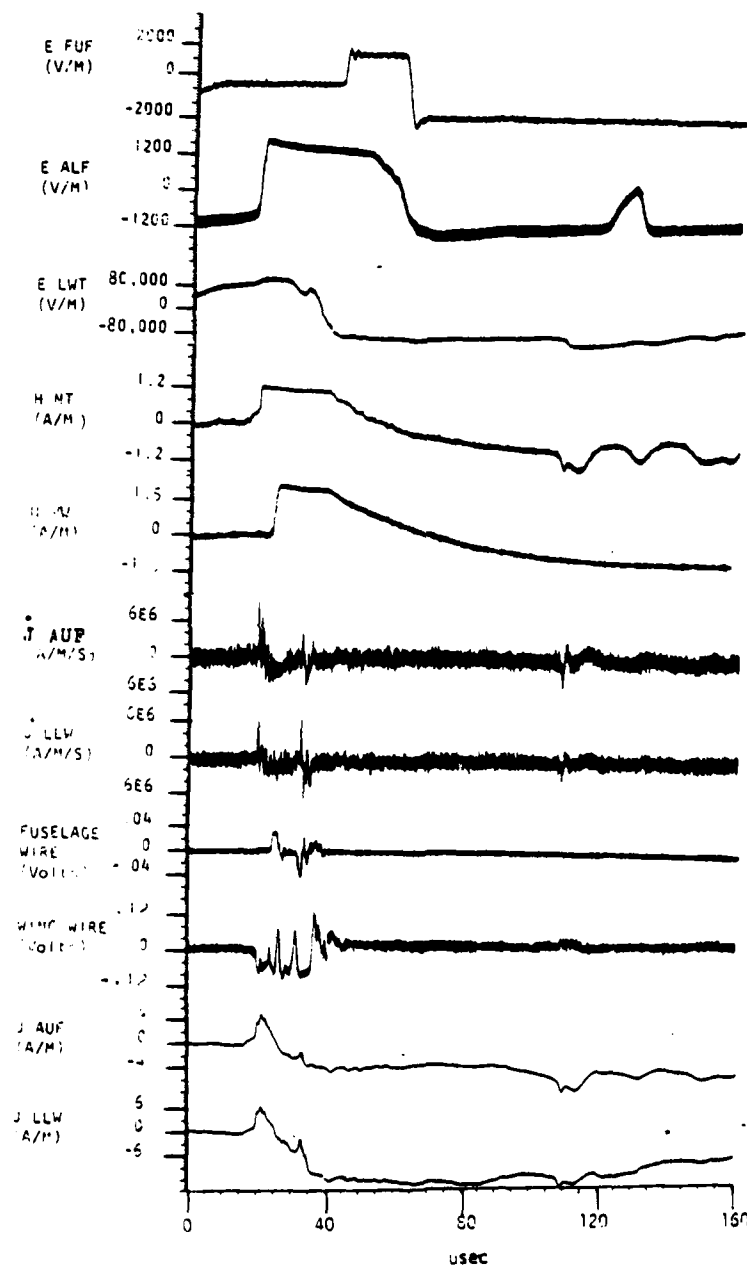
Figure 79. A 164 usec Data Window that Includes One of the Largest
Pulses during the Second Attachment.

155

Table 7

Maximum Magnitudes and Derivatives of Unsaturated Pulses
Pulses during the Lightning Attachment on 26 Aug 81

Quantity	Magnitude	Derivative
Uniform Current	3 kA	3 kA/m-μsec
Electric Field	150 kV/m	250 kV/m-μsec
Magnetic Field	1.5 A/m	3.2 A/m-μsec
Induced Voltage	140 mV	26 kV/μsec

active phase. These two current pulses were integrated to determine the uniform current flow and the charge transfer by each pulse. Since the pulse durations are 20 μsec and 17.5 μsec, respectively, the charge transfers for these two pulses were 30 mC and 47 mC. These types of pulses probably account for most of the charge transfer during the flash.

Table 8 shows the risetimes which were calculated using the standard 10% to 90% of the fastest portion of the curve for all ten pulses. These risetimes were determined for unsaturated pulses only, so magnitude changes over the risetime of the pulse are also presented. The maximum risetime for these pulses was about 3 μsec and the minimum risetime was limited by the recorder bandwidth.

Table 8. Risetimes and Magnitude Changes for Several Pulses during the Lightning Attachment on 26 Aug 81.

PULSE #	1	2	3	4	5	6	7	8	9
E LWT	2700	-	820	3000	2500	-	800	-	1100
H NT	1000	1468	400	-	420	1000	-	-	410
J LLW	248*	593	274*	2003	800	-	800	331*	2000
J AUF	-	900	242*	-	3000	-	-	410	-
Wing Wire	-	1000	900	1500	2000	-	800	1000	2000
Fuselage Wire	-	-	-	1500	310*	1000	-	-	-

a. Risetimes in nanoseconds
   The asterisk (*) indicates that the risetime measured is at the limit of the recorder bandwidth.

	1	2	3	4	5	6	7	8	9
E LWT V/M/µS	3.764	-	1.4E5	2E4	2.8E5	-	9.4E5	-	5.5E4
H NT A/M/µS	.05	.11	.75	-	1.66	.7	-	-	1.46
J LLW A/M/µS	5.2	.51	.5	5.9	11.25	-	4.6	5.43	11.5
J AUF A/M/µS	-	1.0	1.65	-	6.33	-	-	4.39	-
Wing Wire V/µS	-	.019	.13	.166	.07	-	.175	.22	.12
Fuselage Wire V/µS	-	-	-	.002	.13	.03	-	-	-

b. Magnitude changes for the risetime calculations of a.

157

3. SUMMARY OF THE CHARACTERISTICS OF THE TWO DIRECT LIGHTNING
   ATTACHMENTS TO THE AIRCRAFT

During both attachments the aircraft was more than 50 km from the ground site. The electric field change at the ground site was not monitored at the most sensitive scale at which the polarity of the electric field could be used to distinguish ground from cloud flashes. If there had been a ground flash, the leader, after contacting the aircraft, would have propagated to ground. Since the aircraft was about 4.8 km above the ground in both cases, leader propagation from the aircraft to the ground would require about 5 msec. At that time, the return stroke would have propagated up the channel and a fraction of a millisecond later should have caused an electric field change at the aircraft. This type of pattern or any other variations in the waveforms that could be interpreted as a cloud-to-ground lightning flash was not observed. In addition, the slow electric field change at the aircraft only lasted about 350 usec before the first sharp discontinuity was observed. This implies an initial leader propagation of only a few hundred meters prior to attachment to the aircraft and no apparent leader propagation after attachment. This pattern suggests that the aircraft initiated the lightning discharge. However, by comparing sets of correlated pulses, some differences can be observed at the beginning of these two strikes. On 17 July the initial slow electric field variation does have a correlated H NT variation as shown in Figure 70. As the leader propagation started, a small current flow was detected along the fuselage. It may be that

some type of streamer propagated from the aircraft fuselage during the initiation of the flash. However, as pointed out by Shaeffer (Ref 39), for streamer initiation an external field at some point on the aircraft must exceed the breakdown of free space. The static field was not measured and it cannot be concluded with certainty that a leader propagated from the aircraft. The correlated electric/magnetic field pulses were not observed during the 26 August strike leading to the assumption that the entire leader propagation was from the cloud toward the aircraft.

During both strikes the aircraft was flying in cloud in areas of slight or slushy precipitation. From the Stormscope display it appeared that no natural lightning discharges were occurring closer than about 5 km from the aircraft. The aircraft penetrated these clouds at 16,000-17,000 feet MSL and the cloud tops were only at 22,000 and 30,000 ft. These low cloud tops rarely produce lightning discharges. Therefore, it is highly unlikely that either of these flashes was a natural intracloud discharge which happened to make contact with the aircraft. On the basis of the data presented here, it is believed that both of these lightning strikes were triggered by the presence of the aircraft.

The total duration and overall structure of the train of pulses presented here for the two direct attachments (Figures 68 and 74) are consistent with other reported aircraft lightning strikes (Ref 13 and 40). The direct strikes lasted 295 msec and 460 msec with a maximum pulse repetition rate of 10^4 pulses/sec. Fitzgerald (Ref 41) does not show the total duration of his 55 direct lightning strikes but claims a pulse repetition rate of

103 pulses/sec. The direct strike reported by Nanevicz (Ref 13) lasted 700 msec with a pulse repetition rate of 0.2 x 103 pulses/sec. Trost and Pitts (Ref 40) reported a strike to the NASA F-106 that lasted over 760 msec and had more than 100 pulses. Our pulse repetition rate of at least one order of magnitude larger is probably due to the fact that our instrumentation was calibrated to detect smaller pulses. This type of pulse repetition rate observed on aircraft lightning discharges probably indicates that the aircraft continues to neutralize small pockets of charge located within a few hundred meters of the aircraft in the oppositely charged region that initiated the discharge.

When comparing the magnitude of our maximum uniform current flow of 800 A and 3 kA for any pulse in the flash with those appearing in the reported data (Refs 37, 40, and 41), it appears that our direct strikes were of lower intensity than the expected average. Fitzgerald reported peak current values of 5.8 kA, 14.5 kA, 2.8 kA, and 22 kA for direct strikes to the nose boom, right wing tip, left wing tip, and vertical stabilizer, respectively. The French ONERA group (Ref 17) flying a C-160 aircraft reported 13 direct strikes with a maximum current of 70 kA. The data collected in the F-106 NASA program of 20 direct strikes for the summers of 1980 and 1981 indicate a maximum current of 14 kA (Ref 42).

Table 9 shows a comparison of the characteristics of our two direct strikes. Most of the features of this table have been discussed in the preceding sections. The risetimes for the

largest unsaturated pulses of the lightning attachment were summarized in Tables 6 and 8. The risetimes of the pulses during lightning attachment reported in the literature (Refs 16 and 17) range from tens of nanoseconds to about 10 μsec.

Table 9
Comparison of the Characteristics of the
Two Direct Lightning Attachments to the C-130 Aircraft

	17 July	26 August
Flash Duration	295 msec	460 msec
Maximum Pulse Repetition Rate	10^4 pulses/sec	10^4 pulses/sec
Total Number of Pulses	150 - 200	200 - 300
Maximum Uniform Current Flow in a Single Pulse	800 A	3 kA
Maximum Electric Field Change in a Pulse	2000 V/m (Saturation Level)	200,000 V/m
Maximum Magnetic Field Change in a Pulse	1.8 A/m (Saturation Level)	1.8 A/m (Saturation Level)
Risetime	Max: 12 μsec Min: about 20% below BW limit of 350 nsec	Max: 10 μsec Min: about 25% below BW limit of 350 nsec
Continuing Current	50 A	--------------

SECTION VI

CONCLUSIONS

Partial results of the Air Force Flight Dynamics Laboratory three-year (1979-1981) airborne lightning characterization program have been presented. The intent of this report has been to document the results and to provide detailed information on all aspects of the program, including assumptions and tradeoffs made to permit interpretation of the data.

The program was conceived because new technology being used on the latest production aircraft and on aircraft designs under development can cause vulnerability to Electromagnetic Interference (EMI) from atmospheric electromagnetic radiation and to induced transients from the radiation. This new technology includes low voltage solid state devices and micro-circuits, high speed electronics which perform critical flight functions, and non-metallic structural materials that do not provide any or sufficient electromagnetic shielding of aircraft electronics.

Several thousand events were recorded which resulted in thousands of waveforms for electric and magnetic fields and surface currents at the aircraft and on the ground. The data were recorded in analog and digital formats and were time-correlated at all measuring locations. Three different sets of data were presented in Sections IV and V. Section IV shows nearby and far field data between 5 and 35 km of the discharge. Five of the

lightning flashes discussed were correlated between the ground and the aircraft recorders. The characteristics of the data recorded during several other flashes were also discussed. Section V describes the characteristics of the two direct strikes.

At the present time about 40% of the data has been processed and another Technical Report will be published after all the data have been analyzed. However, this report contains sufficient information on the signature of the electromagnetic fields measured at the aircraft surface to provide a better understanding of lightning interaction with the aircraft and to permit designing experiments for future lightning characterization programs using similar instrumentation.

Many important conclusions were reached after this partial analysis of the data. Most of these conclusions were stated in the report and summarized at the end of the respective sections in the data interpretation. Here, a brief summary is provided of some of the most important conclusions.

1. The signatures of the electric field with 2 MHz frequency response recorded on the ground and in the aircraft (1500 to 16,000 ft MSL) for flashes 7 to 35 km away are similar. However, the magnitude of the fields at the aircraft was larger than on the ground by an enhancement factor as large as 3. This enhancement factor accounts for some of the differences between the measured surface fields on the aircraft and the aircraft incident field which was not measured. Within a 2 MHz frequency response, the aircraft surface fields had characteristics similar to those of the incident field measured on the ground.

2. The risetimes for return strokes in cloud-to-ground

163

flashes were found to range from less than 100 nsec to several microseconds. However, there are many other pulses in cloud-to-ground and intracloud flashes with risetimes equal to or faster than the risetimes of return strokes. These pulses are of smaller magnitudes than return strokes and are found primarily during the preliminary breakdown stage of cloud-to-ground flashes. They have also been observed during K-changes in the interstroke process and in intracloud discharges.

3. The surface fields measured on the aircraft for flashes 3 to 7 km away show a significant frequency content in the 2 to 5 MHz range. The surface fields are affected considerably by the resonant frequencies of the aircraft for nearby flashes.

4. From the data presented here and a review of the literature, it appears that most direct lightning attachments to the aircraft are triggered by the presence of the aircraft and are not natural lightning discharges. The duration of these direct lightning strikes is comparable to natural discharges (0.5 sec) and they exhibit a unique pulse repetition rate of around 10^3 or 10^4 pulses/sec. The uniform current related to these pulses can range between hundreds of amps to tens of kiloamperes.

For the two attachments described in this report the data indicate that the aircraft triggered both discharges. In both cases minor damage occurred to the aircraft. In one case, the attachment broke an antenna on the aircraft surface and in the other case an internal transient produced a dump in the navigation computer memory. These types of damage could jeopardize the completion of a mission and are serious enough to study in detail.

164

SECTION VII

RECOMMENDATIONS

Our most important recommendation is that the task of processing the remainder of the 1981 data be completed. Only forty percent of these data has been processed to date. Several research papers and a final technical report should be published after completion of the data analysis. One research paper should be written on the properties of the airborne electric and magnetic fields. This paper should contain statistics for the rise-time and frequency response of hundreds of return strokes and other fast pulses in cloud-to-ground and intracloud flashes. Another research paper should be published on the behavior of the surface fields measured on the aircraft with 20 MHz bandwidth as a function of the distance to the flash. In this manner, it may be possible to fully understand the variations between the incident field and the surface fields for nearby flashes. As shown in this report, the aircraft resonant frequencies (2 to 5 MHz) have a significant effect for flashes less than 7 km from the discharge.

After completion of the tasks previously stated, we will have further improved our understanding of the interaction of the aircraft with nearby lightning flashes; however, additional data are still needed to understand direct lightning attachments to aircraft. The data in the two direct strikes presented here

answer some questions but raise many others. Most of the questions which are raised from analysis of the data in Section V cannot be answered even after close study of all previously reported studies of lightning direct attachment to aircraft (Refs 4, 13, 14, 16, 17, 40-42). Additional programs are needed in which the aircraft electromagnetic fields are measured during the attachment of a cloud-to-ground lightning discharge.

References

1. P.B. Corn, "Aircraft and Environmental Factors Influencing Lighting Strikes," AIAA 19th Aerospace Sciences Meeting, St. Louis, Mo., Jan 1981.

2. P.B. Corn, "Lightning as a Hazard to Aviation," Preprints, American Meteorological Society 11th Conference on Severe Local Storms, 301-306, October 1979.

3. J.A. Plumer, "Lightning Effects on General Aviation Aircraft," FAA Conference, Report No. FAA-RD-79-6 Supp 1, Melbourne, Fla, March 1979.

4. F.A. Fisher and J.A. Plumer, "Lightning Protection of Aircraft," NASA REference Publication 1008, October 1977, 550 pp.

5. R.K. Baum, "Airborne Lightning Characterization,"Lightning Technology Conference, FAA-RD-80-30, NASA Langley Research Center, Hampton, Virginia, April 1980.

6. C.D. Weidman and E.P. Krider, "The Fine Structure of Lightning Return Stroke Wave Forms," J. Geophys. Res., 83, 6239-6247, December 1978.

7. J.A. Tiller, M.A. Uman, Y.T. Lin, and R.D. Brantley, "Electric Field Statistics for Close Lightning Return Strokes Near Gainesville, Florida," J. Geophys. Res., 81, 4430-4434, August 1976.

8. R. J. Fisher and M.A. Uman, "Measured Electric Field Risetimes for First and Subsequent Lightning Return Strokes," J. Geophys. Res., 77, 399-407, 1972.

9. N. Kitagawa, "On the Electric Field Change Due to the Leader Process and Some of their Discharge Mechanisms," Papers in Meteorology and Geophysics, 7, 4004.14, 1957.

10. N. Kitagawa and M. Brook, "A Comparison of Intracloud and Cloud-to-Ground Lightning Discharge," J. Geophys Res., 65, 1189-1201, 1960.

11. T. Ogawa and M. Brook, "The Mechanism of the Intracloud Lightning Discharge," J. Geophys Res., 69, 5141-5150, 1964.

12. P.L. Rustan, "Properties of Lightning Derived from Time Series Analysis of Radiation Data, Ph.D. Dissertation, Univ. of Florida, 397 pp, 1979.

13. J. Nanevicz, R. Adams, and R. Bly, "Airborne Measurement of Electromagnetic Environment near Thunderstorm Cells" (TRIP-76), Stanford Research Institute, March 1977.

14. B.J. Peterson and W.R. Wood, "Measurements of Lightning Strikes to Aircraft," Final Report No. DS-68-1, Federal Aviation Administration, Aircraft Development Service, Washington D.C. 20590.

15. J.T. Dijak, "Airborne Measurements of Transient Electric Fields and Induced Transients in Aircraft due to Close Lightning," Air Force Flight Dynamic Lab Tech Rep 77-64, 62 pp, 1977.

16. F.L. Pitts, "Electromagnetic Measurements of Lightning Strikes to Aircraft," AIAA 19th Aerospace Sciences Meeting, Paper No 81-0083, Jan 1981.

17. Centre D/Essais Aeronautique De ToLouise, "Measure Des Characteristiques De La Foudre En Altitude," Essais No 76/650000 P.4 FINAL, July 1979.

18. G.I. Serham, M.A. Uman, D.G. Childers, and Y.T. Lin, "The RF Spectra of First and Subsequent Lightning Return Strokes in the 1-200 km Range," Radio Science, Vol 15, 1089-1094, 1980.

19. F. Horner, "Radio Noise from Thunderstorms," in Advances in Radio Research, 2, J.A. Saxton (ed), Academic Press, New York, 122-215, 1964.

20. E.T. Pierce, "Atmospherics and Radio Noise," Lightning, Chapter 20, Associated Press, edited by R.H. Golde, 1977.

21. A.S. Dennis and E.T. Pierce, "The Return Stroke of the Lightning Flash to Earth as a Source of VLF Atmospherics," Radio Science, 68D, 779-794, 1964.

22. C.E. Baum, "Electromagnetic Pulse Sensor Handbook," EMP Measurement 1-1, June 1971.

23. C.E. Baum, E.L. Breen, J.C. Giles, J.P. O'Neill, and G.D. Sower, "Electromagnetic Sensors for General Lightning Application," Symposium on Lightning Technology, NASA Hampton, VA, April 1980.

24. C.E. Baum, E.L. Breen, J.C. Giles, J.P. O'Neill, and G.D. Sower, "Sensors for Electromagnetic Pulse Measurements Both Inside and Away from Nuclear Source Regions," IEEE Trans. on Antennas and Propagation, Vol. AP-26, No 1, Jan 1978.

25. C.E. Baum, "A Technique for Distribution of Signal Inputs to Loops," AFWL EMP Sensor and Simulation Notes, AFWL EMP 1-1, Note 23, Dec 1966.

26. C.L. Lennon, Minutes of Frequency Management Group, Range Commander Council, R1-R25, White Sands Missile Range, New Mexico, 1975.

27. P.L. Rustan, M.A. Uman, D.G. Childers, W.H. Beasley, and C.L. Lennon, "Lightning Source Locations from VHF Radiation Data for a Flash at Kennedy Space Center," J. Geophys. Res., 85, 4893-4903, September 1980.

28. D.E. Proctor, "A Hyperbolic System for Obtaining VHF Radio Pictures of Lightning," J. Geophys. Res., 76, 1470-1489, February 1971.

29. E.P. Krider and R.C. Noggle, "Broadband Antenna Systems for Lightning Magnetic Fields," J. of Applied Meteorology., 14, 252-256, March 1975.

30. D.E. Proctor, "VHF Radio Pictures of Cloud Flashes," J. Geophys. Res., 86, 4041-4071, May 1981.

31. Y.T. Lin and M.A. Uman, "Electric Radiation Fields of Lightning Return Strokes in Three Isolated Florida Thunderstorms, J. Geophys. Res., 78, 7911-7915, 1973.

32. M.A. Uman, R.D. Brantley, Y.T. Linn, J.A. Tiller, E.P. Krider and D.K. McLain, "Correlated Electric and Magnetic Fields from Lightning Return Strokes," J. Geophys. Res., 80, 373-376, January 1975.

33. C.D. Weidman, E.P. Krider, and M.A. Uman, "Lightning Amplitude Spectra in the Interval from 100 KHz to 20 MHz, Geophys. Res. Lett., 8:931-934, (1981).

34. M. Brook and N. Kitagawa, "Radiation from Lightning Discharges in the Frequency Range 400 to 1000 Mc/s," J. Geophys. Res., 69, 2431-2434, 1964.

35. M.J. Master, M.A. Uman, Y.T. Lin, and R.B. Standler, "Calculations of Lightning Return Stroke Electric and Magnetic Fields Above Ground," J. Geophys. Res., Vol 86, No. C12, 12, 127-12-132, Dec 1981.

36. C.D. Weidman and E.P. Krider, "The Radiation Field Waveforms Produced by Intracloud Lightning Discharge Processes," J. Geophys. Res., 84:3157-3164 (1979).

37. M.A. Uman, "Lightning," McGraw-Hill, New York, 1969.

38. B.J.C. Burrows   "Atsolute Calibration of B and J Sensors on FY80 WC 130 Aircraft," USAF Contract No. F61708-81-M0140, June 1981.

39. J. F. Shaeffer, "Aircraft Initiation of Lightning," 1972 Lightning and Static Electricity Conference, USAF Report AFAL-TR-72-325, December 1972.

40. T. F. Trost and F.L. Pitts, "Analysis of Electromagnetic Fields on an F-106B Aircraft During Lightning Strikes," NASA Techical Report 1981.

41. D.R. Fitzgerald, "Aircraft and Rocket Triggered Natural Lightning Discharges," Lightning and Static Electricity Conference, AFAL Rep. TR-68-290, Part II, December 1968.

42. F.L. Pitts and M.E. Thomas, "1980-1981 Direct Strike Lightning Data," NASA Tech Memorandum 81946 and 83273, Feb 1981 and March 1982.

tromagnetic
ng Strikes,"

red Natural
Electricity
ber 1968.

rect Strike
d 83273, Feb

END

DATE

FILMED

8 — 8

DTIC